VLÁKNA A TEXTIL

FIBRES AND TEXTILES

TECHNICAL
UNIVERSITY
OF LIBEREC

STU
FCHPT

Trenčianska univerzita
Fakulta priemyselných technológií v Púchove
Alexandra Dubčeka v Trenčíne

VUTCH
RESEARCH INSTITUTE OF TEXTILE CHEMISTRY
VÝSKUMNÝ ÚSTAV TEXTILNEJ CHÉMIE

CHEMOSVIT
FIBROCHEM

VÚCHV

ZSVTS

VLÁKNA A TEXTIL

http://www.vat.ft.tul.cz

VLÁKNA A TEXTIL
Volume 31, Issue 2, September 2024

CONTENT

DETERMINATION ON NITROGEN CONTENT OF ANTIBACTERIAL COTTON FABRIC TREATED WITH CHITOSAN

LUU, THI THO[1]; VU, THI HONG KHANH[2*]; NGUYEN, TUAN ANH[3] AND NGUYEN, THI KIM THU[4]

[1]   Hanoi University of Industry, 298D, Cau Dien St, Bac Tu Liem Dist, Hanoi City, Vietnam
[2]   Industrial University of Ho Chi Minh City, 12 Nguyen Van Bao St, Ward 4, Go Vap Dist, Ho Chi Minh City, Vietnam
[3]   Ho Chi Minh City University of Technology and Education, No 1, Vo Van Ngan St, Thu Duc Dist, Ho Chi Minh City, Vietnam
[4]   Hanoi University of Science and Technology, No 1, Dai Co Viet St, Hanoi City, Vietnam

ABSTRACT

The study aims to evaluate the nitrogen content on antibacterial cotton fabrics treated with chitosan using four different quantitative determination methods: field-emission scanning electron microscopy with energy dispersive X-ray spectroscopy (FESEM-EDX), dyeability of antibacterial treated samples based on color strength (K/S), elemental analyses via combustion tests, and antibacterial ability under dynamic contact conditions or the dynamic shake flask test. The nitrogen content was analyzed under the effects of molecular weight (MW) of chitosan (2.6 kDa and 187 kDa), crosslinkers including citric acid (CA) and dimethylol dihydroxyethyleneurea (DMDHE), and washing cycles. The findings from these measurements not only determined the nitrogen content of antibacterial cotton fabric but also elucidated the bonding mechanism between cellulose and chitosan in the presence of crosslinking compounds. Consequently, the antibacterial activity of cotton fabrics treated with chitosan could be indirectly assessed through the nitrogen content obtained from the amine groups of finishing compounds.

KEYWORDS

Nitrogen content; Antibacterial activity; Crosslinker; Chitosan; Cotton fabric; Dyeability.

INTRODUCTION

Chitosan is a natural linear polysaccharide produced by the deacetylation of chitin, which is derived from shrimp shells, insect cuticles, and cell walls of fungi and algae. These are abundant biopolymers second only to cellulose derivatives [1-4]. Notably, commercial chitosan samples, deacetylated chitin from crustacean sources, are soluble in aqueous acidic solutions with a pH lower than 6.5, such as acetic acid, formic acid, and lactic acid [5-8]. The solubility of chitosan is a crucial for its chemical conversion into thin films and yarns. Chitosan contains more active groups than chitin, especially amine groups, which can inhibit bacterial growth of bacteria due to their positive charge [3]. In acidic solution, amine groups in chitosan transform into quaternary ammonium cations, enabling it to prevent both gram-negative and gram-positive bacteria [4]. Outstanding properties of chitosan include nontoxicity, biocompatibility, and biodegradation, offering benefits such as antibacterial ability, anticancer properties, and antibody abilities [5, 9]. The main application fields of commercial chitosan are biotechnology, pharmaceutics, wastewater treatment, cosmetics, agriculture, food science, and textiles [2]. Chitin is insoluble in diluted acetic acid but if its degree of N-acetylation is higher than 60%, it transforms into chitosan, which is soluble in acidic solutions [4, 10, 11]. In addition, molecular weight of chitosan, dependent on its origin and acetylation conditions (time, temperature and sodium hydroxide concentration), is significant.

In textile finishes, chitosan is primarily used for antibacterial treatments on cotton fabrics due to high economic efficiency and excellent human health protection [5]. The antibacterial properties of cotton fabrics treated with chitosan were attributed to the interaction between cationic chitosan and anionic bacterial and fungal surfaces, which alters cell wall absorption or causes cytoplasmic leakage [12-14]. Chitosan with positive charges and low molecular weight can bind to DNA in bacterial and fungal cells, inhibiting biosynthesis [15]. Studies have shown that the antibacterial effectiveness of cotton fabric treated with chitosan is influenced by factors such as molecular weight, degree of acetylation, pH value, temperature, concentration and additives. Some researchers have demonstrated that lower molecular weight chitosan results in higher antibacterial effectiveness [5, 16] and lower moisture or water absorption [17]. However, the relationship between

antibacterial ability and molecular weight of chitosan is still debated due its natural variability and range of acetylation degrees, making its effects difficult to determine. Chitosan with a higher degree of acetylation possesses more quaternary amine cations, thus enhancing its antibacterial activity [18]. Additionally, the antibacterial efficacy of chitosan is optimal at pH value around 5.0 [13, 19, 20]. The best antibacterial effectiveness is observed when treating samples with chitosan at temperature between 25 ºC and 37 ºC, while it decreases below 25 ºC [21]. To enhance the linkage of chitosan to cotton fabrics, crosslinkers such as citric acid (CA), 1,2,3,4-butanetetracarboxylic acid (BTCA), glutaraldehyde and dimethylol dihydroxyethyleneurea (DMDHEU) have been used in previous researches [22, 23].

Some methods for evaluating the antibacterial ability of fabrics treated with chitosan include dynamic contact methods according to ASTM E2149-01, AATCC 100 and AATCC 147 standards, commonly testing gram-positive bacteria (e.g., Staphylococcus aureus) and gram-negative bacteria (e.g., Escherichia coli) [5]. In addition, advanced techniques such as scanning electron microscope (SEM), Fourier transform infrared spectroscopy (FTIR), nuclear magnetic resonance (NMR), X-Ray diffraction analysis (XRD are also applied to confirm the presence of chitosan in fabric structure. Some methods like dyeing, mass comparing and nitrogen content determination were reported [9, 24-26]. In this study, the authors will determine the nitrogen (N) content on antibacterial treated cotton fabrics with chitosan, as this quantitative evaluation allows for assessing antibacterial ability. Many studies have shown that amine groups in chitosan interact with anionic bacterial cell to inhibit microbial growth.

EXPERIMENTS

Materials and chemicals

Pretreated cotton fabrics were provided by Nam Dinh Textile Garment JSC (Vietnam). The cotton fabrics were specified as 2/1 twill with a weft count 16 (Ne), a warp count 34 (Ne), and 175 and 410 threads per centimeter (TPC) in crosswise and lengthwise directions, respectively, and a weight of 230 grams per square meter (GSM).

Chitosan with deacetylated degree (DD of about 75% was purchased from Vietnam Chitosan Co. Ltd, and was extracted from shrimp shells. The molecular weight of the chitosan was reduced using gamma irradiation. Two types chitosan with different molecular weights, 6.9 kDa (CTS1) and 187 kDa (CTS2), were determined through solution viscosity and calculated using the Mark–Houwink equation [27].

Since chitosan can not form covalent bonds with cellulose, citric acid (CA) and dimethylol dihyroxyethyleneurea (DMDHEU) were used as crosslinking agents. Acid dyes, commercially named Lanaset® Yellow 2R, were purchased from Huntsman Corporation, and applied at pH of 4.5. Additionally, acetic acid, ethanol, sodium hypophosphite (SHP) for CA agent, catalyst NKC for DMDHEU agent and a nonionic wetting agent (Hostapal MRN) were used as additives.

Instrument and methods

Cotton fabrics were washed, desized and bleached according to AATCC 187-2013 and stored in a conditioner (M250-RH, Mesdan) for 24 hours. Chitosan was dissolved in citric acid (7%) or acetic acid (2 g/l) using a magnetic stirrer (Starlet), and the dyeing medium was controlled by a pH meter (Mettler Toledo). The prepared solution (chitosan, crosslinker, wetting agent, catalyst, etc.) was applied to the cotton fabrics using a padding mangle (Roaches machine) and a setting drier (Hisaka). All treated samples were cleaned in a washing machine (Quickwash Plus) to evaluate color fastness and chemical retention.

A recipe with liquor ratio of 1/50, 0.5% on weight of fabric (owf) of acid dyes, and 2g/l acetic acid was used to dye the treated cotton fabrics with chitosan and crosslinkers at 98 ºC in 130 minutes using exhaust dyeing equipment (Colorstar) and an infrared dyeing machine (Starlet-2). The color strength (K/S) of dyed samples was measured using a UV-vis 1601PC and a UV spectrophotometer (Gretag Color-Eye 2180, daylight D65). Furthermore, an elemental analysis method (Elementar Analysensysteme GmbH) and a field emission scanning electron microscope with energy dispersive X-ray spectroscopy (FESEM-EDX, JSM 7600) were used to determine and evaluate the nitrogen content of antibacterial treated cotton fabric with chitosan and crosslinkers (CA and DMDHEU).

Escherichia coli (E. coli), a type of gram-negative bacteria stored at minus 40 ºC, provided by Proteomics lab, was used to examine the antibacterial activity of treated samples according to ASTM E2149-01 test method under dynamic contact conditions. The bacterial reduction was evaluated after 60 minutes and 2 minutes of exposure.

RESULTS AND DISCUSSION

Determination on nitrogen content of treated fabrics based on FESEM images coupled with EDX spectra

In previous works, chitosan was cross-linked by citric acid (CA) via an amidation reaction (i.e., amide group replaces a hydrogen atom on amino group) at an elevated temperature [28]. CA agent can dissolve chitosan completely. DMDHEU is also known as an excellent anti-wrinkle finishing agent on cotton fabric. Both CA and DMDHEU can react with hydroxyl groups and amine groups in cellulose and chitosan as illustrated in the proposed mechanism.
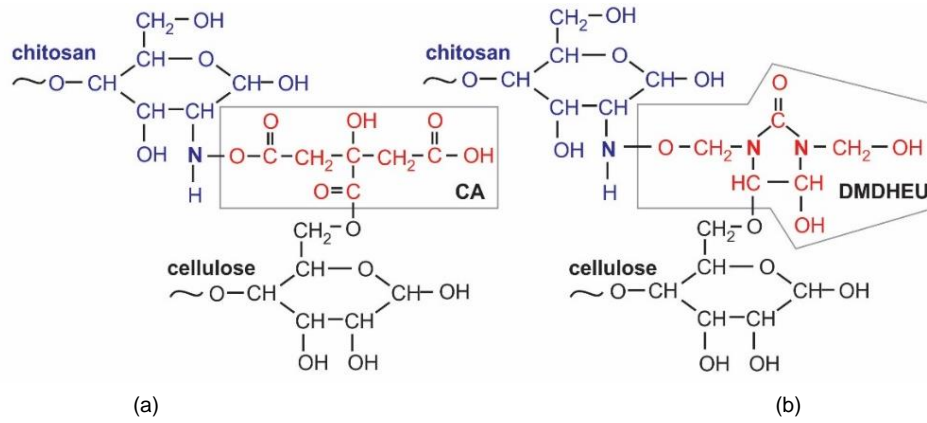
Figure 1. Proposed bonding mechanism of cellulose and chitosan in the presence of crosslinkers (CA and DMDHEU): (a) Chitosan – CA – Cellulose, (b) Chitosan – DMDHEU - Cellulose.

(a)

(b)

(c)

5

(d)

(e)
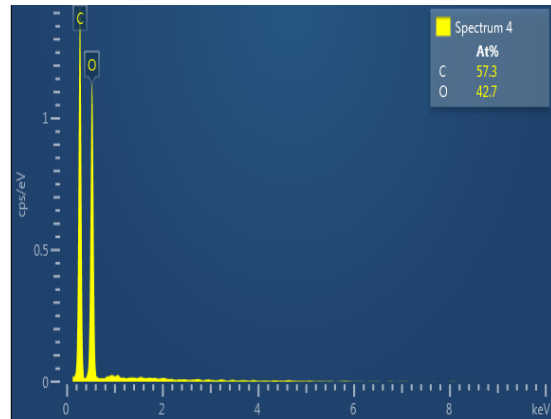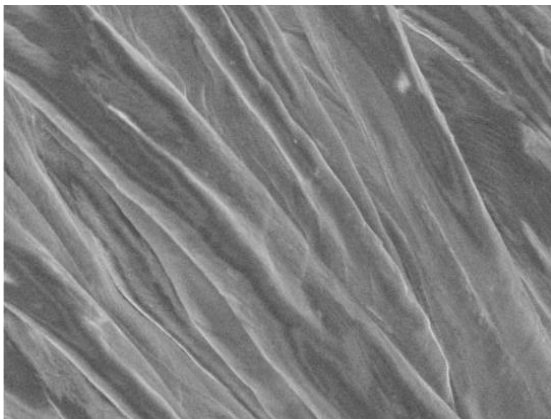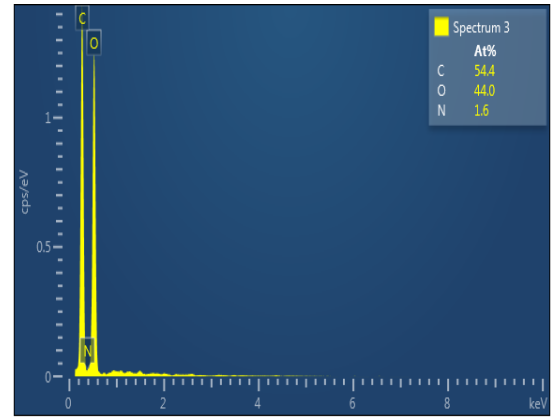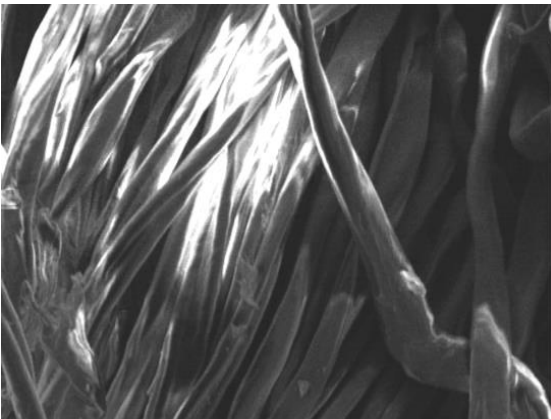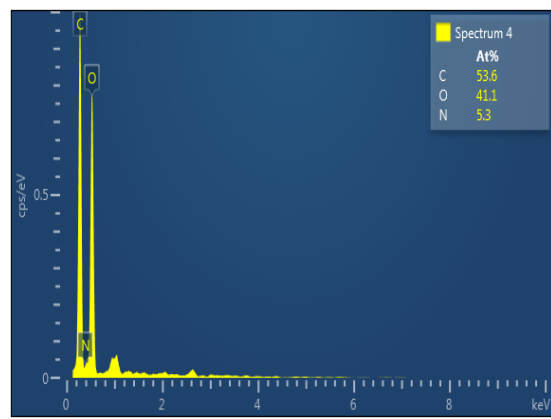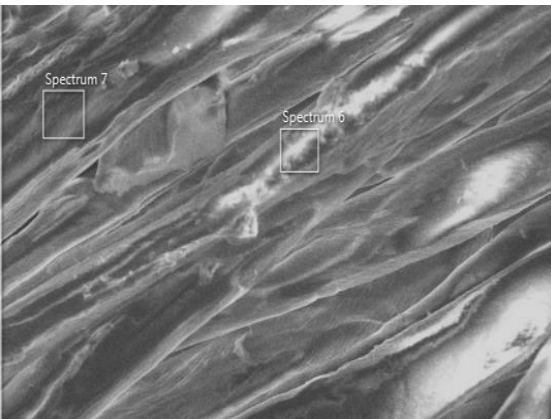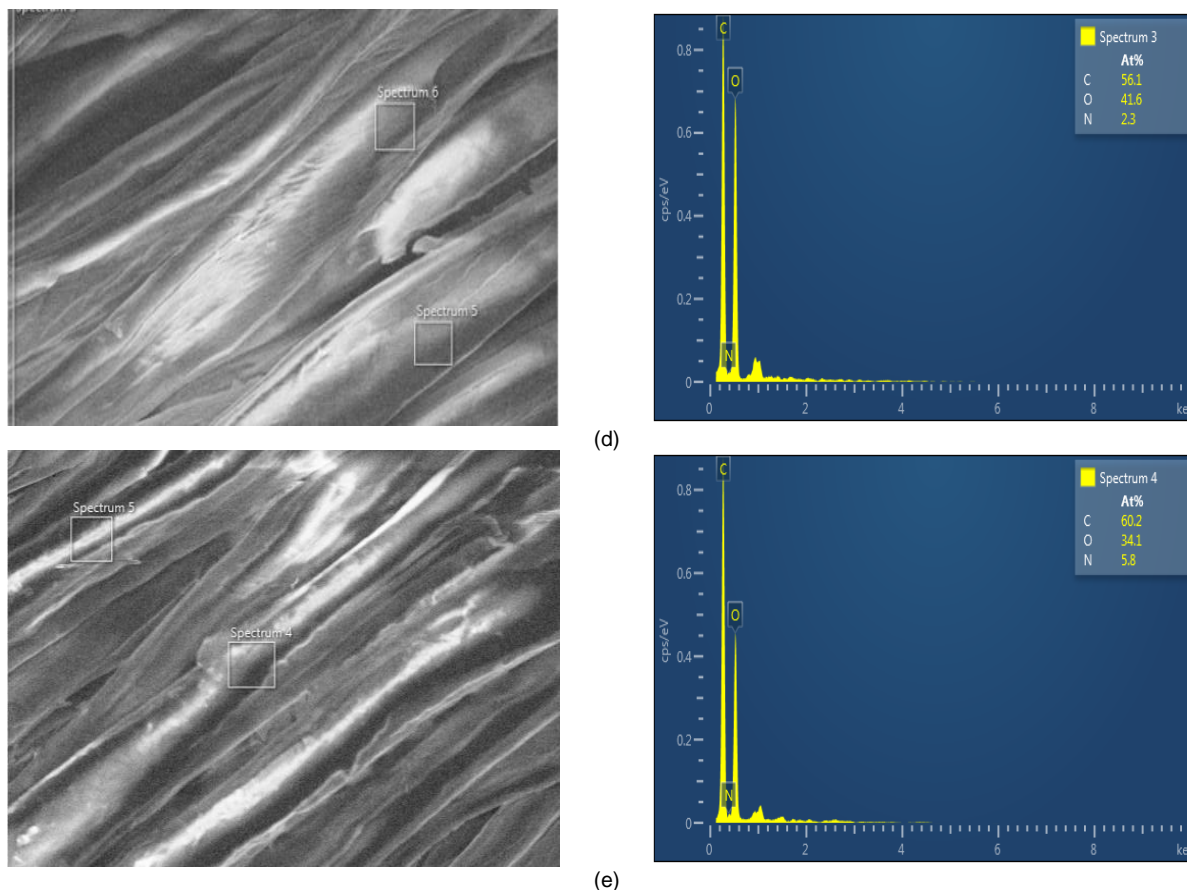
Figure 2. FESEM photos and EDX spectra of (a) untreated sample, treated with b) CTS1 and CA, c) CTS2 and DMDHEU, d) CTS1 and CA, and e) CTS2 and DMDHEU.

Table 1. Total content of carbon (C), oxygen (O) and nitrogen (N) atoms for untreated sample and treated samples with CTS1-CA, CTS2-CA, CTS1-DMDHEU, and CTS2-DMDHEU based on EDX spectra.

Sample	Molecular weight (kDa)	Content (%)		
		Carbon	Oxygen	Nitrogen
Untreated	-	57.3	42.7	0.0
CTS1-CA	2.6	54.4	44.0	1.6
CTS2-CA	187	56.1	41.6	2.3
CTS1-DMDHEU	2.6	53.6	44.1	5.3
CTS2-DMDHEU	187	60.2	34.1	5.8

For the antibacterial treatment of cotton fabrics with chitosan, two types of molecular weight of chitosan (2.6 kDa and 187 kDa, referred to as CTS1 and CTS2) and two types of crosslinker (CA and DMDHEU) were used. As shown in Figure 2 and Table 1, FESEM images and EDX spectra demonstrated that nitrogen atoms were not detectable in untreated sample with chitosan in the presence of CA. However, nitrogen atoms were present in all antibacterial samples treated with CTS1 and CTS2. For the same crosslinker, the nitrogen content of samples treated with CTS2 was higher than that of those treated with CTS1 (specifically, being 2.3 % vs. 1.6 % for CA, being 5.8 % vs. 5.3% for DMDHEU, respectively). Moreover, for the same chitosan type, the nitrogen content of antibacterial treated cotton fabrics crosslinked with CA was significantly lower than those crosslinked with DMDHEU due to absence of nitrogen atoms in the chemical structure of citric acid (specifically, 1.6% vs. 5.3 % for CA and 2.3 % vs. 5.8 % for DMDHEU). In other words, a significant nitrogen content was added to the cotton fabrics due to the nitrogen atoms present in both chitosan and DMDHEU, as illustrated in Figure 1.

Not only N atoms but also O and C atoms were detected in EDX spectra. When replacing CA with DMDHEU, the C content decreases from 54.4% to 53.6% for CTS1 and increases from 56.1% to 60.2% for CTS2 while O content decreases from 44.0% to 41.1% for CTS1 and from 41.6 to 34.1% for CTS2. Besides, as shown in **Figure 2**, FE-SEM photos provide further evidence of morphological variations in antibacterial treated cotton samples compared to untreated sample, with a small amount of finishing agent scattered across the surface of cotton fibers.

Evaluation on nitrogen content of treated fabrics based on dyeability

It is known that cellulose fibers cannot be dyed with acid dyes, but antibacterial treated cotton fibers with chitosan possess amine groups that may bond to acid dyes. Hence, nitrogen content could be determined through the content of acid dyes. The content of absorbed acid dyes was equivalent to the amount of amine groups inside treated cotton fabrics [29].

Antibacterial treated fabrics were dyed with acid dyes, and their dyeability was evaluated by color strength (K/S). This is because K/S is proportional to the content of chitosan linked to amine groups, allowing nitrogen content be determined indirectly. To ensure objectively K/S values of treated samples, an investigation was conducted to detect tthe maximum wavelength in the range from 360 to 700 cm^{-1} in various acid concentrations (including 1, 5, 10, 20, 25, 50 and 100 g/l) through UV-vis measurements. The experimental results indicated that the most suitable wavelength was 440 cm-1, at which the highest absorbance (1.1906 au) was found, as shown in Figure 3.

At this wavelength, the relationship between the absorbance (A) of antibacterial treated samples with chitosan and dye concentration (C) is expressed by the following linear calibration equation

$$A = 0.0084C + 0.0033, R^2 = 0.9999 \qquad (1)$$

Acid dyes could be removed from cotton fabrics because of relatively weak physical interactions (i.e., no chemical bonds). Therefore, the content of acid dyes was measured over several washing cycles, as presented in **Figure 4**. It can be observed that after 0, 5, 10, 15 and 20 of washing cycles, the contents of acid dyes on samples treated with CTS1 and CTS2 were slightly decreased, being 83.97, 79.78, 71.76 and 64.13 % for CTS1 and 90.73, 86.54, 84.99 and 80.35% for CTS2, respectively. Clearly, acid dyes formed a relatively durable linkage with textile fibers due to strong interactions between amine groups of chitosan. However, dyed samples with CTS1 exhibited less washing durability than those with CTS2. In other words, the amine groups of higher molecular weight chitosan on antibacterial treated cotton fabrics were bonded to dyestuffs more effectively [16].

Additionally, the decrease in K/S value of treated samples with CTS1 and CTS2 over washing cycles was represented as a linear function (as shown in Figure 5). The negative slopes of these lines were -0.006 and -0.012 for treated samples with CTS1 and CTS2, respectively, indicating that the content of acid dyes on antibacterial treated cotton with high molecular weight chitosan decreases more quickly with washing cycles. It can be affirmed that the higher the content of acid dyes, the darker the color on the fabric, and the higher the K/S value.
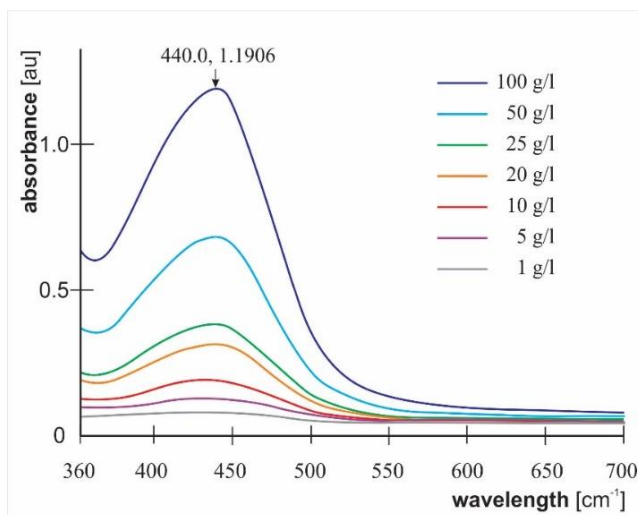
Figure 3. UV-vis spectra of antibacterial treated samples with 0.1% owf of chitosan at various concentrations of acid dyes (1, 5, 10, 20, 25, 50 and 100 g/l).
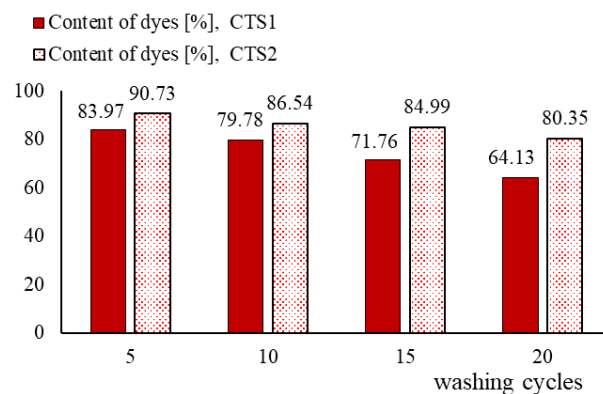
Figure 4. Decrease in content of acid dyes on antibacterial cotton fabrics treated with CTS1 and CTS2 after 5, 10, 15 and 20 washing cycles.
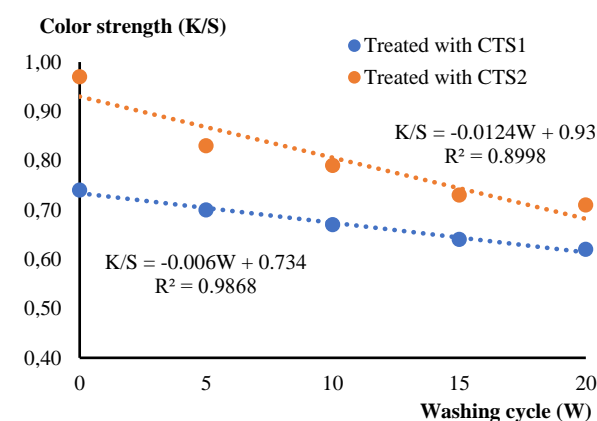
Figure 5. Curve of color strength (K/S) versus washing cycle (W) for antibacterial treated cotton fabrics with CTS1 and CTS2.
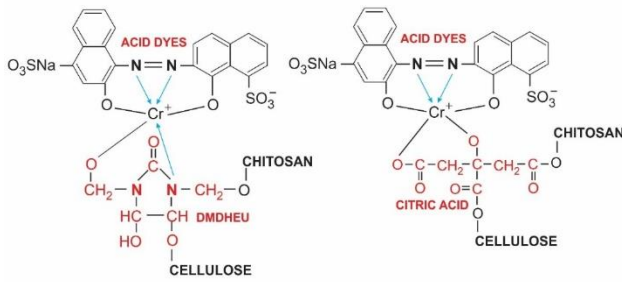
Figure 6. Proposed bonding mechanism of acid dyes with CA and DMDHEU owing to metal complex formation on antibacterial treated cotton fibers with chitosan.
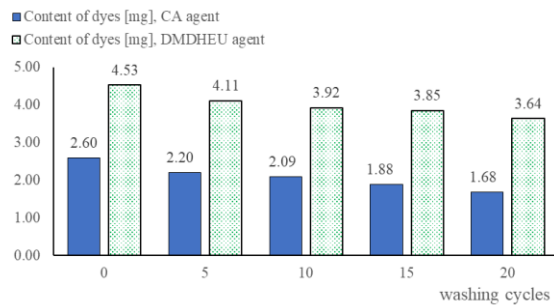
Figure 7. Content of acid dyes on antibacterial treated cotton fabrics with CTS2, CA and DMDHEU after 0, 5, 10, 15 and 20 washing cycles.

The role of crosslinkers, including CA and DMDHEU, in dyeing cotton fabrics with chitosan was also examined under washing conditions. A bonding mechanism among acid dyes, metal complexes, CA/DMDHEU, CTS1/CTS2 and cellulose was proposed, as illustrated in Figure 6. Metal ions played an important role in forming complexes to coordinate acid dyes with CA and DMDHEU.

The content of acid dyes fixed with CA/DMDHEU due to metal complex formation on antibacterial treated fabrics with CTS2 is shown in Figure 7. The nitrogen content absorbed into cotton fabrics (M_{abs}) is calculated based on the following equation:

$$M_{abs} = M_{pre} - M_{post} - M_{wash} \qquad (2)$$

where M_{pre} and M_{post} are the masses of dyes in pre-dyed and post-dyed solution, respectively, and M_{wash} is the mass of dyes in the washing solution after various cycles.

Accordingly, the content of acid dyes bonded with amine groups (M_{amine}) is determined as follows

$$M_{amine} = M_{abs(treated)} - M_{abs(untreated)} \qquad (3)$$

where $M_{abs(treated)}$ is the content of acid dyes on untreated sample with chitosan and $M_{abs(untreated)}$ is the content of acid dyes on treated sample with chitosan.

Based on the obtained results, it is demonstrated that the content of acid dyes on treated fabrics with DMDHEU is much higher than that with CA after all washing cycles. This may be because DMDHEU possesses hydroxyl groups and azo groups which promote more metal complex formation with acid dyes, while CA possesses hydroxyl groups only. Consequently, the content of acid dyes on all treated samples with CA was much lower than that with DMDHEU after several washing cycles.

To evaluate the chemical retention of antibacterial treated cotton fabrics with CTS1 in the presence of CA and DMDHEU through the amount of acid dyes bonded to amine groups, the reduction in the content of acid dyes was investigated after 5, 10, 15 and 20 washing cycles, as reported in Table 3. The results indicated that the content of acid dyes on samples crosslinked with DMDHEU seemed to be reduced more rapidly than those crosslinked with CA after the first washing cycles, but these reductions became similar after 20 washing cycles.

In summary, the nitrogen content of antibacterial cotton fabrics treated with chitosan can be quantitatively determined based on the amount of acid dyes using the calibration curve of absorbance versus dye concentration, as represented in Equation (1).

Table 3. The content of acid dyes in antibacterial treated cotton fabrics with CTS1 crosslinked with CA and DMDHEU after 0, 5, 10, 15 and 20 washing cycles (denoted as CTS1-CA00, CTS1-CA05, CTS1-CA10, CTS1-CA15, CTS1-CA20, CTS1- DMDHEU00, CTS1-DMDHEU05, CTS1- DMDHEU10, CTS1- DMDHEU15, and CTS1-DMDHEU20, respectively) (M_{pre} is 10mg).

Sample	Washing cycle	M_{post} [mg]	M_{wash} [mg]	M_{amine} [mg]	Reduction [%]
CTS1-CA00	0	4.4606	3.2478	2.2920	-
CTS1-CA05	5	4.7668	2.9698	2.2600	1.4
CTS1-CA10	10	4.1051	3.7886	2.1063	8.1
CTS1-CA15	15	4.1973	3.8178	1.9840	13.44
CTS1-CA20	20	4.3797	3.8870	1.7330	24.39
CTS1-DMDHEU00	0	3.9822	3.2771	2.7410	-
CTS1-DMDHEU05	5	4.1885	3.3502	2.4610	6.8
CTS1-DMDHUE10	10	4.2178	3.3502	2.4320	14.4
CTS1-DMDHEU15	15	3.9808	3.6574	2.3600	18.33
CTS1-DMDHEU20	20	4.3377	3.4965	2.1660	24.14

Table 4. Nitrogen content of antibacterial treated cotton samples with CTS1-CA and CTS2-CA after 0, 5, 10, 15 and 20 washing cycles.

Washing cycles	Nitrogen content [%]			
	CTS1-CA		CTS2-CA	
	Content [%]	Reduction [%]	Content [%]	Reduction [%]
0	0.1458	-	0.1770	-
5	0.1393	4.40	0.1500	15.25
10	0.1394	4.38	0.1319	25.48
15	0.1238	15.01	0.1315	25.70
20	0.1052	27.85	0.1364	22.90

Evaluation on total nitrogen content of treated fabrics using elemental analysis method

The Dumas method, also known as combustion method, is an elemental analysis technique used to quantitively determine total nitrogen content in chemical substances, particularly for assessing crude protein concentration in food specimens). In this method, a specimen of known weight is combusted at extremely high temperature in the presence of oxygen, releasing carbon dioxide (CO_2), water (H_2O) and nitrogen (N_2). A special column containing potassium hydroxide (KOH) absorbs all molecules of CO_2 and H_2O, allowing nitrogen content to be measured. The determination results of nitrogen content using elemental analysis are presented in Table 4.

In an initial investigation, an insignificant nitrogen content about 0.0083 % was detected in untreated samples with chitosan due to the minimal nitrogen presence in cotton cultivation. Conversely, all treated samples with CTS1 and CTS2 had significantly higher nitrogen content than untreated samples, by at least 12.67 times. Table 4 presents the nitrogen content of antibacterial treated cotton fabrics obtained from two different types of molecular weight (i.e., 2.6 kDa and 187 kDa) and after 5, 10, 15 and 20 washing cycles. In general, the nitrogen content of samples treated with both CT1-CA and CTS2-CA significantly decreased with washing cycles. Notably, the elemental analysis method concluded that the nitrogen content in samples treated with CTS2 decreased more rapidly with washing cycles compared to those treated with CTS1. For examples, after 5 washing cycles, the nitrogen content dropped to 15.25 % and 4.4 % for treated sample with CTS2 and CTS1, respectively.

Evaluation of nitrogen content on treated fabrics based on antibacterial ability

Since antibacterial agent is not easy to diffuse into an aqueous solution, it may cause suspension issues. Accordingly, the antibacterial activity of treated cotton fabrics with chitosan should be examined under dynamic contact conditions. These tests were conducted with a predominant gram-negative bacterium, Escherichia coli, following the E2149–01

standard method. The antibacterial ability of immobilized agents on antimicrobial treated cotton fabrics was quantitatively determined through bacterial reduction after 60 and 2 contact minutes. The percent reduction of bacteria in the solution after contacting treated samples, compared to the initial solution without a sample (R_o) and with an untreated control sample (R_c), is calculated using the following equations.

$$R_o \, [\%] = 100 \frac{N_o - N_n}{N_o} \qquad (4)$$

$$R_c \, [\%] = 100 \frac{N_c - N_n}{N_c} \qquad (5)$$

where N_o is the number of colonies in the initial bacterial solution [CFU/ml], and N_c and N_n are the numbers of colonies in the bacterial solution (CFU/ml) after incubating the untreated sample and treated sample with chitosan for a given time under standard conditions.

The evaluation results of antibacterial activity on treated cotton fabrics with CTS1 or CTS2, which were crosslinked with CA or DMDHEU under various washing conditions, are reported in Table 5 and Figure 8. It can be concluded that the antibacterial activity of all treated samples with chitosan decreased with washing cycles. It rapidly reduced from 0 to 5 washing cycles and gradually reduced from 5 to 20 washing cycles. At the same washing cycle, the antibacterial activity of treated samples crosslinked with DMDHEU was always lower than that crosslinked wth CA. Furthermore, the antibacterial fastness of samples treated with DMDHEU was also much better than those treated with CA. For instance, after 15 washes, the bacterial reduction on antibacterial treated sample with CTS1 and CA in 60 minutes of exposure was 59%, while it was 38% for those treated with CTS1 and DMDHEU. Similarly, the reduction was 67.4% for sample treated with CTS2 and CA, while it was 49.2% for those treated with CTS2 and DMDHEU. The investigation results also suggested that using chitosan with a higher molecular weight on cotton fabrics ensures better antibacterial ability and maintains its antibacterial durability through washing conditions. These results are consistent with the evaluations and explanations in previous sections (i.e., results of image analysis, dyeability, elemental analysis).

Table 5. Bacterial reduction (R_c) of cotton fabrics treated with CTS1/CTS2 and CA/DMDHEU after 0, 5, 10, 15 and 20 washing cycles.

Sample	Washing cycles	R_c [%]	
		2 min	60 min
CTS1-CA00	0	56.0	100.0
CTS1-CA05	5	16.7	69.7
CTS1-CA10	10	13.6	62.0
CTS1-CA15	15	9.0	59.0
CTS1-CA20	20	6.0	57.6
CTS1-DMDHEU00	0	48.0	80.0
CTS1-DMDHEU05	5	16.6	53.7
CTS1-DMDHEU10	10	11.1	48.1
CTS1-DMDHEU15	15	7.4	38.0
CTS1-DMDHEU20	20	3.7	35.0
CTS2-CA00	0	60.0	100.0
CTS2-CA05	5	47.8	74.0
CTS2-CA10	10	39.0	71.7
CTS2-CA15	15	30.4	67.4
CTS2-CA20	20	30.4	63.0
CTS2-DMDHEU00	0	48.0	84.0
CTS2-DMDHEU05	5	16.6	60.0
CTS2-DMDHEU10	10	11.1	56.9
CTS2-DMDHEU15	15	7.4	49.2
CTS2-DMDHEU20	20	3.7	40.0

(a)

(b)

(c)

(d)
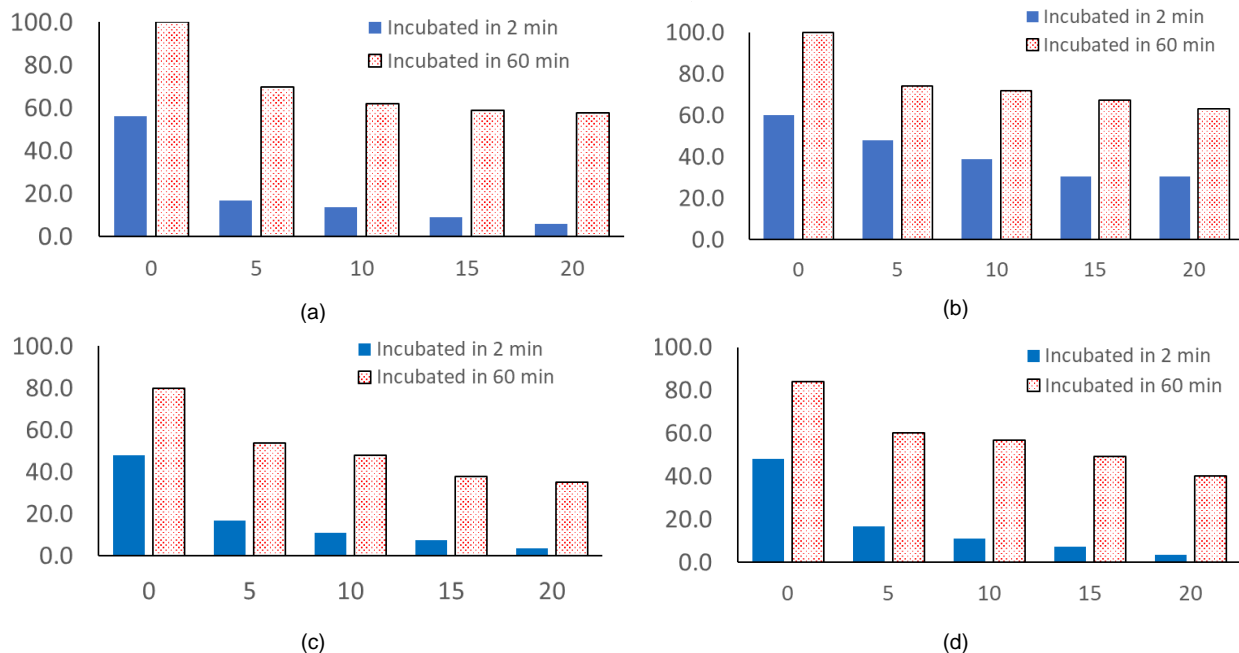
Figure 8. Bacterial reduction *Re* [%] of treated cotton fabrics with (a) CTS1 and CA, (b) CTS2 and CA, (c) CTS1 and DMDHEU and (d) CTS2 and DMDHEU after 0, 5, 10, 15 and 20 washing cycles.

CONCLUSIONS

This work used four different methods including electron microscopy, additional dyeability, elemental analysis through combustion test and antibacterial experiments under dynamic contact conditions to determine N content, thereby evaluating antibacterial activity of treated fabrics with chitosan. Besides, two types of chitosan (CTS1 and CTS2) and two types of crosslinkers (CA and DMDHEU) were applied to clarify bonding mechanism and effectiveness of antibacterial treated fabrics. Actually, the relationship between antibacterial ability and molecular weight of chitosan as well as washing durability is still being debated because it is a naturally occurring polymer with a wide range of degrees of acetylation, making it

difficult to determine its effects. The authors attempted to conduct this work to demonstrate that the nitrogen content in chitosan with low/high molecular weight and crosslinkers could be determined in four different ways, so that the antibacterial ability of treated fabrics could be evaluated both directly and indirectly.

REFERENCES

1. Lim S.-H.: Synthesis of a fiber-reactive chitosan derivative and its application to cotton fabric as an antimicrobial finish and a dyeing-improving agent. North Carolina State University, 2003.
2. Lim S.-H., Hudson S.M.: Synthesis and antimicrobial activity of a water-soluble chitosan derivative with a fiber-reactive group. Carbohydrate research, 339(2), 2004, pp. 313-319. https://doi.org/10.1016/j.carres.2003.10.024
3. Kim Y.H., Choi H.-M., Yoon J.H.: Synthesis of a quaternary ammonium derivative of chitosan and its application to a cotton antimicrobial finish. Textile Research Journal, 68(6), 1998, pp. 428-434. https://doi.org/10.1177/004051759806800607
4. Enescu D.: Use of chitosan in surface modification of textile materials. Roumanian Biotechnological Letters, 13(6), 2008, pp. 4037-4048.
5. El-Tahlawy K.F., et al.: The antimicrobial activity of cotton fabrics treated with different crosslinking agents and chitosan. Carbohydrate polymers, 60(4), 2005, pp. 421-430. https://doi.org/10.1016/j.carbpol.2005.02.019
6. Sajomsang W.: Synthetic methods and applications of chitosan containing pyridylmethyl moiety and its quaternized derivatives: A review. Carbohydrate Polymers, 80(3), 2010, pp. 631-647. https://doi.org/10.1016/j.carbpol.2009.12.037
7. Fouda M.M.G.: Use of natural polysaccharides in medical textile applications. Disertasi. Fachbereich Chemie Universitas Duisburg-Essen, Germany, 2005.
8. Hon D.N.-S.: Chitin and chitosan: Medical applications, in Polysaccharides in medicinal applications, Routledge, 2017, pp. 631-649.
9. Lou C.-W., et al.: Preparation of polyethylene oxide/chitosan fiber membranes by electrospinning and the evaluation of biocompatibility. Textile Research Journal, 78(3), 2008. pp. 254-257. https://doi.org/10.1177/0040517507089752
10. Domard A., Rinaudo M.: Preparation and characterization of fully deacetylated chitosan. International Journal of Biological Macromolecules, 5(1), 1983, pp. 49-52. https://doi.org/10.3390/md15050141
11. Kumar M.N.R.: A review of chitin and chitosan applications. Reactive and functional polymers, 46(1), 2000, pp. 1-27. https://doi.org/10.1016/S1381-5148(00)00038-9
12. Hwang J., et al.: Bactericidal activity of chitosan on E. coli. Advances in chitin science, 3, 1998, pp. 340-344.
13. Sudarshan N., Hoover D., Knorr D.: Antibacterial action of chitosan. Food biotechnology, 6(3), 1992, pp. 257-272.
14. Fang S.W., Li C.F., Shih D.Y.: Antifungal activity of chitosan and its preservative effect on low-sugar candied kumquat. Journal of food protection, 57(2), 1994, pp. 136-140. https://doi.org/10.4315/0362-028X-57.2.136
15. Aiba S.-i.: Preparation of N-acetylchitooligosaccharides by hydrolysis of chitosan with chitinase followed by N-acetylation. Carbohydrate research, 265(2), 1994, pp. 323-328. https://doi.org/10.1016/0008-6215(94)00243-6
16. Shin Y., Yoo D., Jang J.: Molecular weight effect on antimicrobial activity of chitosan treated cotton fabrics. Journal of Applied Polymer Science, 80(13), 2001, pp. 2495-2501. https://doi.org/10.1002/app.1357
17. Strnad S., et al.: Influence of chemical modification on sorption and mechanical properties of cotton fibers treated with chitosan. Textile Research Journal, 78(5), 2008, pp. 390-398. https://doi.org/10.1177/0040517507085395
18. Zhang Z., et al.: Antibacterial properties of cotton fabrics treated with chitosan. Textile research journal, 73(12), 2003, pp. 1103-1106. https://doi.org/10.1177/004051750307301213
19. Elsabee M.Z., et al.: Surface modification of polypropylene films by chitosan and chitosan/pectin multilayer. Carbohydrate polymers, 71(2), 2008, pp. 187-195. https://doi.org/10.1016/j.carbpol.2007.05.022
20. Hashem M., Refaie R., Hebeish A.: Crosslinking of partially carboxymethylated cotton fabric via cationization. Journal of Cleaner Production, 13(9), 2005, pp. 947-954. https://doi.org/10.1016/j.jclepro.2004.05.002
21. Fei Liu X., et al.: Antibacterial action of chitosan and carboxymethylated chitosan. Journal of applied polymer science, 79(7), 2001, pp. 1324-1335. https://doi.org/10.1002/1097-4628(20010214)79:7
22. Huang K.-S., et al.: Application of low-molecular-weight chitosan in durable press finishing. Carbohydrate Polymers, 73(2), 2008, pp. 254-260. https://doi.org/10.1016/j.carbpol.2007.11.023
23. Öktem T.: Surface treatment of cotton fabrics with chitosan. Coloration Technology, 119(4), 2003, pp. 241-246. https://doi.org/10.1111/j.1478-4408.2003.tb00179.x
24. Xu D., et al.: Modified chitosan hydrogels for the removal of acid dyes at high pH: modification and regeneration. Industrial & engineering chemistry research, 50(10), 2011, pp. 6343-6346. https://doi.org/10.1021/ie101987w
25. Gupta D., Haile A.: Multifunctional properties of cotton fabric treated with chitosan and carboxymethyl chitosan. Carbohydrate Polymers, 69(1), 2007, pp. 164-171. https://doi.org/10.1016/j.carbpol.2006.09.023
26. Fouda M.M., et al.: Use of chitosan/polyamine biopolymers based cotton as a model system to prepare antimicrobial wound dressing. International Journal of Diabetes Mellitus, 1(1), 2009, pp. 61-64. https://doi.org/10.1016/j.ijdm.2009.05.005
27. Terbojevich M., Cosani A.: Molecular weight determination of chitin and chitosan. Chitin handbook: 1997, pp. 87-101.
28. Jiang S., et al.: Structure and properties of citric acid cross-linked chitosan/poly (vinyl alcohol) composite films for food packaging applications. Carbohydrate Polymers, 312, 2023, 120842 p.
29. Fu X., et al.: Chitosan derivatives with dual-antibacterial functional groups for antimicrobial finishing of cotton fabrics. Carbohydrate Polymers, 85(1), 2011, pp. 221-227. https://doi.org/10.1016/j.carbpol.2011.02.019

THE EFFECT OF ELECTRIC PULSE TREATMENT ON THE PROPERTIES OF HEMP FIBRE

RASTORHUIEVA, MARIIA[1]; YEVTUSHENKO, VALENTYNA[1]; SHVETS, GALINA[2]; ANDRONOV, VLADIMIR[3]; DANCHENKO, YULIYA[3] AND OLIJNYK, HALINA[2*]

[1] Kherson National Technical University, Instytutska str.11, Khmelnytskyi, 29016, Ukraine
[2] Khmelnytskyi National University, Instytutska str.11, Khmelnytskyi, 29016, Ukraine
[3] National Academy of the National Guard of Ukraine, 3 Zakhysnykiv Ukrainy sq., Kharkiv, 61001, Ukraine

ABSTRACT

The production of competitive textile products can be ensured by using natural, environmentally friendly fibres, which include hemp fibre, as raw materials. To expand the possibility of its use, an essential operation is the pre-treatment of the fibre. The use of electric pulse processing of hemp fibre will provide the ability to control the depth of cottonization, select optimal parameters that collectively evaluate the spinning ability of the fibre and correspond to the permissible similar indicators of cotton fibre. The purpose of the work done is to study the mechanism of electric pulse processing of hemp fibre by identifying its structural characteristics under various processing modes for further use. The work carried out studies of the process of cottonization of hemp fibre by a physical-mechanical method using an electric pulse discharge from 500 to 2500 cycles. An effective mode of electric pulse processing of fibres has been established, amounting to 2500 pulses of electric discharges, which makes it possible to obtain cottonized hemp fibre with the required spinning ability. The parameters of cottonized hemp fibre have been determined, allowing the use of hemp cottonin to produce mixed yarn using a card spinning system on cotton spinning equipment.

KEYWORDS

Electric pulse treatment; Hemp fibre; Microscopic sections; Cottonization; Morphological structure; Yarn.

INTRODUCTION

The production of competitive textile products can be achieved by using various threads and yarn made from natural, environmentally friendly fibres as raw materials for input.

Today, textile materials are subject to requirements for the efficient and rational use of the potential resource of their fibrous base, ensuring the necessary durability of finished products, their level of environmental safety, and, in general, their level of competitiveness in the market [1, 2].

An alternative to cotton can be bast fibres (flax and hemp). Textiles from bast fibres have higher medical, biological and protective properties than cotton. The environmental properties of hemp fibre and their positive impact on human health in terms of everyday clothing use and ecological impact, consistent with the European Green Deal Strategy, are presented in [3]. The authors of [4] provide recommendations for the use of hemp fibre for the production of environmentally friendly building materials, cosmetics and medicines, as this is supported by environmental legislation, due to which there is a growth in the market for biodegradable and recyclable materials. Thanks to such a unique set of properties of bast fibres, such as hygiene, high strength, low electrical resistance, comfort, and natural bactericidal properties, the demand for textile products made from bast fibres, not only for technical but also for household purposes, is growing all over the world.

Thanks to natural antiseptic properties, items made from hemp fibre are hypoallergenic. In addition, hemp fibres have high hygroscopic and thermophysical characteristics. These materials are a priority for clothing manufacturers since modern consumers prefer high-quality and comfortable products. Apparel and textile research focuses on intelligent production. Modern, environmentally friendly textile materials can enhance selected design solutions that meet high aesthetic properties and requirements. Therefore, when creating clothing, it is necessary to use new scientific achievements when choosing methods for processing raw textile materials [5-10], methods for the calculation of different garment types patterns [11, 12], using digital tools for calculating indicators of

material properties [13], and the sewing techniques of garment manufacturing [14].

The problems of processing industrial hemp into spinning fibre have been raised by researchers who have used mechanical cottonization methods and ultrasonic cavitation to increase the degree of decomposition of complex hemp fibres. The hydroacoustic effect was used, but it was limited due to the complexity of the technological process [5]. The method of mechanical cottonization, which consists of processing the core (stem) material of bast fibre by using structural developments of node connections of devices for processing bast fibre raw materials, has been considered by scientists [6].

Research of the method of mechanical cottonization of bast fibres, namely the process of stomping best raw materials, along with which the separation of woody parts, removal of scales, and separation of fibres from the woody part and non-fibrous impurities takes place; proposed new methods of stem destruction, promoting stem disintegration and increasing fibre separation, were considered by scientists in the article [7]. Researchers [8] considered the use of ultrasonic cavitation and chemical-mechanical cottonization to improve the water absorption (moisture properties) and mechanical (tensile and elongation strength, increased linen, colour fastness) properties of hemp fibres that were pre-treated with the enzyme laccase.

The study was carried out on the diameter of the stem of industrial hemp, on which the yield of bast depends, and the results of mathematical planning of the experiment were proposed, which made it possible to obtain optimal regimes for processing the stems with 5-6% cleaning of the bast from the fire [9]. The method of biochemical cottonization, which consists of the pre-treatment of hemp seeds with a biological method to retain moisture and chemical processes to increase resistance to diseases, is dedicated to the work of researchers [10]. These seed treatments have improved the survival rate of hemp seeds in terms of disease incidence.

Research [15] reviews the structure and properties of hemp and possible directions for further technological development. Particularly noteworthy is the use of hemp components in industrial products. Attention is drawn to potential areas of research on the use of cannabis in the medical industry. The study [16] proposed using hemp fibres modified with graphite oxide as an environmentally friendly and effective solution for water purification.

The aim of the [17] was to discuss the issues of processing industrial hemp into goods for various functional purposes. The presented research is relevant for creating its raw material base for pulp and paper enterprises and light industry enterprises. The goal [18] is to produce cottonized hemp fibres with improved thermal stability. It was first found that the fine hemp fibres produced from technical non-retted

hemp fibres by steam explosion exhibited enhanced thermal stability. Tests of yarn obtained by mixing cotton with 50% hemp fibre content were carried out [19]. Hemp fibres are also suitable for vortex spinning, and Air vortex yarn, made from a blend of hemp and Tencel fibres, has less hairiness and roughness than ring-spun and dry-spun yarns. Fabric from this type of blended yarn significantly improves elasticity and shape development [20]. Hemp bast fibres were degummed using combined microwave energy (MWE) and deep eutectic solvent (DES) to generate pure hemp cellulose fibres for potential textile applications. The treated fibres had much enhanced thermal stability due to removing the gummy materials [21].

Of interest are studies related to the use of electric pulse processing. Researchers [22] proposed processing seed pulp to increase the efficiency of obtaining cottonseed oil from industrial hemp seeds using an electric pulse processing method. Thanks to electric pulse processing, it is possible to increase the amount of oil extracted from seeds and reduce the cost of electricity, which is successfully sold in the food industry.

Investigation [23] presents studies on using electric pulse processing in metallurgy for plastic moulding of metals; attention is paid to forming blanks for stainless steel packages.

However, there is currently a lack of research on electrical pulsing in the textile field, specifically pulsing hemp fibre to improve its spinnability.

The research aim is to study the mechanism of electric pulse processing of hemp fibre by identifying its structural characteristics under various processing modes for further use.

Today, issues related to the production of mixed yarn are of great importance in the textile industry. This is explained by the fact that mixtures of fibres, different in properties, design and structure, make it possible to satisfy the conflicting market requirements for textile products. However, the technological process for obtaining yarn, the quality and the cost of the products largely depend on the composition of the selected mixture. Therefore, the choice of the technological chain and optimization of the parameters of the yarn production process parameters must be carried out in each case for each type.

The fact that the specific weight of the cost of raw materials in the cost price of the finished yarn is 70–80% further emphasises the need to optimise the technology of fibre mixing processes to include in the composition of the mixture relatively cheap fibres of domestic origin - flax and hemp. One way to increase hemp's spinning ability is the technological process of cottonization of hemp fibres, which is an integral part of preparing hemp fibres for spinning. Cottonization is used to intensify the process of fibre separation and shortening and remove contaminants. Thanks to this,

hemp fibres become suitable for mixtures with other fibres in cotton spinning equipment. However, pre-processing is necessary to obtain hemp fibre suitable for use in finished products in a mix with other fibres. One of the methods of such processing may be the physical and mechanical cottonization of hemp fibres using an electric pulse method, after which the fibre becomes suitable for spinning; the process of grinding and shortening the fibres and removing debris is intensified. This process makes hemp fibre ideal for use in multi-component mixtures.

The current method of electric pulse processing of hemp fibre is that the electrical discharge in water, which causes energy conversion, leads to destruction processes and the destruction of the physical and mechanical forces of the fibrous materials. The result will be an increase in product duration and supply. Under the influence of underwater electrical discharges, chemical-mechanical processes lead to chemical reactions to remove lignin and pectin and mechanical damage to the fibre surface, that is, the splitting of bundles into individual elementary fibres. An important task is to select the conditions for grinding hemp fibre and the optimal mode for obtaining high-quality cottonized hemp fibre that can be used in spinning.

MATERIALS AND METHODS

Microscopic and instrumental methods were used to study the structure of hemp fibre after electric pulse treatment.

The essence of the microscopic examination method was to determine the percentage of groups of fibres containing different numbers of cottonized fibres (from 1 to 9) and varying depending on the mode of electric pulse treatment from 500 to 2500 cycles.

An orthoscopic eyepiece was used to determine the number of elementary fibres in groups, and a photographic glass was used to project an image of a cross-section of fibres onto photographic film. The studies were carried out using a biological microscope MBR-1, designed for studying transparent objects in penetrating light. Microscopic studies of cross sections of hemp fibres were conducted at a general microscope magnification of U_0=160 and a microscope field of view diameter of D_0=1mm.

The preparation of cross-sections of fibres was placed on the microscope stage and moved to find the necessary area for the examined object. Under a microscope, the number of elementary fibres in bundles of about 100 square meters was visually inspected. Ten microscopic sections of fibres were monitored and separated under different electric pulse processing modes, ensuring 95% reliability of the traceability used in the textile industry.

Light microscopy of fibre cross-sections was used to assess the effectiveness of the hemp fibre cottonization process. In this method, a thin bundle of test fibres, lightly twisted by hand, is pulled in a loop through a small circular hole in a thin metal plate. As a result, the fibre bundle is clamped in a perpendicular hole in the plate. The ends of the protruding bundle of fibres are cut off with a razor on both sides at the level of the plate. The plate is placed under a microscope to view the cross-section in reflected light.

Instrumental studies were carried out on an experimental installation for electric pulse processing, the central part of which is a discharge chamber with an electronic system in which a powerful discharge and the destruction and removal of encrusting substances from the fibre are carried out [24].

Non-flowing process water without heating and chemicals was used as a working medium during the experiment. The processing of hemp fibre was based on the principle of a powerful electrical discharge in the liquid into which the hemp fibre being processed was immersed.

The discharge technological unit, containing working electrode systems, is designed to convert electrical energy into other types of energy and transfer it to the processing object. The pulse current generator (power source) converts electrical energy to form a powerful discharge of the liquid in which the fibre is immersed. In this case, the discharge circuit connects the technological unit with the power source. The block of primary devices moves the organs performing processing and the working environment, and the block of auxiliary devices loads and unloads hemp fibres and removes processing waste.

The integrated control unit coordinates the operation of the pulse current generator and the technological process of cottonization in a given sequence. The auxiliary systems block is designed to transport and regenerate the working fluid and perform control functions.

The main technological unit that forms the basis of the equipment for electric pulse processing of hemp fibre is a discharge chamber with an electrode system - a metal cube measuring 350x350x350 mm^3 with an observation window. The chamber volume is 42.875 l. Following the requirements of resource-saving technology, tap water with a resistivity of 8-10 Ohm·m, surface tension - 72.75 erg/cm^2 (at 20°C) is used as the working medium – 30 l of water was used for the study.

Hemp fibre processing was based on the principle of a powerful electrical discharge in water. As a result of this treatment, complex fibres are split into elementary ones while maintaining the integrity of the cellulose component of the fibres. A high-voltage electric discharge in water is accompanied by some physicochemical phenomena, one of which is electric discharge cavitation. Water is simultaneously a medium for generating and reproducing electrical discharges, transporting the energy of electrical discharges to the processing object, and placing

various processing objects in it. At the same time, it not only surrounds the processing object - the fibre but also penetrates inside, ensuring movement inside the fibre. This flow brings new germs of cavitation (cavitation inside the fibres that does the work of splitting the fibre, destroying lignin, pectins and other non-cellulosic substances).

The electric pulse installation [24] operates as follows. The processed batch of fibre weighing 5 kg is loaded into the technological discharge unit and placed in the observation area through the viewing window. Electric discharges from the control panel unit launch a pulse current generator for fibre processing.

During the experiments, the electrical parameters of the discharge circuit of the installation can vary in the range: voltage U_0 of charging the capacitor bank from 14 to 50 kV; capacitance from 0.5 to 3 μF; pulse frequency v from 0.5 to 5 Hz; The radius of curvature of the tip of the positive electrode is from 5 to 6 mm. The inductance of the discharge circuit L is 3.4 μH. The reserve energy of the discharge circuit W_0 varies from 100 to 2000 J. The length of the interelectrode gap is 10 to 35 mm (considering the specific resistance of the working medium – 8...15 W·m, necessary for processing hemp fibre).

The pulse voltage is changed within a given range using a block of auxiliary devices. Removing encrusting substances from hemp fibre is controlled through a viewing window using a translucent lamp. After eliminating encrusting substances is completed, the auxiliary systems unit replaces the working fluid to remove processed waste from the fibre's surface.

After the electric pulse processing of hemp fibres is completed, the primary device unit unloads the discharge technological unit, from which the processed batch of fibre is extracted.

As a result of this treatment, complex fibres are split into elementary ones while maintaining the integrity of the cellulose component of the fibres. For cottonization, a batch of hemp fibre was used after primary processing in the conditions of the scientific and experimental laboratory of the Department of Commodity Research, Standardization and Certification of the Kherson National Technical University. The amount of fibre to be processed was 50 kg.

To destroy and remove encrusting substances and subsequent separation of technical fibres into elementary ones, the original fibres were subjected to electric pulse processing in an aqueous environment with 500, 1000, 1500, 2000, and 2500 electric discharge pulses.

$$t = \frac{n}{60\,f} \qquad (1)$$

where: t – action time, min.; n – number of pulses; f – pulse frequency [Hz].

Therefore, the fibre processing times in the chamber were 5, 8, 11, 13, and 16 min.

The technological mode of electric pulse processing of hemp fibre, selected following the theoretical and experimental studies of the electric pulse influence on fibrous structures, is presented in Table 1.

During the electric pulse processing of hemp fibre, the capacitor's capacitance, the pulses' frequency, and the length between the electrode (discharge) gaps remained unchanged.

Fibre length was determined by measuring the straightened length of individual fibres according to the standard [25] using the measuring scale on the test board. The fibre was extended to full extension without stretching the fibre along the measuring scale. The fibre length was red to the nearest 1.0 mm (0.02 in.)

The load [cN] of cottonin was determined using the method for cotton fibre, that is, the breaking of fibre bundles on tensile testing machine DSH-3M according to the standard [26].

RESULTS AND DISCUSSION

As a result of research, we found that electric pulse treatment is an effective and environmentally friendly method of cotonization. Indeed, when using this method of processing industrial hemp, the process of obtaining hemp cottonin is accompanied by 7-8 kilowatt-hours of electricity per 1 kg of fibres. This increased energy allows us to bring this method to an energy-saving.

Electropulse processing of hemp fibre occurs due to a pulsed electrical discharge in a liquid, a process with a high concentration of energy. The most commonly used operating voltage range is from 10 kV to 70 kV.

Variating the physical parameters of the colonization process, modes, and type of emitters can achieve complete or partial removal of encrusting substances. However, to prevent cellulose destruction, it is necessary to additionally control the duration and intensity of exposure to physical processes on the fibre.
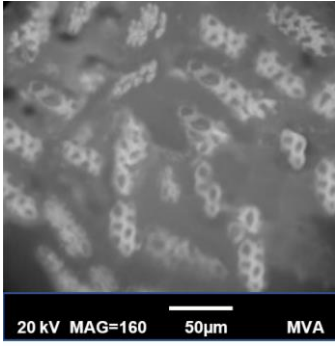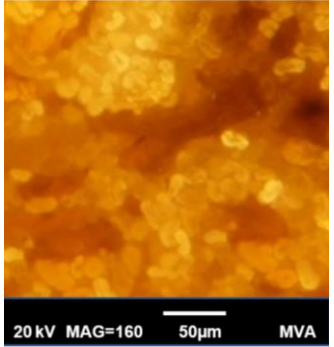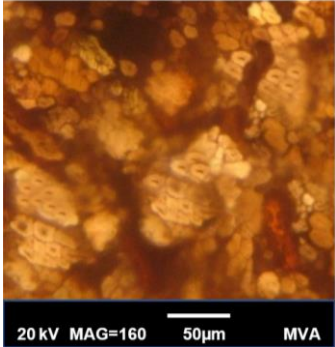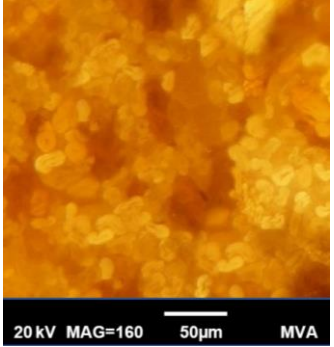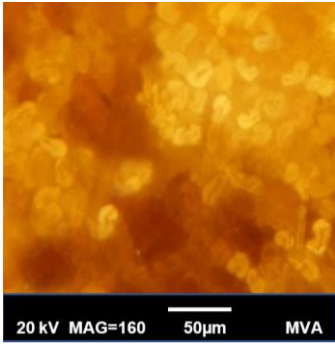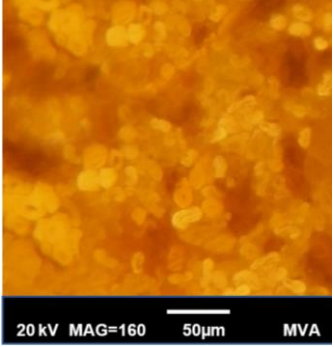
The physical model of an electrical discharge in a liquid and the mechanism of destruction of lignified plant cell walls is as follows. A voltage exceeding the breakdown voltage of this medium and applied to pairs of electrodes immersed in a weak electrolyte causes a powerful electrical discharge. The resulting energy heats the liquid substance to a temperature of 103 K, and the pressure rises to 102 mPa. That is, high plasma pressure is transferred to the water-fibre medium, under the influence of which it is compressed.

In this case, a complex stress state arises in the fibrous material, which can cause various types of destruction, crushing, etc. As a result, the fibre is freed from accompanying substances.

Table 1. The technological regime of electric pulse processing of hemp fibre.

Voltage, U [kV]	The capacitance of capacitor, C [μF]	Pulse frequency, f [Hz]	Number of pulses, n	Discharge gap length, l [mm]	Working environment temperature, t [°C]
34 – 38	0.5	3	500 – 2500	20	30 – 40

Table 2. General view of microscopic sections of hemp fibre depending on the number of electrical discharge pulses.

Fibre sample	Number of electrical discharge pulses	Photographs of microscopic sections	Fibre sample	Number of electrical discharge pulses	Photographs of microscopic sections
Reference sample	0		Sample 3	1500	
Sample 1	500		Sample 4	2000	
Sample 2	1000		Sample 5	2500	

For the study, several fibres were taken from 30 locations to form 6 groups of helm fibres (6 samples).

Six samples of hemp fibre were studied for the structure of hemp cotton, which were exposed to different numbers of electric discharge pulses. Microscopic sections of hemp fibre were assessed before and after treatment with electric pulse discharge, and changes in its morphological structure were recorded using a microscope. Photographs of microscopic sections are presented in Table 2.

Photos of microscopic sections of hemp fibre are presented in Table 2, which testify to changes in the structure of fibres, which led to the splitting of complex fibres into elementary ones and the formation of complexes from them due to electropulse treatment. After processing, elementary fibres were combined into complexes with different numbers of elementary fibres in them. The number of elementary fibres in the complexes was counted under a microscope. The complexes identified in the studied samples consisted of 1 elementary fiber or contained 2, 3, 4, 5, 6, 7, 8, or 9 elementary fibers. It should be noted that the number of complexes with a certain number of fibres (for example, 9 elementary fibres in

a complex) varied depending on the number of processing pulses of samples.

It should be noted that even when industrial hemp fibre is treated in an aqueous medium with 500 pulses of electric discharge (sample 1), a change in the fibre structure and formation of complexes of elementary fibre is observed. Thus, in sample 1: complexes containing 1 elementary fibre make up 15% of the total number of complexes identified in this sample; complexes containing 2 elementary fibres - 18%; complexes with 3 elementary fibres - 20%, etc.

Images of a section of technical hemp fibre to be processed in an aqueous environment with 1000 pulses of electric discharge (sample 2) show significant changes in the fibre structure and a decrease in the number of complexes with the number of elementary fibres of 7, 8, and 9 fibres. At the same time, a more significant number of complexes with a small number of elementary fibres (1, 2, 3 or 4 fibres in each complex) is observed.

Photos of sections of industrial hemp fibres treated in an aqueous environment with electric discharge pulses of 1500, 2000 and 2500 (samples No. 3-5) show an increase in the number of small complexes, including 1-4 elementary fibres.

A visual examination of microscopic sections of hemp fibres obtained after electric pulse treatment at varying degrees of intensity confirmed the hypothesis that such treatment changed the structure of the fibres and increased the number of elementary fibres.

Based on the experimental data obtained, graphs of the distribution of fibres in complexes were constructed after treating hemp fibres with an electric pulse discharge. The graph (Fig. 1) shows the share (%) of complexes with a certain number of elementary fibres in the total number of isolated fibre complexes in a particular sample after processing. The reference sample was not processed.

When processing fibres with an intensity of 500 pulses of electric discharge, sample 1 contains the entire range of fibre complexes. In this case, the share of fibre complexes containing 4 elementary fibres is the most significant (22%).

The next mode of processing hemp on an electric pulse installation was 1000 pulses of electric discharge - sample 2. Based on the diagram analysis (Fig. 1), it was found that with a processing intensity of 1000 cycles, the number of complexes, which contain from 4 to 7 elementary fibres noticeably decreases. At the same time, complexes containing 8 and 9 fibres disappeared because they were split into smaller ones. As a result of processing, the most significant number of complexes includes 2 and 3 elementary fibres, which is 26%.

At a processing intensity of 1500 cycles of electrical discharges (sample 3), the number of groups containing 2 fibres increased to 40%.

In a processing mode with an intensity of 2000 pulses of electric discharge (sample 4), complexes, which contain 1 to 5 elementary fibres, are observed in microscopic sections. The most significant share comprises complexes containing 2 elementary fibres (42%).

It has been established that the most effective mode of electrical pulse processing of fibre is 2500 pulses of electric discharge, which allows one to obtain cottonized hemp fibre with the most significant change in structure. This change is caused by splitting complex technical fibres into elementary fibres. In these samples, 32% are complexes containing 1, 2 and 3 elementary fibres, which creates the prerequisites for obtaining a thin and uniform yarn structure.

However, based only on microscopic sections about the change in the fibre structure caused by splitting complex fibres into elementary ones, one cannot judge the possibility of using them in mixtures with other fibres for further processing into yarn. The criterion for the suitability of fibres for further technological processing on spinning equipment is the study of the physical and mechanical parameters of hemp cottonin obtained at 2500 pulses of electric discharge, which allows one to evaluate the spinning ability of the fibre.

The length of cottonin fibres (short and long) was assessed by measuring single fibres according to the method [25], after which the share of fibres of a certain length in the total number of fibres in the experimental group was determined. Using the same method, the length of cotton fibre was determined, a group of which was also subjected to electric pulse treatment of 2500 pulses of electric discharge. A comparison of the properties of cottonin and cotton was carried out to confirm the possibility of using cottonin fibres in spinning production instead of cotton.

According to the study results, hemp cottonin obtained with 2500 processing cycles (Fig. 2) has a staple length of 37.9 mm, corresponding to the cotton fibre length. At the same time, the percentage of short fibres and fluff is 17.2%, staple fibres are 75.8%, and a length of more than 45 mm is about 7% (Fig. 3), corresponding to the standardised indicators.

Analysis of the hemp fibre diameter distribution diagram showed that the largest number of fibres (Fig. 4) have diameters from 10 to 27 μm. In this case, the average diameter is 15.46 μm, corresponding to the thickness of medium-fibre cotton used in the carded spinning system, equal to 0.28 tex.

The diagram of the distribution of fibres by strength (Fig. 5) shows that the maximum strength of cottonin (30.8 cN/tex) is 4.4 cN/tex higher than the maximum value of cotton fibres (26.4 cN/tex).

The diagram of the strength distribution of hemp cottonin (Fig. 5) shows that the average strength of
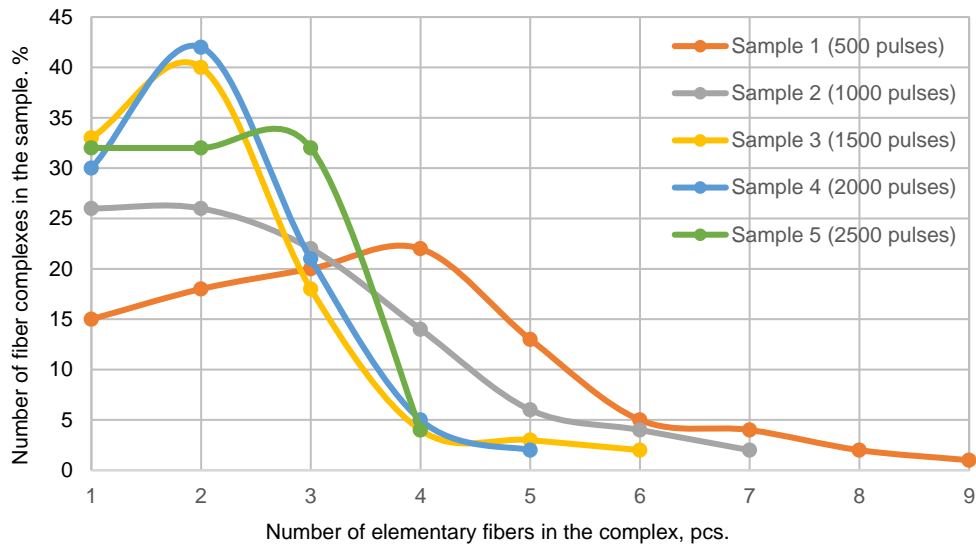
Figure 1. The influence of the number of cycles of electric pulse processing on the change in fibre structure.
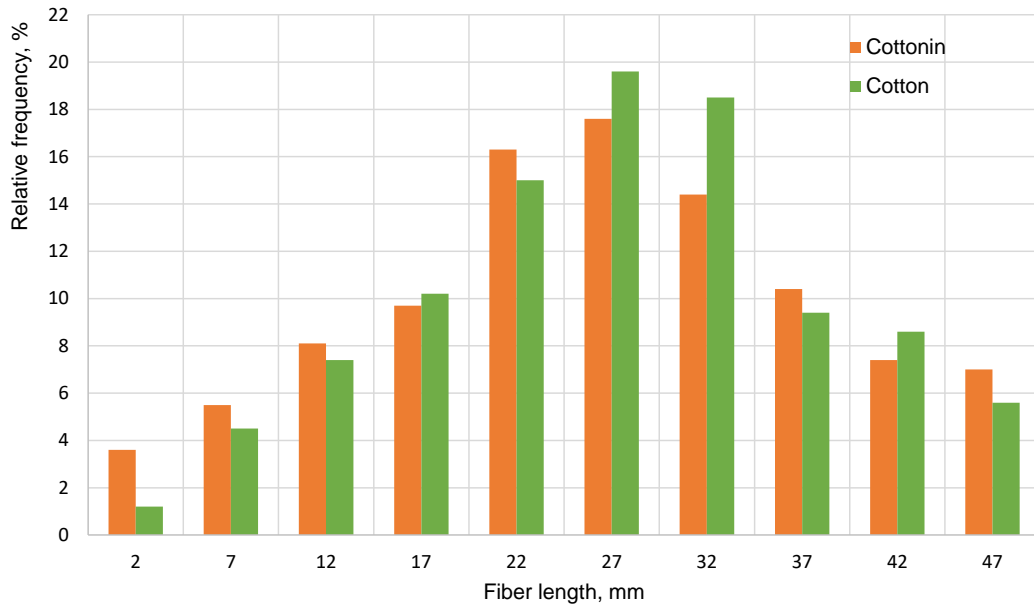
Figure 2. Diagram of the length distribution of hemp cottonin.
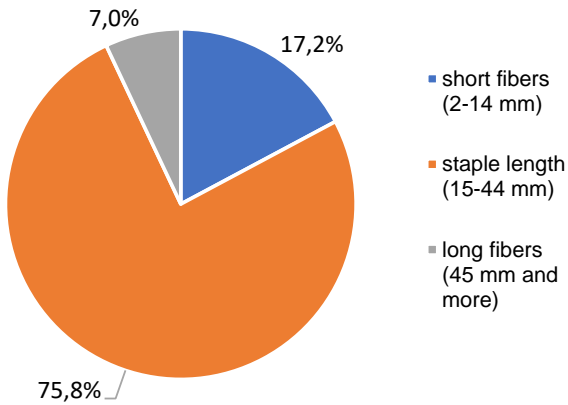
Figure 3. Distribution percentages of staple length in the sample with 2500 processing cycles.
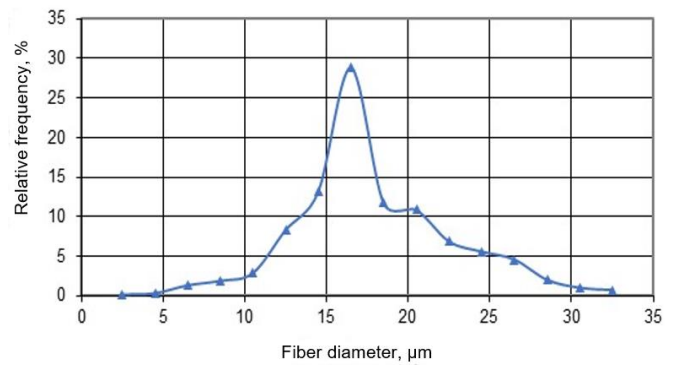
Figure 4. Diagram of distribution of hemp cottonin by diameter.
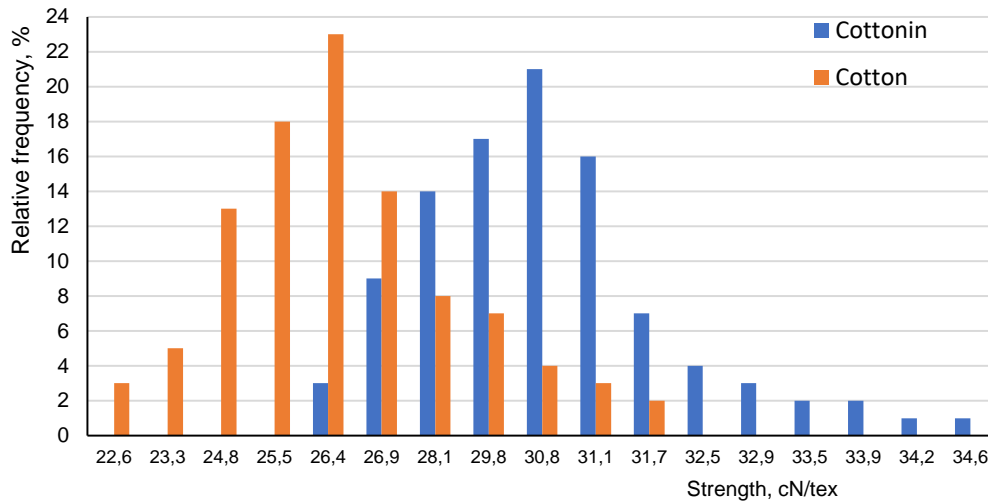
Figure 5. Diagram of distribution of hemp cottonin by strength.

Table 3. Calculation results of fiber properties after 2500 processing cycles.

Fiber properties	Mean ±SD		95 % CI		CV [%]	
	cottonin	cotton	cottonin	cotton	cottonin	cotton
Upper half mean length, UHML [mm]	26.8 ± 6.89	28.39 ± 8.09	(22.53 ; 31.07)	(23.38 ; 33.4)	25.7	28.5
Fiber diameter, *D* [µm]	15.5 ± 4.07	13.4 ± 3.27	(12.94 ; 17.98)	(11.37 ; 15.43)	26.3	24.4
Strength, *F* [cN/tex]	31.1 ± 3.36	26,9 ± 3.2	(22.26 ; 31.54)	(25.01; 28.79)	10.8	11.9

cottonin is 30.8 cN/tex, and the coefficient of variation is 10.8%, less than medium-fibre cotton.

The strength of medium-fibre cotton ranges from 24 to 27 cN/tex, indicating its spinning ability. The experimental strength values are within the required limits.

The sample size, providing a 95% confidence level, was 1300 fibers, used to determine fiber length, diameter, and strength. The research results are presented in Table 3.

Thus, hemp cottonin, obtained through 2500 cycles of processing using the electric pulse method, corresponds to medium-fibre cotton in its main physical and mechanical parameters and can, therefore, be used to form yarn using a carded spinning system at cotton factories.

The results of experimental studies of the physical and mechanical parameters of hemp cottonin after the process of electric pulse processing of hemp suggest that processing hemp fibre in a mode corresponding to 2500 pulses gives a good result, and the resulting fibre can be used in the preparation of multicomponent mixtures with other natural and chemical fibres.

CONCLUSIONS

The process of colonization of hemp fibre was studied using physical and mechanical methods, including electric pulse discharge.

An effective mode of electric pulse processing of fibres has been established, amounting to 2500 pulses of electric discharges, which makes it possible to obtain cottonized hemp fibre with the necessary spinning ability.

The parameters of customized hemp fibre were determined, which together evaluate its spinning ability: average fibre length 26.8 mm, fibre diameter 15.5 µm, and average strength 30.8 cN/tex.

The spinning ability of cottonized hemp fibre corresponds to the permissible similar indicators of cotton fibre, which allows hemp cottonin to produce blended yarn using a carded cotton spinning system.

REFERENCES

1. Schumacher A., Pequito S., Pazour J.: Industrial hemp fibre: A sustainable and economical alternative to cotton. Journal of Cleaner Production 268, 2020, 122180, ISSN 0959-6526. https://doi.org/10.1016/j.jclepro.2020.122180
2. Olijnyk H., Danchenko Y., Kornytska L.: Research on light resistance of the chenille cotton fabrics' coloring. Vlakna a Textil 30(3), 2023, pp. 31-36. https://doi.org/10.15240/tul/008/2023-3-004
3. Zimniewska M., Romanowska B.: Bast Fiber Textiles Addressed Improvement of Human Life. Natural Fiber, IntechOpen, November 2, 2022, Chapter 3, pp. 35–61. ISBN 978-1-80355-213-2. https://doi.org/10.5772/intechopen.105161
4. Manjakkal L., Jain A., Nandy S., et al.: Sustainable electrochemical energy storage devices using natural bast fibres. Chemical Engineering Journal, Volume 465, 2023, 142845, ISSN 1385-8947 https://doi.org/10.1016/j.cej.2023.142845

5. Hych O., Rastorhuieva M., Zakora O.: Analysis of the problem of processing industrial hemp into spinnable fibre. Visnyk of Kherson National Technical University 76 (1), 2021, pp. 132-140.
https://doi.org/10.21303/2313-8416.2021.002042

6. Berezovsky Yu., Kuzmina T., Lialina N., et al.: Technical and technological solutions of the process of obtaining fibres from bast crops. INMATEH – Agricultural Engineering 60(1), 2020, pp. 137-146.
https://doi.org/10.35633/inmateh–60–16

7. Berezovsky Yu.: Technical solution for scutching the raw bast material. Science and innovation 14(1), 2018, pp. 24-35.
https://doi.org/10.15407/scin14.01.026

8. Merdan N.: Effects of environmental surface modification methods on physical properties of hemp fibres. Materials Science 23 (4), 2017, pp. 416-421.
http://doi.org/10.5755/j01.ms.23.4.17469

9. Boyko G., Tikhosova H., Ternova T.: Optimization of the decortication process of industrial hemp stems by mathematical planning method. INMATEH – Agricultural Engineering 60(1), 2020, pp. 53-60
http://doi.org/10.35633/inmateh-60–06

10. Mayton H., Amirkhani M., Loos M., et al.: Evaluation of industrial hemp seed treatments for management of damping-off for enhanced stand establishment. Agriculture 12(5), 591, 2022.
https://doi.org/10.3390/agriculture12050591

11. Zakharkevich O., Poluchovich I., Kuleshova S., et al.: «CloStyler» – mobile application to calculate the parameters of clothing blocks. IOP Conference Series: Materials Science and Engineering 1031 (1), 2021, 012031.
https://doi.org/10.1088/1757-899x/1031/1/012031

12. Zakharkevich O., Koshevko J., Shvets G., et al.: Development of the Mobile Application to Calculate Parameters of Underwear Patterns. Terotechnology XII Materials Research Proceedings 24, 2022, pp. 309–315
https://doi.org/10.21741/9781644902059-45

13. Shvets G., Zakharkevich O., Kuleshova S., et al.: "Matved" – Mobile application to support the educational process in garment design. AIP Conf. Proc., December 7, 2023, 2889 (1): 040007.
https://doi.org/10.1063/5.0173472

14. Zakharkevich O., Paraska O., Koshevko J., et al..: Development of a mobile application to study sewing techniques for manufacturing fur and leather clothes. Fibres & Textiles in Eastern Europe 31 (2), 2023, pp. 1–10.
https://doi.org/10.2478/ftee-2023-0011

15. Tutek K., Masek A.: Hemp and Its derivatives as a universal industrial raw material (with particular emphasis on the polymer industry) – a review. Advanced Eco-friendly Wood-Based Composites 15(7), 2022, 2565
https://doi.org/10.3390/ma15072565

16. Viscusi G., Lamberti E., Gorrasi G.: Hemp fibres modified with graphite oxide as green and efficient solution for water remediation: Application to methylene blue. Chemosphere 288(3), 2022, 132614, ISSN 0045-6535
https://doi.org/10.1016/j.chemosphere.2021.132614

17. Lialina N., Yudicheva O., Samoilenko A., et al.: Evaluation of the quality of cellulose semi-finished products from technical hemp and the possibility of their further use. Fibres and Textiles 30(3), 2023, pp. 48-54.
https://doi.org/10.15240/tul/008/2023-3-006

18. Moussa M., Hage R., Sonnier R., et al.: Toward the cottonization of hemp fibres by steam explosion. Flame-retardant fibres, Industrial Crops and Products 151, 2020, 112242, ISSN 0926-6690.
https://doi.org/10.1016/j.indcrop.2020.112242

19. Sisti L., Totaro G., Vannini M., et al.: Retting process as a pretreatment of natural fibres for the development of polymer composites. Lignocellulosic Composite Materials, 2018, pp. 97–135.
https://doi.org/10.1007/978–3–319–68696–7_2

20. Kim H., Kim S.: Hand and wear comfort of knitted fabrics made of hemp/tencel yarns applicable to garment. Fibres Polym. 19, 2018, pp. 1539–1547.

21. Ahmed B., Wu Q., Lin H., et al.: Degumming of hemp fibres using combined microwave energy and deep eutectic solvent treatment. Industrial Crops and Products 184, 2022, 115046, ISSN 0926-6690.
https://doi.org/10.1016/j.indcrop.2022.115046

22. Ibragimov M., Turdiboyev A., Akbarov D.: Effects of electric pulse processing in increasing the efficiency of cotton oil from technical seeds. IOP Conference Series Earth and Environmental Science, Civil and Agricultural Engineering, October 14-16, 2021.
https://doi.org/10.1088/1755-1315/939/1/012004

23. Deng J. D., Han T., Li W. T., et al.: A study on electric pulse treatment of stainless steel constructive forming process. Proceedings of 19th International Conference on Metal Forming, September 11 – 14, 2022, 1270 012027.
https://doi.org/10.1088/1757-899X/1270/1/012027

24. Timanow V. M., Bojcshenko A. V., Krasnjanska O.M., et al.: Pat. No.8566 UA. Sposib pidgotowku ljonovolokna do prjadinnja. MKR D0 21 C 1/00. No.u 200500026; declareted: 14.01.2005, published: 15.08.2005, Bul. No. 9, 2s

25. ASTM D5103-07: Standard test method for length and length distribution of manufactured taple fibers, 2018, online:
https://img.antpedia.com/standard/files/pdfs_ora/20210202/ASTM%20D5103%20-%2007(2018.pdf

26. ASTM D5035-06: Standard Test Method for Breaking Force and Elongation of Textile Fabrics (Strip Method), 2008, online: https://www.wewontech.com/170421001.pdf

DEVELOPMENT OF ANTIFUNGAL FINISHES FOR WATER HYACINTH PRODUCTS

POOMFUANG, KRIT[1]; JARIYAPUNYA, NAREERUT[1*]; HATHAIWASEEWONG, SUNEE[1]; ROUNGPAISAN, NANJAPORN [1]; THONGSALEE, AREEYA [1]; JINGJIT, PIYANUT[1] AND VENKATARAMAN, MOHANAPRIYA[2]

[1] Department of Textile Engineering, Faculty of Engineering, Rajamangala University of Technology Thanyaburi, Pathum Thani, 12110, Thailand
[2] Department of Material Engineering, Faculty of Textile Engineering, Technical University of Liberec, Liberec, 461 17, Czech Republic

ABSTRACT

This work discusses the research conducted to develop an appropriate agent to enhance the anti-fungal properties of water hyacinth stalks, which are commonly used in handicraft products in Thailand. The objective of the research was to find an agent that would prevent fungal infestations, prolong the shelf life of the products, and ultimately increase the income for the craft makers. The initial experiment involved treating cotton fabrics with three different antifungal solutions: Chitosan, Zinc Pyrithione, and Poly (allylamine hydrochloride). These treated samples were then tested with Aspergillus niger, a common fungal strain, using the standard antifungal test AATCC 30. Among the three finishes, the fabric treated with Poly (allylamine hydrochloride) displayed the highest anti-fungal properties. However, the fabric treated with Zinc Pyrithione effectively inhibited fungal growth but left visible white particles on the fabric. Chitosan, on the other hand, did not significantly inhibit fungal growth. Based on these test results, it was concluded that a solution of Poly (allylamine hydrochloride) can be employed as a finishing agent for water hyacinth to enhance its antifungal properties in water hyacinth-based products. Additionally, it was found that a higher concentration of Poly (allylamine hydrochloride) (100 g/L) is necessary to effectively prevent fungal growth on water hyacinth stalks. By utilizing this research, local Thai communities can enhance the durability and longevity of their water hyacinth handicraft products, reducing the impact of fungal infestations and increasing their income.

KEYWORDS

Poly(allylamine hydrochloride); Antifungal; Water hyacinth.

INTRODUCTION

Water hyacinth, scientifically known as Eichhornia crassipes, is one of the invasive species that flourishes and reproduces in aquatic ecosystems due to its free-floating characteristics. This plant is commonly seen in stagnant swamps, lakes, reservoirs, and rivers, where it multiplies swiftly [1]. Water hyacinth has been causing significant harm to the environment and societies in tropical regions [2-3]. Despite the obstacles presented by these challenges, water hyacinth offers various advantages such as its medicinal properties and potential as an organic bioenergy source for biogas, briquettes, and fertilizer and additionally, it can be transformed into handmade products [4-5]. Although water hyacinth is widely known to contribute to water pollution due to its rapid growth and extensive spread, leading to a decline in water quality [6]. Various innovative strategies are being explored to harness the potential of water hyacinth, particularly utilizing its stalks as a raw material for producing local handicraft items [7]. The water hyacinth stalks were dried in order to be utilized as raw materials for a variety of products, such as handicrafts, furniture, bags, and other goods [8]. Regrettably, these products tend to have a limited shelf-life [9], which restricts income opportunities for handicraft-makers, primarily stems from the absence of anti-fungal properties in dried water hyacinth stalks [10]. It is advisable to store most handicraft products made from dried water hyacinth stalks away from moisture in order to mitigate the risk of potential damage, as exposure to water can result in deformation and a decrease in the strength of the products. Figure 1 depicts the manifestation of fungus on a product crafted from dried water hyacinth stalks. The appearance of fungal growth on the surface of this product provides a visual representation of the issue being addressed in the academic context.

Figure 1. Fungal growth detected on handicrafts made from dried water hyacinth stalks.

Antifungal agents play a vital role in various industries, including agriculture, healthcare, and textiles, to control fungal growth and prevent associated diseases. Among the different agents available, Chitosan (CS), Zinc Pyrithione (ZnPT), and Poly(allylamine hydrochloride) (PAH) have gained significant attention for their antifungal properties. Chitosan, with its biocompatibility and complete biodegradability, has proven to be effective in inhibiting fungal growth in plants like papaya sprouts [11]. It has also shown potential in managing common cucumber diseases [12] and acting as a preventive measure against crop diseases [13-15]. This makes Chitosan a versatile agent in agricultural practices. Zinc Pyrithione, widely used in shampoos to treat dandruff and seborrheic dermatitis, has gained recognition for its antifungal properties [16-17]. Its effectiveness against fungal infections makes it a valuable component in personal care products. Poly(allylamine hydrochloride) (PAH), popular in the textile industry, has been extensively studied for its antifungal and antibacterial properties [18-20]. Its efficacy in preventing fungal growth on fabrics highlights its potential in improving product quality and increasing the shelf life of textile products.

The continuing research endeavor seeks to enhance antifungal agents and evaluate their efficacy in improving fungal resistance, specifically in relation to dried water hyacinth stalks. The initial phase of the experiment will involve testing these agents on fabric made of 100% cotton. Following this, the chosen agent will be tested on dried water hyacinth stalks. The researchers aim to assist producers in achieving superior product quality by increasing the fungal resistance of dried water hyacinth stalks, thereby extending their shelf life.

EXPERIMENTAL

Materials

In order to compare with 100% cotton fabric, the dry fiber of water hyacinth was utilized. This decision was based on the fact that water hyacinth fiber contains a cellulose content ranging from approximately 55% to 67% [21-23].

Similarly, cotton fibers are considered the purest form of cellulose, the most abundant polymer in nature. Approximately 90% of cotton fibers are composed of cellulose [24]. For the experiment, three anti-fungal solutions were employed, namely Chitosan (CS), Zinc Pyrithione (ZnPT), and Poly (allylamine hydrochloride) (PAH). The primary goal of the initial experiment was to evaluate the antifungal effectiveness of these agents using 100% cotton woven fabric, which has a cellulose content referring to that of dried water hyacinth stalks. This standardization of methodology was crucial to ensure accurate and reliable results.

Evaluation of antifungal treatment activity on 100% cotton fabric

This section employs 100% cotton woven fabric characterized by a plain weave structure, with an approximate weight of 113.23 ± 2.13 grams per square meter (GSM) and a thickness of 0.26 ± 0.005 millimeters (mm). The anti-fungus treatment experiment on 100% cotton fabric involved immersing the fabric in a solution of antifungal agent with a concentration of 50 g/L. All antifungal agents utilized in this study are water-based. Drinking water with a pH range of approximately 6.5 – 7 was utilized to guarantee compatibility and encompass the pH range of the agents as outlined in Table 1. The fabric was dipped and subsequently padded with a wet pickup of 30% by weight, dried, and cured in a hot air convection oven at a temperature of 120 °C for 1 minute, as shown in Figure 2. The experiment also included the preparation of three antifungal agent solutions, each with a concentration of 50 g/L, to evaluate fungal growth. These solutions consisted of Chitosan (CS), Zinc Pyrithione (ZnPT), and Poly (allylamine hydrochloride), as indicated in Table 1.

Circular pieces of antifungal fabrics produced from treatment processing with various solutions were cut to a diameter of approximately 2.45 centimeters. These pieces of fabric were then subjected to laboratory testing according to the AATCC30 Antimicrobial Test standard (Test III) using agar plates infused with Aspergillus niger. In preparation for the growth of the Aspergillus niger strain on agar medium, a solution was created containing 3 g/L of Ammonium nitrate (NH_4NO_3), 2.5 g/L of Potassium dihydrogen phosphate (KH_2PO_4), 2 g/L of Dipotassium hydrogen phosphate (K_2HPO_4), 0.2 g/L of Magnesium sulfate ($MgSO_4$), 0.1 g/L of Ferrous sulfate ($FeSO_4$), and 20 g/L of Agar. This solution was then sterilized under pressure at 121 °C and poured into the growth medium to form a solid gelatinous matrix. The prepared Aspergillus niger was placed onto the matrix and incubated at a temperature of 28 ± 1 °C for a period of 7 to 14 days.

Table 1. Antifungal solution preparation for 100% cotton fabric.

Solution	Agent	Agent [pH]	Water [pH]	Concentration [g/L]	Temperature [C°]	Time [Sec]
1	CS	5.5 – 7.2	6.5 - 7	50	120	60
2	ZnPT	6.5 - 9	6.5 - 7	50	120	60
3	PAH	5.5 - 7	6.5 - 7	50	120	60
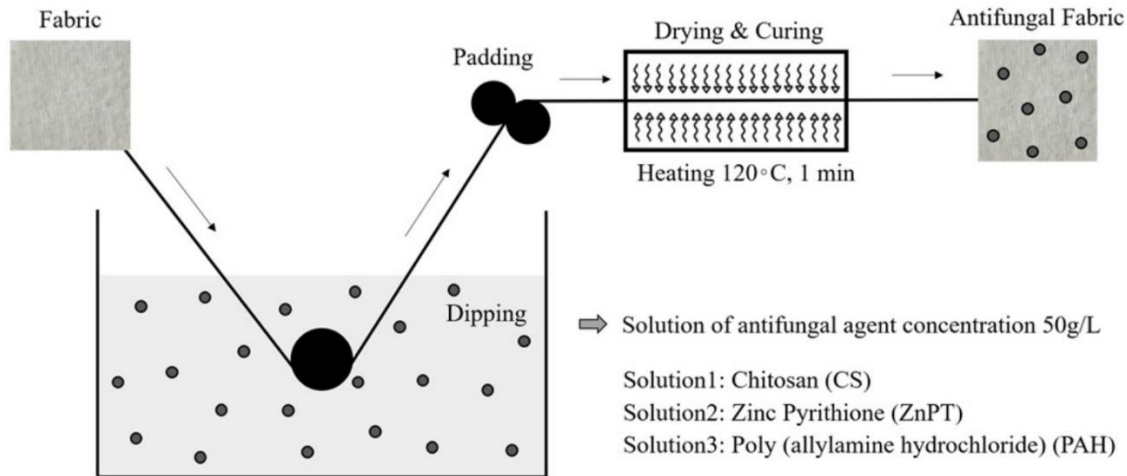
Figure 2. Antifungal treatment methods for cotton fabric with various solutions.

Evaluation of antifungal treatment activity on dried water hyacinth stalks

The experiment was conducted with the objective of creating a treatment to combat fungus in water hyacinth stalks. In the initial stage, the fresh water hyacinth stalks were dried under sunlight for a period of three days before applying the anti-fungus treatment. It was observed that for every one kilogram of fresh water hyacinth stalks, only 150 to 200 grams of dried water hyacinth stalks were obtained. These dried stalks were then prepared for the anti-fungus treatment, where the selection of a suitable anti-fungal solution for fabrics was assessed. The quality of the anti-fungal fabric was determined based on the AATCC30 standard, which influenced the choice of solution for this experiment.

The solution that was identified during the preliminary experiment was used to formulate the anti-fungal treatment for water hyacinth stalks. The dried stalks were immersed and soaked in the solution, employing a method similar to that of cotton fabric, with a concentration of 50 g/L for one minute. Afterward, they went through a 30-minute drying phase, followed by heating with hot air at 120°C for one minute.

Later on, the specimens underwent testing in accordance with the AATCC30 Antimicrobial Test Standard (Test III), using Agar Plate with Aspergillus niger for evaluation. Subsequently, a spraying process was employed to develop an anti-fungus treatment and compare hyacinth stalks.

This development has the potential to improve the quality of products made from water hyacinth and increase their value by incorporating antifungal finishes for water hyacinth fiber products.

RESULTS AND DISCUSSION

The results from the AATCC30 Antimicrobial Test Standard (Test III) results indicated that three 100% cotton fabrics were immersed in the solutions of antifungal agents consisted of Chitosan (CS), Zinc Pyrithione (ZnPT), and Poly (allylamine hydrochloride) (PAH) each with a concentration of 50 g/L. The fabric treated with CS solution did not effectively prevent the growth of the fungus Aspergillus niger, as depicted in Figure 3. Conversely, both ZnPT and PAH demonstrated the ability to inhibit fungal growth, However, the application of ZnPT resulted in the presence of visible white particles on the fabric, indicating that the ZnPT solution exhibits a white color appearance. In contrast, no particles were observed on the fabric treated with PAH due to its transparent nature, as illustrated in Figure 3.

Based on the results obtained from the antimicrobial experiments carried out on cotton fabric, it was concluded that the most effective antifungal agent for water hyacinth stalks is PAH at a concentration of 50 g/L. The methodology involved preparing dried water hyacinth stalks, immersing them in a solution containing PAH at a concentration of 50 g/L for a duration of 1 minute, as depicted in Figure 4. This was followed by a drying period of 30 minutes and a final

Figure 3. Antimicrobial results of CS, ZnPT, and PAH on cotton fabric at a concentration of 50 g/L.

step of subjecting the stalks to hot air at a temperature of 120°C for one minute.
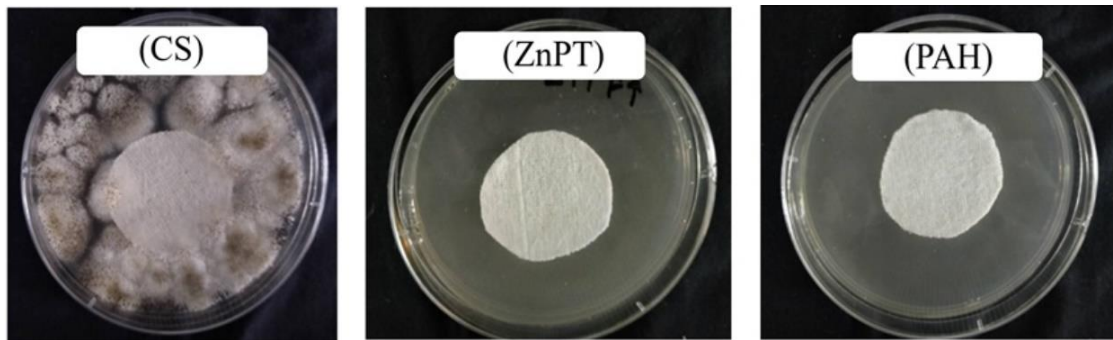
Based on the findings, it was determined that the dried water hyacinth sample was immersed in a solution with a PAH concentration of 50 g/L for 1 minute. Subsequently, it was tested in the laboratory following the AATCC30 Antimicrobial Test standard (Test III) on an Agar Plate. The results indicated that the treatment was unable to prevent fungal contamination, as illustrated in Figure 5(a).

For sample A, the 100% cotton fabric's high absorbability, which allows it to absorb moisture up to 24-27 times its own weight, made it unable to prevent fungal growth. Consequently, a concentration of 50 g/L of PAH effectively inhibited fungal contamination on the cotton fabric. In contrast, dried water hyacinth stalks have a smooth surface and a lower capacity to absorb the PAH solution at 50 g/L. Therefore, increasing the concentration of PAH could enhance its absorption by the dried water hyacinth stalks, thereby more effectively inhibiting fungal contamination. Moreover, the concentration of PAH can vary based on the application method. The padding method on cotton fabric ensures an even coating without oversaturation, achieving a wet pickup of 30% by weight. Conversely, immersion is a suitable method for coating antifungal agents on dried water hyacinth stalks and can vary depending on factors such as the initial concentration of the PAH solution, the duration of immersion, and the absorption capacity of the dried water hyacinth stalks.

PAH adheres to dried water hyacinth stems through chemical binding via ionic interactions, where the positively charged ammonium groups ($-NH_3^+$) in PAH bind with negatively charged groups on the cell walls of water hyacinth, and through hydrogen bonding, where amine groups in PAH form hydrogen bonds with hydroxyl and carboxyl groups in the water hyacinth. Moreover, the concentration of PAH affects its antifungal efficacy on dried water hyacinth stems, making the appropriate concentration crucial for maximizing effectiveness. Upon analysis of the results, it became evident that the water hyacinth sample, which had been subjected to a brief immersion in a solution containing 50 g/L PAH concentration for a duration of 1 minute, and

subsequently subjected to laboratory testing using the AATCC30 Antimicrobial Test standard (Test III) Agar Plate, failed to effectively inhibit fungal contamination. Specifically, the fungus Aspergillus niger exhibited the ability to proliferate, as visually represented in Figure 5(a). These findings underscore the limited antimicrobial efficacy of the tested PAH concentration and need for additional research and an elevation in the PAH concentration suggests a potential avenue for refining the antimicrobial treatment protocol.

The experiment involved modifying the PAH antifungal concentration according to the information provided in Table 2.

The experimental setup entailed the creation of Sample B with a PAH concentration of 70 g/L and Sample C with a PAH concentration of 100 g/L. Significantly, our analysis unveiled that Sample B retained discernible traces of Aspergillus niger fungus, as depicted in Figure 5(b), indicating the ongoing fungal presence. In contrast, Sample C displayed a conspicuous absence of fungal growth, as clearly depicted in Figure 5(c), emphasizing the effectiveness of the higher PAH concentration in preventing fungal colonization.

Figure 4. Immersion in PAH solution of dried water hyacinth stalks.

Table 2. Preparation of PAH antifungal concentrations for water hyacinth.

Solution	Antifungal Agent	Concentration	Sample
1	PAH	50 g/L	A
2	PAH	70 g/L	B
3	PAH	100 g/L	C
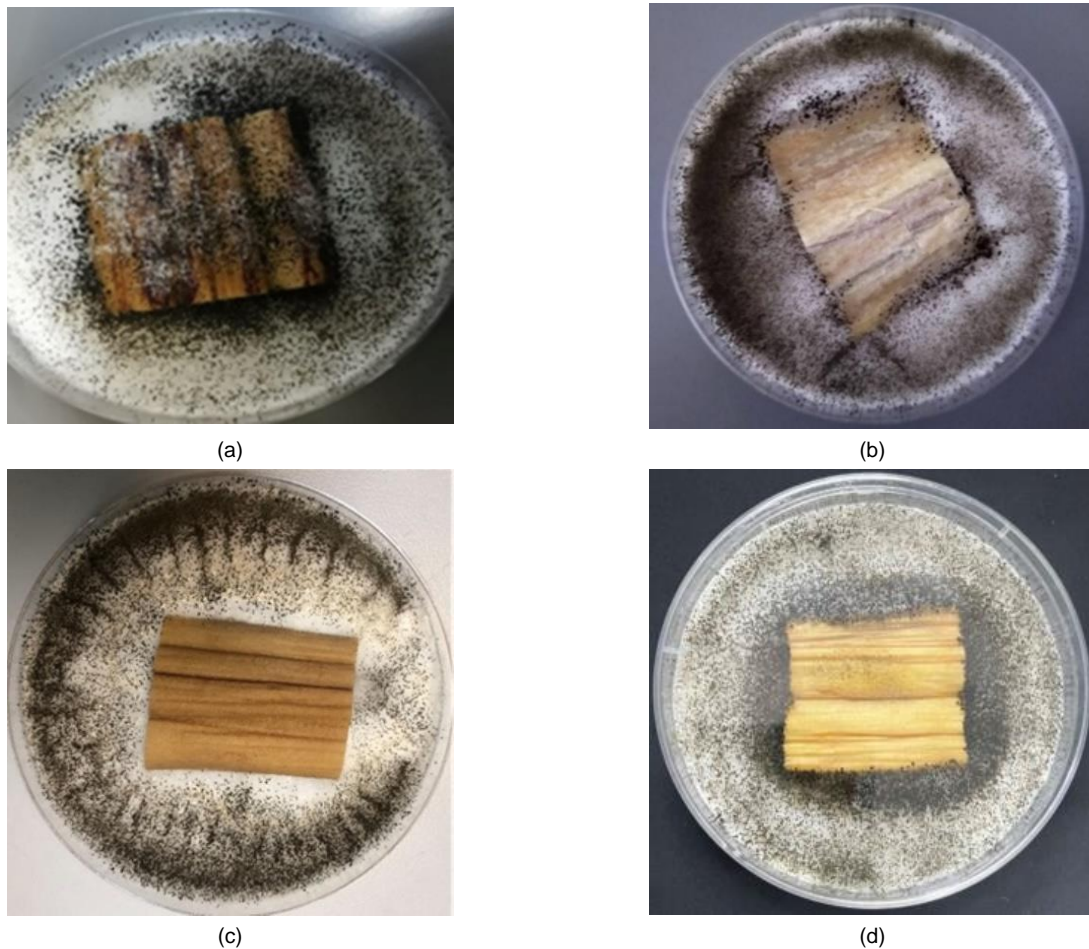
Figure 5. Antimicrobial result of sample: (a) A with PAH concentration 50 g/L, (b) B with PAH concentration 70 g/L, (c) C with PAH concentration 100 g/L, (d) D after immersion in the water for 1 minute.

To confirm the antimicrobial efficacy of PAH at a concentration of 100 g/L, an additional test was conducted using dried water hyacinth stalks treated with PAH. The experiment involved exposing the dried water hyacinth stalks to water for 1 minute, followed by drying them for 30 minutes and then using hot air at a temperature of 120°C for 1 minute. The fungal resistance of the dried water hyacinth stalks was then assessed according to the AATCC 30 Antimicrobial Test standard (Test III) using an agar plate. The results for Sample D demonstrated that most of the dried water hyacinth stalks' surfaces maintained their fungal resistance, as shown in Figure 5(d).

Based on the experimental results, it is evident that the PAH concentration has an impact on inhibiting the growth of fungi. This can contribute to enhancing the quality of processed products derived from water hyacinth stalks. This observation underscores the potential for incorporating 100 g/L of PAH antifungal agents during the preparatory phase of water hyacinth stalks to ensure their suitability for subsequent product development, ultimately leading to improved quality in water hyacinth-derived products.

In addition to preparing water hyacinth stalks for subsequent product development, the researchers conducted antifungal testing on finished water hyacinth products, as depicted in Figure 6. This was achieved by directly applying antifungal agents using a spray technique to the prepared products. Immersing the finished products in a solution was deemed impractical due to concerns about potential structural integrity alterations caused by excessive solvent absorption. Therefore, a spray technique was employed to evaluate and enhance the protection of water hyacinth-derived products against fungal contamination, utilizing a solution with a concentration of 100 g/L of PAH (Preservative Antifungal Agent with High potency) to assess its effectiveness.

The resistance testing performed on water hyacinth-derived products, using a spray method with a concentration of 100 g/L of PAH of Sample E, demonstrated its capacity to provide protection against fungal contamination, albeit with less efficiency when compared to pretreating the water hyacinth stalks with antifungal agents prior to product formation, as shown in Figure 7. Nevertheless, the test results unequivocally indicate that the spray technique can effectively safeguard products against fungal growth in the absence of prior antifungal solution immersion.

Figure 6. Spray technique of PAH solution on dried water hyacinth stalks.

Figure 7. Antimicrobial result of sample E utilizing spray technique at PAH concentration of 100 g/L.

CONCLUSION

The objective of this research was to develop and evaluate antifungal agents for dried water hyacinth stalks. The experiments demonstrated that PAH exhibited efficient antifungal propertie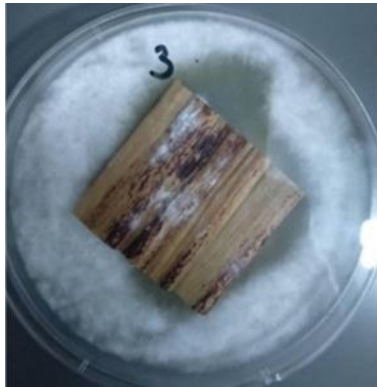s, both on 100% cotton fabric with a concentration of 50 g/L and on water hyacinth with a concentration of 100 g/L. The data indicated that the effectiveness of retaining antifungal agents on cotton fabric was superior, as it absorbed the antifungal solution more effectively than dried water hyacinth stalks. Therefore, increasing the concentration of antifungal agents significantly contributes to enabling water hyacinth stalks to effectively resist fungi, requiring a concentration of PAH substances as high as 100 g/L.

In addition to the efficient antifungal effects achieved through immersing dried water hyacinth stalks in a concentrated PAH solution, it is observed that employing the PAH spray technique with the same concentration can also effectively inhibit fungal growth in finished products. This demonstrates that finished water hyacinth products can effectively prevent fungal contamination using the spray technique, extending the product's shelf life and adding value to the water hyacinth product efficiently.

REFERENCES

1. Jirawattanasomkul T., Minakawa H., Likitlersuang S., et al.: Use of water hyacinth waste to produce fibre-reinforced polymer composites for concrete confinement: Mechanical performance and environmental assessment. Journal of Cleaner Production, 2021, 292, pp. 1–13. https://doi.org/10.1016/j.jclepro.2021.126041
2. Zhang Q., et al.: Simple cellular automaton-based simulation of ink behaviour and its application to Suibokuga-like 3D rendering of trees, The Journal of Visualization and Computer Animation, 10(1), 1999, pp. 27-37. Harun I., Pushiri H., Amirul-Aiman A.J., et al.: Invasive Water Hyacinth: Ecology, Impacts and Prospects for the Rural Economy. Plants 2021, 10, 1613. https://doi.org/10.3390/plants10081613
3. Gezie A., Assefa W.W., Getnet B., et al.: Potential impacts of water hyacinth invasion and management on water quality and human health in Lake Tana watershed, Northwest Ethiopia. Biol Invasions, 2018, 20, pp. 2517–2534. https://doi.org/10.1007/s10530-018-1717-0
4. Wimalarathne H.D., Perera P.R.: Potentials of water hyacinth as livestock feed in Sri Lanka. Indian Journal of Weed Science, 2019, 51(2), pp. 101–105. https://doi.org/10.5958/0974-8164.2019.00024.8
5. Harun I., Pushiri H., Amirul-Aiman A.J., et al.: Invasive water hyacinth: Ecology, impacts and prospects for the rural economy. Plants, 2021, 10(8), pp. 1-23. https://doi.org/10.3390/plants10081613
6. Madikizela L.M.: Removal of organic pollutants in water using water hyacinth (Eichhornia crassipes). Journal of Environmental Management, 2021, 295, 113153. https://doi.org/10.1016/j.jenvman.2021.113153
7. Agustin D., Anggriani N., Dewi A.S., et al.: Training on the Utilization of Water Hyacinth Waste into Handicraft Products for PKK Women in Tambak Oso Village, Sidoarjo. Nusantara Science and Technology Proceedings, 2023, pp. 32-40 https://doi.org/10.11594/nstp.2023.3305
8. Amante K., Ho L., Lay A., et al.: Design, fabrication, and testing of an automated machine for the processing of dried water hyacinth stalks for handicrafts. In IOP Conference Series: Materials Science and Engineering, 2021, 1109 (1), 012008. https://doi.org/10.1088/1757-899X/1109/1/012008
9. Lubembe S.I., Okoth S., Turyasingura B., et al.: WaterHyacinth, an Invasive Species in Africa: A Literature Review. East African Journal of Environment and Natural Resources, 2023, 6(1), pp. 243-261. https://doi.org/10.37284/eajenr.6.1.1293
10. Gaur S., Singhal P.K., Hasija S.K.: Relative contributions of bacteria and fungi to water hyacinth decomposition. Aquatic Botany, 1992, 43(1), pp. 1-15. https://doi.org/10.1016/0304-3770(92)90010-G
11. Asawatreratanakul P., Asawatreratanakul K.: Chitosan Induction of fungal resistance in papaya seedling. ASEAN Journal of Scientific and Technological Reports, 2012, 15(3), pp. 1-6.
12. Tonma S., Tibkampor N.: Effect of Herb Crude Extracts Mixed on Chitosan to Inhibit Cucumber Pathology. Ramkhamhaeng Research Journal of Sciences and Technology, 2019, 22(2), pp. 23-34.
13. Kaomek M.: Antifungal Activity of Chitooligosaccharides From Samanca Saman (Jacq) Merr., Leucaena Leucocephala De Wit, Oryza Sativa Rd.6 And Sorghum Vulgare Ku 630 Produced by Chitinase. VRU Research and Development Journal Science and Technology, 2020, 15(2), pp. 119-130.
14. Kaomek M.: Screening, Characterization and Antifungal of Chitosanase From Thai Plants. VRU Research and Development Journal Science and Technology, 2019, 14(1), pp. 1-10.
15. Lopez-Moya F., Suarez-Fernandez M., Lopez-Llorca L.V.: Molecular mechanisms of chitosan interactions with fungi and plants. International Journal of Molecular Sciences, 2019, 20(2), 332.

https://doi.org/10.3390/ijms20020332

16. Mangion S.E., Holmes A.M., Roberts M.S.: Targeted delivery of zinc pyrithione to skin epithelia. International Journal of Molecular Sciences, 2021, 22(18), 9730.
https://doi.org/10.3390/ijms22189730

17. Park M., Cho Y.J., Lee Y.W.,et al.: Understanding the Mechanism of Action of The Anti-Dandruff Agent Zinc Pyrithione Against Malassezia Restricta. Scientific reports, 2018, 8(1), 12086 p.
https://doi.org/10.1038/s41598-018-30588-2

18. Asghari-Paskiabi F., Jahanshiri Z., Shams-Ghahfarokhi M., et al.: Antifungal Nanotherapy: A Novel Approach to Combat Superficial Fungal Infections. Nanotechnology in Skin, Soft Tissue, and Bone Infections, 2020, pp. 93-107.
https://doi.org/10.1007/978-3-030-35147-2_5

19. Vidiasheva I.V., Abalymov A.A., Kurochkin M.A., et al.: Transfer of cells with uptaken nanocomposite, magnetite-nanoparticle functionalized capsules with electromagnetic tweezers. Biomaterials science, 2018, 6(8), pp. 2219-2229.
https://doi.org/10.1039/C8BM00479J

20. Zhao Z., Li Q., Gong J., et al.: A Poly (allylamine hydrochloride)/poly (styrene sulfonate) Microcapsule-coated Cotton Fabric for Stimulus-responsive Textiles. RSC advances, 2020, 10(30), pp. 17731-17738.

https://doi.org/10.1039/D0RA02474K

21. Arivendan A., Jebas Thangiah W.J., Irulappasamy S., et al.: Study on Characterization of Water Hyacinth (Eichhornia Crassipes) Novel Natural Fiber as Reinforcement with Epoxy Polymer Matrix Material for Lightweight Applications. RSC advances, 2022, 51(5), pp. 8157S-8174S.
https://doi.org/10.1177/15280837211067281

22. Ewnetu Sahlie M., Zeleke T.S., Aklog Yihun F.: Water Hyacinth: A Sustainable Cellulose Source for Cellulose Nanofiber Production and Application as Recycled Paper Reinforcement. Journal of Polymer Research, 2022, 29(6), 230 p.
https://doi.org/10.1007/s10965-022-03089-0

23. George S., Thomas S., Nandanan Nedumpillil N., et al.: Extraction and Characterization of Fibers from Water Hyacinth Stem Using a Custom-Made Decorticator. Journal of Natural Fibers, 2023, 20(2), 2212927.
https://doi.org/10.1080/15440478.2023.2212927

24. Elmogahzy Y., Farag R.: Tensile properties of cotton fibers: importance, research, and limitations. In Handbook of properties of textile and technical fibres, Woodhead Publishing, 2018, pp. 223-273.
https://doi.org/10.1016/B978-0-08-101272-7.00007-9

ANTIVIRAL TEXTILES AND ANTIVIRAL ACTIVITY TESTING - THE USE OF BACTERIOPHAGE SURROGATE FOR ANTIVIRAL ACTIVITY TESTING

TVRZOVÁ, LUDMILA[1]*; BLAHOVÁ, ANNA[1]; FOJT, JAKUB[1]; DOUBKOVÁ, HANA[1] AND PROCHÁZKA, JIŘÍ[2]

[1] Textile Testing Institute, Cejl 12, 602 00 Brno, Czech Republic
[2] SINTEX, Moravská 1078, 560 02, Česká Třebová, Czech Republic

ABSTRACT

The risk of dissemination of highly contagious viral diseases (as COVID-19, Ebola) led in the increasing need to develop functional textiles and surfaces with antiviral effect. Antiviral textiles are designed to reduce the viability and infectivity of viruses on their surfaces and by this way to reduce the cases of infection (including re-infection or cross-infection with contaminated textiles). Different antiviral agents and diverse techniques of their application are used for functionalized textiles manufacturing. The most often used antivirals are metallic and ionic silver and copper, iron oxide, quaternary ammonium salts. The aim of the process is to prepare textiles with long-term durable finishing effective in viral activity inhibition. The basic step of functionalized antiviral textiles development is antiviral effectivity testing. The safe method of testing with the use of Phi6 bacteriophage, SARS-CoV-2 and Ebola virus surrogate, was modified for antiviral textiles testing. The samples of textiles with antiviral finishing were tested by the bacteriophage-based method and excellent antiviral activity was detected for all tested materials. The woven cotton was used as reference untreated material, the different textile cotton structures with similar square weight were compared and no statistically significant difference was found between the resulting antiviral efficacy values. A simple and quickly feasible screening method for determining the antiviral properties of textiles, especially with leaching-type of treatment, was also designed and tested.

KEYWORDS

Antiviral; Bacteriophage; Finishing; Textiles; Virus.

INTRODUCTION

The fast spread of the COVID-19 virus in the last years together with continuous emergence of other infectious diseases (SARS, H1N1 influenza, Ebola haemorrhagic fewer), bring the highest need for development and testing of antiviral textiles [1] [2]. Textiles help to protect human from un-favorable conditions of environment, but for protection from microorganisms and viruses they need to be treated by antimicrobial finishings. Antiviral treatment of the personal protection equipment and the textiles used in public space can reduce the risk of viral infection transmission due to the contact with contaminated textiles and objects [3-5]. For this reason, there is a growing need for the development of efficient and accessible methods of antiviral activity testing, and hand in hand with them to optimize the testing methods as well.

The mainly used strategy for producing antiviral and antipathogenic textiles, in general, is physically load additives on the surface of the fabric and/or microfibers, although new fabrication methods are available too (copper ion-textile based on fundamentally different principle of incorporating copper ions into the cotton structure at the molecular level described by Quian et al. [6]). Antiviral chemicals (inorganic metals and metal nanoparticles, such as silver, zinc or copper, quaternary ammonium compounds or organic compounds with antiviral properties [5] [7] can be applied to textiles through various chemical finishes. Surface modifications (microencapsulation, plasma treatment, electrospinning) can help to improve durability and provide long-lasting effect of antiviral or generally antipathogenic treatment [4] [5] [8]. The selection of a particular method depends on factors such as the desired level of antiviral activity, fabric type, intended use, cost, and regulatory considerations [4].

Independently on the antiviral compound, the method of antiviral textile production and the way of the use, there is a need for the antiviral effectivity testing in the

---

course of antiviral fabrics development. Specific viruses are chosen for antiviral effectivity testing, depending on the use of textile product and the availability of the testing method. The international standard ISO 18184 "Textiles - Determination of antiviral activity of textile products." [9] mentions the use of human influenza virus as a representative of enveloped viruses, and feline calicivirus as a representative of non-enveloped viruses. The use of another evaluated virus is possible. The testing virus could be a carefully chosen surrogate virus, used as a substitute for specific human viruses. Surrogate viruses possess similar properties to their human counterparts, allowing researchers to study antiviral activity in a controlled laboratory setting [10]. Calicivirus or Vaccinia virus are commonly used as a surrogate or model viruses in antiviral testing. Bacteriophages are the promising biosafety level 1 (BSL-1) substitutes of human viruses, due to their resistance towards antimicrobials, environmental conditions and antiviral compounds [11-13]. The Phi6 bacteriophage (double-stranded RNA enveloped virus) has been used in a wide range of testing applications as a valuable surrogate of human enveloped viruses, such as SARS-CoV-2 virus, influenza virus and Ebola virus, due to their lipidic surface structures [2] [3] [12] [14]. As safe infectious testing particle enables testing in conditions where the use of an animal virus would not be safe [1] [2]. The example of the use are materials for face masks and the testing of antiviral effectivity and viral filtration efficiency with the same virus [13].

Due to the limited availability of antiviral activity testing, our work was focused on the development and application of an effective and affordable method for testing the antiviral activity of textile materials. Based on the previously published data and the comparison of structural properties of viruses, the bacteriophage phi6 was chosen as a suitable enveloped surrogate virus for the determination of antiviral activity of functionalized textiles. The aim of this work was to optimize the bacteriophage-based method for determination of antiviral activity of functionalized textiles and overcome the limitations of testing with selected animal viruses (lower titre of particles in suspension, sensitivity to environmental conditions, costs of the testing). The method is based on the common principle of assessment of antiviral activity of textiles - the viral suspension test. In this test, the textile sample is directly exposed to a suspension of the target virus. After a specified contact time, the virus is recovered from the textile, and its infectivity is assessed. The different testing system allows to extend the method by qualitative preliminary test, which was designed besides the quantitative testing.

The resistance of functional adjustments, including antiviral treatments, during using and maintenance of textiles, is important characteristic of treated products. The leaching of antimicrobial agents is important for durability of the treatment and the kind of antimicrobial effect. A non-leaching type of the functionalized textile is generally preferred for clothing as it may retain its activity for a longer time. The leaching type of the treatment is used for medical textiles and disposable materials, the leaching substances are characterized by stronger, biocidal, antimicrobial activity [4]. The bacteriophage-based method of antiviral activity determination can give preliminary and fast information about leaching of the textile treatment.

MATERIALS AND METHODS

Bacteriophage Phi6 DSM 21518 and the host strain *Pseudomonas* sp. DSM 21482 (testing virus and their host) were purchased from German collection of microorganisms (Deutsche Sammlung fur Mikroorganismen und Zellkulturen, DSMZ) – Leibnitz Institute, Braunschweig, Germany. Tryptic soya broth (TSB) and Tryptic soya agar (TSA) for the host strain cultivation, Soybean casein digest medium with Tween 80 and Lecithin (SCDLP) and Tris-buffer base were purchased from HiMedia.

A Phi6 stock solution of 10^{10} plaque forming units (PFU)/ml of TSB was used for the virus propagation and for testing procedure. Liquid lysis method described by DSMZ [15] was used for bacteriophage propagation. Double-layer plaque assay for the infected cells number determination was provided according to Plohl [3] with minor modifications. There were added 3 ml of top agar on the standard 90 mm Petri plate with bottom agar (TSA), and 0.1 ml of host bacteria suspension and 0.1 ml of diluted sample of bacteriophage suspension. SM-buffer [15] was used for bacteriophage dilution. The plates with inoculated top-agar were allowed to solidify and then were cultivated at 25°C. The infectivity titre of the virus was determined as a number of plaque-forming units per ml of suspension [16] from the number of plaques (clear zones) on the plates after 24 hours of cultivation.

Four knitted fabrics of different composition (Table 1(a)) with the same antiviral silver-based treatment harmonized with current biocidal regulation and two woven cotton reference materials (Table 1(b)) were used in this study. All tested materials were manufactured by SINTEX. The negative untreated reference samples of unbleached woven cotton were washed in 10 cycles without detergent at 60°C (10 min followed by 2-time rinsing for 5 min) [9].

Determination of antiviral activity

The test specimens with mass of (0.40 ± 0.05) g were prepared in triplicates and cut on the (20 x 20) mm pieces. The vial containers were used for sterilization of samples in the autoclave at 121°C and 103 kPa for 15 min. The triplicates of control untreated specimens were prepared by the same way, as well as specimens for cytotoxicity testing [9].

Table 1a. The antiviral materials used for the bacteriophage-based method optimization. The same antiviral finishing agent (with preliminary validated antiviral effect) was used for all materials.

	Sample 1	Sample 2	Sample 3	Sample 4
Material structure/colour	single jersey white	doubleface blue	elastic single jersey black	single jersey light blue
Material composition	50 % cotton 50 % polyester	51 % polyester 49 % cotton	90 % polyester 10 % Lycra	100 % cotton
Mass per unit area [g/m²]	158	185	230	131
Width [cm]	176	200	150	163

Table 1b. Reference untreated materials used for the bacteriophage-based method optimization. Woven unbleached cotton was used as reference material for antiviral activity determination.

	736A	737A
Material composition	100 % cotton	100 % cotton
Mass per unit area [g/m²]	113	103
Warp sett [cm⁻¹]	26	39
Weft sett [cm⁻¹]	23	27

Infectivity titre test was used for antiviral activity of textile samples determination. Antiviral activity of the tested products was evaluated on the base of antiviral efficacy value, *Mv*.

The **antiviral efficacy value** was calculated as follows:

$$Mv = lg\,[Va] - lg\,[Vc], \qquad (1)$$

where Mv is the antiviral efficacy value, *lg* [Va] is the common logarithm average of 3 infectivity titre value immediate after inoculation of untreated specimen, *lg* [Vc] is the common logarithm average of 3 infectivity titre value after 2 h contacting with the treated specimen.

The infectivity titre of control specimens (untreated) was determined immediately after inoculation and after contact time (2 h). Logarithm reduction value of infective titre of control specimens was less than 1.0.

At the beginning of every test, 200 µl of the virus suspension (10^7 infection particles per ml, last dilution in sterile distilled water) was applied on the textile test specimen and untreated (reference) sample. After contact time 2 hours (or immediately in the time 0), the virus was recovered from the specimens, 20 ml of sterile washing out solution - SCDLP medium – was added and vials were agitated by Vortex mixer 5 times for 5 s Medium with recovered virus was diluted and appropriate dilutions were inoculated to the top agar, together with the host cells, for infectivity titre determination (Fig. 1).

The double-layer agar plaque assay provides a measure of the viability of viral particles present in a sample, as each plaque corresponds to a single infectious unit. Antiviral efficacy value is calculated as the reduction of viral infectivity by treated textile in comparison with untreated reference sample [9].

Agar diffusion assay

Fabric specimens were cut to squares (2 x 2 cm approx.) and placed on the top TSA agar pre-inoculated by *Pseudomonas* sp. DSM 21482 and bacteriophage Phi6 DSM 21518 (double layer agar in a Petri dish was used). Plates were incubated at 25°C for 24 h. The zones of inhibition were checked visually and microscopically (if no zone was detected). The assay allows to characterize antiviral textile as leaching or un-leaching type. Leaching antiviral agents diffuse to agar surrounding the sample and inhibit the infection process, resulting in inhibition zone appearance.

RESULTS AND DISCUSSION

Four samples of different material composition, with mass per unit area (131 – 230) g/m², treated by the same antiviral compound, were tested for antiviral effectivity by bacteriophage-based method of antiviral textile testing. Two untreated control fabrics (100% cotton, unbleached, 10 times washed) of different woven parameters were used for testing and *Mv* calculation (Table 1(a,b)).

Sample 1 was white single jersey polyester/cotton 50/50 %. Sample 2 was blue doubleface 49 % polyester, 51 % cotton, sample 3 was black elastic single jersey 90% polyester, 10 % Lycra, and sample 4 was light blue single jersey, 100 % cotton. All samples were treated by identical antiviral compound of the same concentration. The reference cotton infectivity titre values were used for the antiviral efficacy value determination. No toxic effect of antiviral textile samples toward host cells has been demonstrated by control test. The infectivity titre of viral suspension used for testing was $3 – 5 \times 10^7$ PFU/ml. The logarithm reduction values of infective titre of control specimens were less than 1, what is the condition of valid test for 2 h contact time concerning ISO 18184 [9].
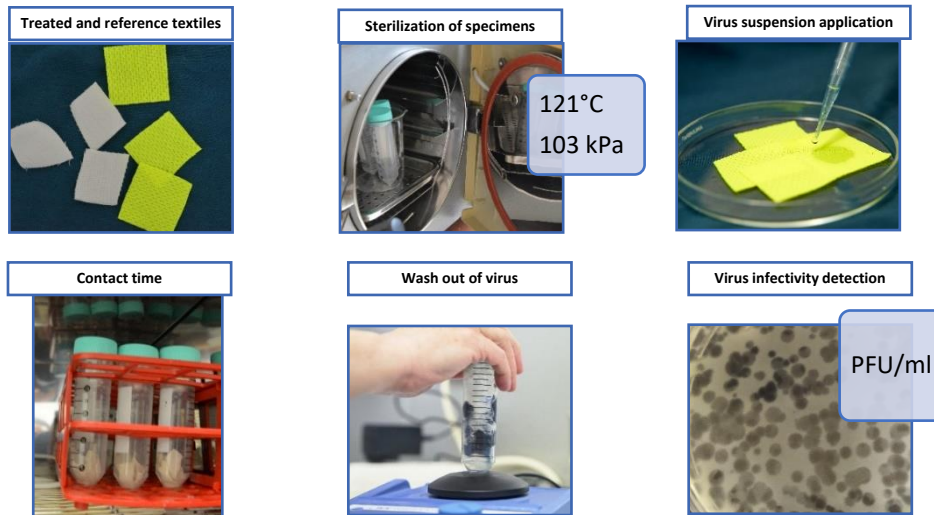
Figure 1. Determination of antiviral efficiency of textile products by the use of bacteriophage-based method. Illustration photos show sample preparation and treatment, virus application and recovery and resulting bacteriophage plaques in top agar.

Antiviral activity of samples 1, 2, 3, 4 tested with references 736A (left plot) and 737A (right plot)
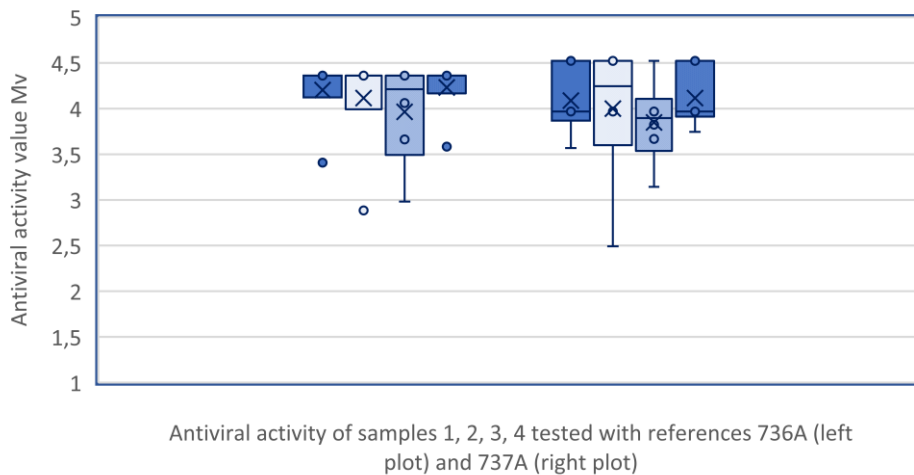
Figure 2. Boxplots of antiviral activity (*Mv*) results distribution. 6 *Mv* values were determined for each sample (1 – 4) with reference 736A and 6 *Mv* values with reference 737A. Average Va value of *lg* (PFU) was taken for Mv calculation.

Table 2a. Antiviral activity values (*Mv*) of treated samples (*lg* reduction Va/Vc, PFU/ml). Outliers were excluded from dataset used for calculation.

	Mv			
	Sample 1	Sample 2	Sample 3	Sample 4
Reference 736A	4.4	4.4	4	4.4
Reference 737A	4	4	3.8	4.1

The samples were compared on the base of *Mv* value, calculated as described in methods part. This value is important for evaluation of effectivity of antiviral treatment (categories according to Annex F of ISO 18184 standard [9]). The two available reference woven cotton materials were used with the aim to confirm or exclude the effect of reference fabric structure on antiviral activity results.

The Shapiro-Wilk test for some of sample results gave p-values by order of magnitude lower than $p = 0.05$, which means, that null hypothesis of normality was rejected and some of datasets were non normal distributed. That's why we used boxplots for identification of outliers, where the box ranges from the first (Q1) to third quartile (Q3), the line inside box represents median and minimum is calculated Q1-1.5*interqaurtile range (IQR) and maximum is calculated Q3+1.5*IQR, points outside the whiskers are outliers (Fig. 2). It shows that there are three outliers in test with reference 736A; these outliers were excluded from our dataset for further calculations (Table 1b). Because of non-normal

distribution of data with different number of values and repeating values, the exact Wilcox test was used. The p-values given by this test when testing all datasets with each other ranged between 0.18 to 1.00, which means the null hypothesis was accepted and antiviral activity of all samples was similar with significance level 5%.

The excellent antiviral treatment effect (*Mv* value above 3) was detected for all samples, concerning categories according to Annex F of ISO 18184 standard [9]. The values of antiviral activity of four tested samples are not significantly different (Figure 2 and Table 2a).

The results of the testing of 4 samples of treated textiles with confirmed antiviral activity have shown, that bacteriophage Phi6 is an optimal surrogate enveloped virus for the testing of antiviral activity of textiles as porous surfaces. Phi6 has many advantages for antiviral activity testing – resistance to environmental conditions, fast and safe processing, temperature optimum near room temperature [14]. The cultivation of bacterial host cells differs from the cultivation and preparation of animal cells as hosts of animal viruses. The advantages of the bacterial host cells are the fast growth, agar-based techniques of detection and the resistance against wide spectrum of environmental conditions. The benefit of

bacteriophage-based method is the possibility of agar-diffusion preliminary test. It is allowed by completely different detection of infectious particles.

The results of the preliminary agar diffusion test (Table 3, Figure 3) have shown the antibacterial and antiviral activity of all tested samples, which confirms the leaching type of the antiviral treatment used for all 4 samples. Inhibition zones slightly differ depending on the textile material and their contact with agar surface. No inhibition was detected with the use of square samples of reference untreated material.

The antiviral substances of the un-leaching type are commonly preferred for the multiply-used products that must retain their antiviral properties over many washing cycles, but leaching type textiles may be more biocidal, on the other side. Specific technics, as dipping-padding-drying process or sol-gel process, help to prepare durable, non-leaching antipathogenic finishing of fabrics. The leaching-type textiles are commonly used for single-used textile products (surgical gowns, surgical caps) and specifically developed for dermatological applications (cotton wound dressing) [4] [17] [18]. The fast preliminary testing of antimicrobial/ antiviral activity and estimation of the stability of the antiviral treatment is the benefit of bacteriophage-based method of antiviral activity determination.

Table 2b. Values of antiviral activity of individual specimens determined with the use of 2 different reference materials signed 736A and 737A. Each test run was provided with 3 treated specimens and 3 untreated reference specimens. Outliers, identified by boxplot analysis, are marked by red colour. Values obtained by the inclusion of outliers are marked by blue colour. Marked values were excluded from dataset used for further calculations.

Reference	736A							
Sample	1	1	2	2	3	3	4	4
Mv1	4.36	4.36	4.36	4.36	3.66	4.36	4.36	4.36
Mv2	4.36	4.36	4.36	4.36	2.98	4.36	3.58	4.36
Mv3	3.41	4.36	4.36	2.88	4.36	4.06	4.36	4.36
SD	0.55	0	0	0.85	0.69	0.17	0.45	0
Mv average	4.04	4.36	4.36	3.87	3.67	4.26	4.10	4.36
Mv	4.20		4.12		3.97		4.23	

Reference	737A							
Sample	1	1	2	2	3	3	4	4
Mv1	4.52	3.97	4.52	3.97	3.82	3.97	4.52	3.97
Mv2	4.52	3.97	4.52	3.97	3.14	3.97	3.74	3.97
Mv3	3.57	3.97	4.52	2.49	4.52	3.67	4.52	3.97
SD	0.55	0	0	0.85	0.69	0.17	0.45	0
Mv average	4.20	3.97	4.52	3.48	3.83	3.87	4.26	3.97
Mv	4.09		4.00		3.85		4.12	

Table 3. Inhibition of growth of cells (*Pseudomonas* sp. DSM 21482) and plaque formation (bacteriophage Phi6 DSM 21518) in agar diffusion test.

	Inhibition of cells and virus in diffusion test			
Treated sample	Sample 1	Sample 2	Sample 3	Sample 4
Inhibition zone	++	++	+	++

(a) no inhibition of host cells (lawn) and virus (plaques) - sample without antiviral finishing

(b) narrow zone of inhibition of pre-inoculated host + virus (sample 3)

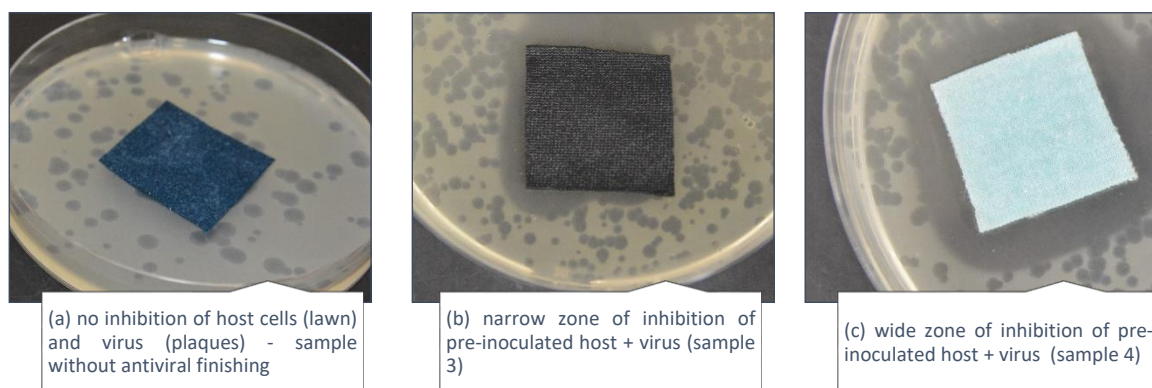(c) wide zone of inhibition of pre-inoculated host + virus (sample 4)

Figure 3. Agar diffusion test of textiles on double layer agar plate. (a) textile sample without antiviral treatment (knitted sample of blue colour), (b) sample 3 – narrow zone of inhibition of host strain and the bacteriophage phi6, (c) sample 4 – wide zone of inhibition of growth of cells and virus.

In this study, the method of antiviral activity testing of textiles was adapted to testing with a bacterial virus, enveloped bacteriophage phi6, surrogate of enveloped human viruses SARS-CoV-2, influenza virus and Ebola virus. The surrogate bacterial virus with different cultivation technique allows for efficient and fast testing without the influence of side effects of host-cell virus system (for example the need for medium dillution or the surface passivation of Ag nanoparticles, described by Imoto [19]). The described method is available for wide spectrum of testing purposes including the testing of antiviral activity of surfaces and textiles directly in the environment where they are used. Testing in real conditions can then follow up the verification of the antiviral effect of the tested material.

The bacteriophage-based method of antiviral activity testing allows to test antiviral properties of comprehensive range of samples in the frame of projects aimed on development of new antiviral textiles. The experimental design based on the comparison of specimens treated by different concentrations of active compound or produced by different finishing methods can work with a sufficient number of samples. Its advantage is rapid and accurate quantification (nearly all bacteriophage particles are infectious) via plaque forming units number determination.

CONCLUSIONS

The development and utilization of antiviral fabrics represent a significant advancement in the field of textile technology, with the potential to contribute to public health and safety. Innovations in the field of antiviral textiles, including biosensor materials, are not possible without effective and safe methods of antiviral activity testing. From this point of view, bacteriophages can be valuable tools in the evaluation of antiviral treatments or materials, providing comparable results for textile products evaluation. This paper describes the optimized method of antiviral efficiency testing available in conditions of BSL-2 laboratory equipped for common microbiological testing. The bacteriophage-based method allows to determine antiviral activity of wide spectrum of textile products, developed for the use in healthcare, public transportation, catering, space research. The effective testing method can help to develop new functional, health-friendly and environmental-friendly textile products.

REFERENCES

1. Nastasi N., Renninger N., Bope A., et al.: Persistence of viable MS2 and Phi6 bacteriophages on carpet and dust. Indoor Air 32, 2022, e12969. https://doi.org/10.1111/ina.12969
2. Whitworth C., Mu Y., Houston H., et al.: Persistence of Bacteriophage Phi 6 on Porous and Nonporous Surfaces and the Potential for Its Use as an Ebola Virus or Coronavirus Surrogate. Appl Environ Microbiol. 86(17), 2020, e01482-20. https://doi.org/10.1128/AEM.01482-20
3. Plohl O., Fric K., Filipić A., et al.: First Insights into the Antiviral Activity of Chitosan-Based Bioactive Polymers towards the Bacteriophage Phi6: Physicochemical Characterization, Inactivation Potential, and Inhibitory Mechanisms. Polymers (Basel). 14(16), 2022; 3357. https://doi.org/10.3390/polym14163357
4. Gulati R., Sharma S., Sharma R. K.: Antimicrobial textile: recent developments and functional perspective. Polym. Bull. 79(8), 2022, pp. 5747–5771. https://doi.org/10.1007/s00289-021-03826-3
5. Zhang Y., Fan W., Sun Y., et al.: Application of antiviral materials in textiles: A review. Nanotechnology Reviews, 10 (1), 2021, pp. 1092-1115. https://doi.org/10.1515/ntrev-2021-0072
6. Qian J., Dong Q., Chun K. et al.: Highly stable, antiviral, antibacterial cotton textiles via molecular engineering. Nature Nanotechnology 18, 2023, pp. 168–176. https://doi.org/10.1038/s41565-022-01278-y
7. Zanchettin G., Falk G. S., González S. Y., et al.: Tutorial review on the processing and performance of fabrics with antipathogenic inorganic agents. Cellulose 30, 2023, pp. 2687–2712. https://doi.org/10.1007/s10570-023-05060-8
8. Ščasníková K., Dubec A.: The influence of high-temperature plasma on permanence of antimicrobial nano-finish. Fibres and Textiles 30(4), 2023, pp. 41-49. https://doi.org/10.15240/tul/008/2023-4-005

9. ISO 18184: Textiles – Determination of antiviral activity of textile products. ISO: Geneva, Switzerland, 2019.

10. Adcock N. J., Rice E. W., Sivaganesan M., et al.: The use of bacteriophages of the family Cystoviridae as surrogates for H5N1 highly pathogenic avian influenza viruses in persistence and inactivation studies. J Environ Sci Health A Tox Hazard Subst Environ Eng. 44(13), 2009, pp. 1362-1366. https://doi.org/10.1080/10934520903217054

11. Weyersberg L., Klemens E., Buehler J., et al.: UVC, UVB and UVA susceptibility of Phi6 and its suitability as a SARS-CoV-2 surrogate. AIMS Microbiol. 8(3), 2022, pp. 278-291. https://doi.org/10.3934/microbiol.2022020

12. Gallandat K, Lantagne D.: Selection of a Biosafety Level 1 (BSL-1) surrogate to evaluate surface disinfection efficacy in Ebola outbreaks: Comparison of four bacteriophages. PLoS One. 12(5), 2017, e0177943. https://doi.org/10.1371/journal.pone.0177943

13. Serrano-Aroca Á.: Antiviral Characterization of Advanced Materials: Use of Bacteriophage Phi 6 as Surrogate of Enveloped Viruses Such as SARS-CoV-2. International journal of molecular sciences, 23(10), 2022, 5335. https://doi.org/10.3390/ijms23105335

14. Prussin A. J., Schwake D. O., Lin K., et al.: Survival of the Enveloped Virus Phi6 in Droplets as a Function of Relative Humidity, Absolute Humidity, and Temperature. Applied and environmental microbiology 84(12), 2018, e00551-18. https://doi.org/10.1128/AEM.00551-18

15. Rohde Ch., Wittmann J.: Supply, storage, propagation and purification of phages, online: https://www.dsmz.de/fileadmin/user_upload/Collection_allg/DSMZ_Cultivation_of_Phages.pdf [cit. 2023]

16. Kropinski A. M., Mazzocco A., Waddell T. E., et al.: Enumeration of bacteriophages by double agar overlay plaque assay. Methods in molecular biology 501, 2009, pp. 69-76. https://doi.org/10.1007/978-1-60327-164-6_7

17. Krishnan P. D., Banas D., Durai R. D., et al.: Silver Nanomaterials for Wound Dressing Applications. Pharmaceutics. 12(9), 2020, 821 P. https://doi.org/10.3390/pharmaceutics12090821

18. Bar G., Biswas D., Pati S., et al.: Antiviral Finishing on Textiles – An Overview. Textile and leather review 4(1), 2021. https://doi.org/10.31881/TLR.2020.17

19. Imoto Y., Seino S., Nakagawa T., et al.: Quantitative Methods for Testing Antiviral Activities of Textile Fabrics. J Antimicrob Agents 3.3, 2017, 146. https://doi.org/10.4172/2472-1212.1000146

SPECTROKINETIC INVESTIGATION OF THE PHOTOCHROMIC SYSTEM UNDER CONTINUOUS UV IRRADIANCE USING REFLECTANCE VS. TIME CURVES

Solanki, Utkarshsinh B.[*]; Viková, Martina and Vik, Michal

Department of Material Engineering (KMI), Technical University of Liberec, Studentska 1402/2, Liberec, Czech Republic

ABSTRACT

The photochromic properties of the dye 5-chloro-1,3,3-trimethylspiro[indoline-2,3'-[3H] naphtho[2,1-b] [1,4]-oxazine] were investigated by exposing it to continuous monochromatic irradiation using 360 nm ultraviolet irradiation using photochromic prints at 293.15 ± 2 K; it undergoes a photocoloration and photodecoloration state, thus following the dynamics of a photochromic cycle of growth and decay phase, respectively. Even if the isolated photo isomeric form of the photochromic dye structure is unavailable, one can quantitatively analyse the photo-induced kinetics of photochromic systems using the raw reflectance data. The quantum colour yield is represented by colour span values [K/S] obtained by converting reflectance data to Kubelka-Munk values. The dynamics of the photoreaction in a photochromic system can be examined by analysing the constants for the rate of colouration and decolouration caused by light. By employing first-order kinetics, the dependent dominant wavelength [λ_{max}] can be determined by fitting the raw data obtained as a change in reflectance values from the FOTOCHROM3 spectrophotometer. The relationship between the colour span values and the concentration of the photochromic dye employed in the photochromic prints is linear.

KEYWORDS

Photokinetics; Photochromic system; Spiroxazine dye; Colour span values; UV irradiance.

INTRODUCTION

Photochromism is a photoinduced reversible phenomenon, as it undergoes colour transformation upon UV irradiance, and its removal goes to its colourless form. Spiro-[-indoline-napthoxa-zines] and spironapthoxazines are two well-known photochromic compounds. They comprise two heterocyclic moieties linked by a tetrahedral spiro-carbon to stop conjugation. Figure 1 shows how the spironapthoxazine-based photochromic dye changes colour when exposed to light. The dye is 5-chloro-1,3,3-trimethylspiro [indoline-2,3'-[3H] naphtho[2,1-b] [1,4]-oxazine].

When light hits the spiroxazine-based chromic dye, the spiro-carbon (C_{spiro}) bond breaks apart. Thermal cis-trans isomerisation into the zwitterionic or quinonoid merocyanine structure follows this process. If you change the amount of UV light that a certain
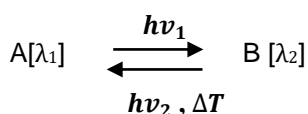
$$A[\lambda_1] \underset{h\nu_2 \,,\, \Delta T}{\overset{h\nu_1}{\rightleftharpoons}} B[\lambda_2]$$

Figure 1. Photochromic phenomena and its interconversion between two states.

type of chromophore absorbs and the number of molecules that make up that light, the molecules change at the molecular level and behave as H-aggregates and J-aggregates. This causes the red and blue shift in the electromagnetic spectrum from its main wavelength. The colourful transformation over the measured UV irradiance cycle is considered a change in energy level between its ground and excited states. This process is crucial for understanding the molecular structure's reactivity, stability, and physical transformation in its pure form. However, the screen-printing method micro-encapsulates the photochromic dye, making it less pure, and prepares the printing paste with additional additives. The stability of these photochromic systems under UV light, the duration of their exposure, and their lack of colour influence their reaction to UV light. These things influence how they react backwards when exposed to visible light [1-3].

Cotton-based photochromic fabrics use technological methods to develop a photoresponsive system, including printing, coating, padding, sol-gel, and exhaust [3]. Some technological procedures for producing photochromic systems include mass dyeing, melt spinning, screen printing, inkjet printing,
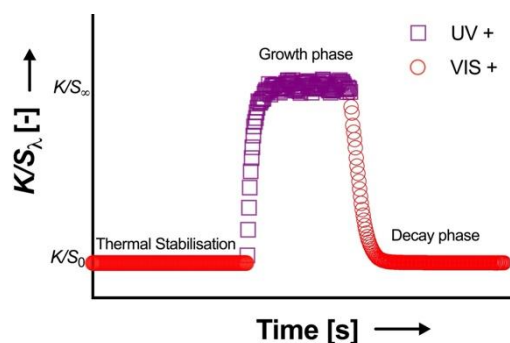
Figure 2. General kinetic profile curve of a photochromic cycle.

pad-dry-cure, exhaustion dyeing, and electrospinning. Each technical method offers distinct merits and drawbacks. Little et al. prepare the photochromic fabric using screen printing and photochromic colourants as dispersed dyes [4,5]. Viková et al. constructed the chromic system using a variety of photochromic prints and studied colorimetric properties using the screen-printing method [6–9]. Solanki et al. developed the photo-fatigue measurement methodology, which irradiates the photochromic system under UV irradiance (the exposure time in seconds) and decolourisation time. This results in the upper plateau of the typical curve of a photochromic cycle for photochromic prints made using screen-printing with the same photochromic dye [8, 9].

The dynamics of kinetic behaviour in a photochromic cycle can be illustrated in Figure 2. The photochromic cycle curve illustrates the colouration and decoloration modes of conduct when a UV light source is present and absent, respectively, in a continuous mode. It starts with the thermal stabilisation (VIS+), followed by the growth phase (UV+) and the decay phase (VIS+) [6-9].

Several studies provide valuable insights for modelling the kinetics of a photochromic system in continuous mode. Pimienta et al. [10] investigate the kinetics of spiropyran photochromic systems under continuous light exposure. This allows us to look into the kinetics of photochromic compounds in solution. Bouas-Laurent & Dürr [11] discuss fatigue, main photochromic parameters, and spectrokinetic aspects, all of which are critical for understanding the behaviour of photochromic systems under continuous irradiation. Maafi et al. [12] present useful spectrokinetic methods for investigating photochromic kinetics, offering formalisms and procedures to analyse photochromic system kinetics. We can learn a lot about how to model the kinetics of photochromic systems in continuous mode by looking at things like fatigue, spectrokinetic methods, structural influences, and different ways to test and characterise the kinetics of photochromic systems. The photokinetics of the photochromic pigment under continuous irradiation vary from one state to another.

However, the essential parameters considered when conducting such studies are the following:

1. Dependence of the absorption of UV irradiance
2. Choice of media or substrate, the polarity of the base material
3. Choices of light sources of a specific wavelength
4. Choice of concentration, following Lambert's law
5. Monitoring the reaction
6. The reaction procedure is temperature control during the measurement, leading to the backward reaction and thus adding photodegradation due to the temperature.

Photo-induced kinetic modelling is essential for understanding the behaviour of photoreversible photochromic systems, which undergo colouration (growth phase) and decolouration (decay phase). The spectral absorbance value (measured with a spectrophotometer), the quantum yield (colouration value), the temperature (measurements were done at room temperature), the concentration of the photochromic dye, and the base substrate can be a solvent form that is applied to the surface of the fabric or doping in the form of a polymeric matrix. All of these things can change the kinetics of photochromic compounds. These factors impact the photochemical and thermal reaction kinetics, which are crucial for predicting the colour performance of photochromic textiles [13, 14]. To understand the photokinetics of photochromic prints, it is essential to consider the complex relationship between photochromic compounds and the kinetic processes governing their colouration and decolouration reactions. Seipel et al. [13, 14] introduced an extended kinetic model that defines rate constants for colouration, decay, and decolouration, allowing for predicting colour performance in photochromic textiles. This model offers a thorough comprehension of how specific fabrication parameters, like inkjet printing and UV-curing processes, can modify the kinetics of the photochromic reaction. We commonly use first-order kinetics models to accurately describe photochromic colour behaviour, representing colouration and decolouration phases with their respective rate constants [17]. Kinetic modelling and its parameters can elucidate the complex interplay of kinetic processes in photochromic prints. By studying the kinetic behaviour of photochromic dye as photochromic prints, researchers can uncover new opportunities for designing smart textiles, optical devices, and functional materials.

EXPERIMENTAL

Photochromic prints preparation

Six photochromic systems were created using different concentrations of a 5-chloro-1,3,3-trimethylspiro[indoline-2,3'-[3H] naphtho[2,1-b] [1,4]-oxazine] dye: 50 g.kg^{-1} (Purple A), 100 g.kg^{-1} (Purple

B), 150 g.kg^{-1} (Purple C), 200 g.kg^{-1} (Purple D), 250 g.kg^{-1} (Purple E), and 300 g.kg^{-1} (Purple F). Figure 1 displays the utilised photochromic dye's closed and open forms.

Kinetic measurements using a FOTOCHROM3 spectrophotometer

The spectrophotometer FOTOCHROM3 (Figure 3(a)) was used to perform photo-induced kinetic measurements to assess the photochromic system's resistance to fatigue induced by continuous UV illumination. The gadget uses the CHROMADYNAMIK software to give real-time colour measurements in UV and visible light sources and deliver continuous irradiance mode spectrum reflectance data. The samples were subjected to continuous and cyclical exposure to both light sources using a measuring aperture with a diameter of 28 mm. The photochromic prints were subjected to a continuous UV LED light with a 360 nm wavelength and a spectrum irradiance strength of 799 W.cm^{-2}. This radiation source was used to assess the photo colouration of the chromic systems. The FOTOCHROM3 device enables the measurement of a photochromic cycle's UV+ and VIS+ phases. It uses a 360 nm UV light source (UV+) and a visible light source (VIS+) to measure the kinetics of the photochromic system. This allows for measuring changes in reflectance data over time during the photocolouration and photodecolouration phases. Figure 3(b) shows the power distribution of the UV LED and visible light sources used in the spectrophotometer, as measured by a spectroradiometer.

The experiment's environmental parameters included an ambient relative humidity of 45–55 % and a measurement device temperature of 20˚C ± 2˚C. The UV irradiance dose was measured as UV dose [mW.s.cm^{-2}] = UV energy received [mW.cm^{-2}] * UV irradiance time [s] used for UV exposure under continuous UV irradiance using the FOTOCHROM 3 device. The photo colouration UV irradiance time was 240 s, and the photo decolouration (photobleaching) time was 360 s for all photochromic systems.

Data treatment

The first-order association model describes the photocolouration transformation reaction process when the photochromic system is exposed to UV irradiance. The first-order dissociation model (Figure 4(a)) represents the photocolouration of colour intensity. Upon removing the UV light source, the chromic system tends to regain its original form under the fluence of the used visible light source; the relaxation phase follows the first-order dissociation model (Figure 4(b)). Under continuous monochromatic irradiation, the photochromic system can reach its photo-steady equilibrium state (the upper plateau curve of the growth phase) and in opened (coloured state) form. Under continuous UV irradiation, we used a base substrate as a textile fabric form. This colour change during the photo colouration phase is measured as a change in the reflectance, absorbance, or scattering, which can be visualised as chromogenic.

When exposed to a UV light source, the photochromic dye's colour change is quantified using the Kubelka-Munk function. The Kubelka-Munk function, along with Beer's law, is characterised by having a single wavelength. The colour values (K/S) were determined using the Kubelka-Munk function, equation 1 [8,9], to the reflectance spectral data.
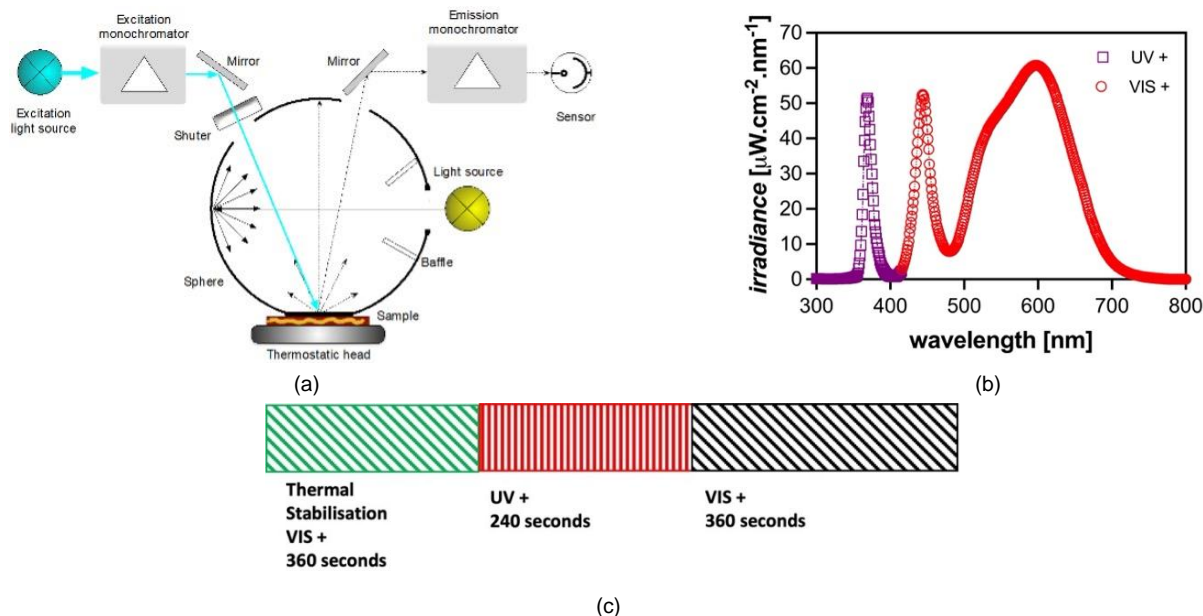

(a)

(b)

(c)

Figure 3. Schematic illustration of a) FOTOCHROM3 spectrophotometer, b) SPD curves of used light sources, c) Fatigue scenario used under continual UV irradiance.
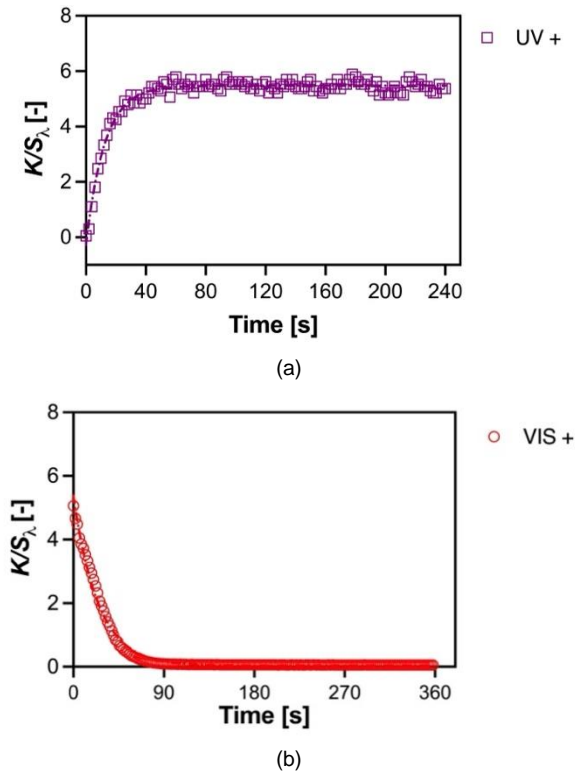
(a)

(b)

Figure 4. Photochromic cycle: a) Growth phase with one-phase association fit, b) Decay phase with one-phase dissociation fit.

$$K/S_\lambda = \frac{(1-R_\lambda)^2}{2R_\lambda}, \qquad (1)$$

where K/S_λ – where K_λ is the absorption coefficient, and S_λ is the scattering coefficient of the photochromic dye observed at its dominant wavelength in the visible spectra of an electromagnetic spectrum

The photo-kinetic behaviour of the photochromic system is analysed using the first-order kinetic model, as demonstrated in earlier research that investigated the kinetic behaviour of several photochromic dyes and pigments [8-13]. This behaviour is described by Equation 2.

$$K/S_{(t)} = \left(K/S_{(0)} - K/S_{(\infty)}\right)\exp(-kt) + K/S_{(\infty)}, \quad (2)$$

where, the subscript t – actual time, 0 – at the beginning of the reaction (photo colouration phase), ∞ - time at infinity (reaching photo-steady equilibrium state, upper plateau and lower plateau for the growth phase and decay phase, respectively), k – rate constant [s^{-1}], t – UV irradiance time used in [s] during the growth phase for each photochromic cycles (n), $K/S_{(\infty)}$ – the upper plateau obtained after fitting the raw data of each growth phase cycles, (n) – is the growth phases of each photochromic cycle.

Equation 2 represents a mathematical model that examines the relationship between photochromic systems' growth and decay phases, thus following the first-order kinetics model. It is used to study the photo-fading behaviour of these systems under

observed cycles of UV irradiation. Nevertheless, this study specifically examines the photo-fading characteristics of development phases, which are assessed across multiple cycles of UV irradiation utilising various modes. The photochromic system exhibits a photo-fading behaviour when subjected to several UV irradiation cycles during consecutive measured growth stages. Thus, the quantity of UV irradiance cycles is denoted as the converted UV dosage required for photo-fading photochromic dye molecules. The data processing begins by converting the acquired reflectance data into colour intensity values at their most prominent wavelength using the Kubelka-Munk (*K/S*) function, as described in Equation 1. Subsequently, the data is further processed for evaluation using Equation 2, as previously mentioned.

The photochromic system's dominant wavelength λ_{max} = 570 nm experiences a transition in colour, shifting from a colourless state to a vivid, deep purple hue. The colour span values were adjusted to a one-phase association model based on its dominant wavelength to calculate the kinetic parameters: rate constant k [s^{-1}], half-life ($t_{1/2}$) and maximum colour span value (K/S_{max}) for the photocolouration phase. Similarly, a one-phase dissociation model was used to analyse the decolouration phase. Observations have been made on the cycles of recorded UV irradiance, the spans acquired, and the behaviour of the plateau in the extended continuous mode. The photodegradation behaviour adheres to a one-phase dissociation model for all measured cycles. Furthermore, we note that the photodegradation behaviour is consistent for the UV mode without a relaxation phase, in which the photochromic system is solely exposed to UV light. The raw data was processed and analysed using the GraphPad 10 (10.3.0) statistical software on the MacOS platform.

RESULTS AND DISCUSSION

The study examines the spectrokinetic analysis of a photochromic dye based on spironapthoxazine. The photochromic system was created as photochromic prints utilising the screen-printing technique. The photochromic dye molecules are deposited on the surface of the textile fabric. We obtained the kinetic measurements using a specialised spectrophotometer known as FOTOCHROM3. This instrument allows us to observe the photoreaction of a photochromic system as it undergoes the growing phase (photocolouration) and decay phase (decolouration) of a general profile curve in a photochromic cycle. We performed the photoexcitation using a monochromatic light source, specifically ultraviolet (UV) light, with a wavelength of 360 [nm]. We conducted the thermal relaxation of a photochromic device by exposing it to visible light from a continuous irradiance source. In the UV irradiance mode, the fabric absorbs the intensity of

the UV light, which partially penetrates and bends back due to its structure. The FOTOCHROM3 device measured the reflectance values of each photochromic system, specifically capturing the changes in photocoloration and decoloration. This measurement was done under the continuous irradiance mode, with the growth and decay phases seen over a specific period.

The reflectance vs. time curves from the FOTOCHROM3 spectrophotometer were used to process the data for each photochromic system using the stepwise method described in the data treatment section. Figure 5 presents the K/S value of each photochromic system at its dominant wavelength during the growth and decay phases, as determined by fitting the one-phase kinetic model. We determined the kinetic parameters by fitting the spectrum data using the one-phase association and dissociation model to analyse the growth and decay phases.

The rate constants for photocoloration and decoloration of each photochromic system are graphed in Figure 6. Furthermore, the half-life values of each photochromic system throughout its growth and decay phases are graphically represented in Figure 7. The colour span values of each photochromic system and their dependence on the dye concentration are linear, as illustrated in Figure 8. The measured energy of the UV irradiance area is 7.9 W.m^{-2}, whereas for the visible region, it is 97.79 W.m^{-2}. The diameter of the aperture for irradiance during excitation and relaxation is 28 mm, and the exposure area is 0.0006154 m^{-2}. The exposure phase lasted 240 s, and the decay phase lasted 360 s. The observed photon flux for UV+ and VIS+ is defined as Φ_{UV+} and Φ_{VIS+}, and the estimated values for Φ_{UV+} are 1.953×10^{22} photons.m^{-2} and Φ_{VIS+} are 2.390×10^{23} photons.m^{-2}, respectively.

(a) (b)

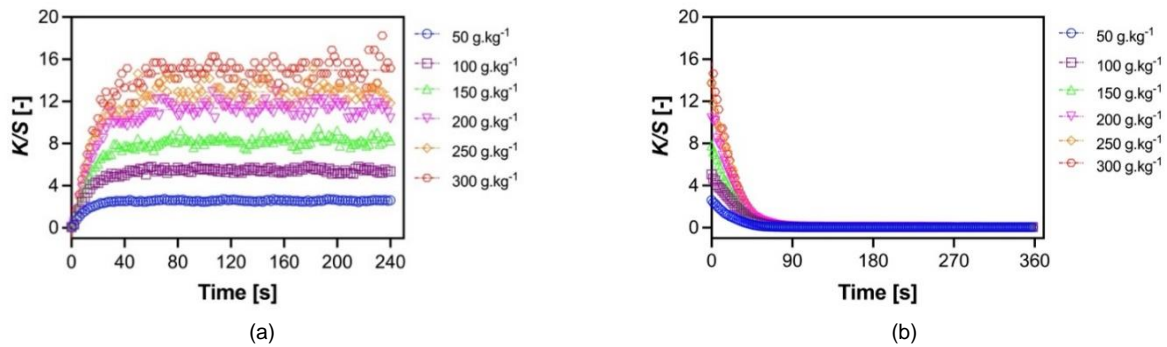**Figure 5.** The photochromic system's: a) Growth phase with one-phase association fit, b) Decay phase with one-phase dissociation fit.
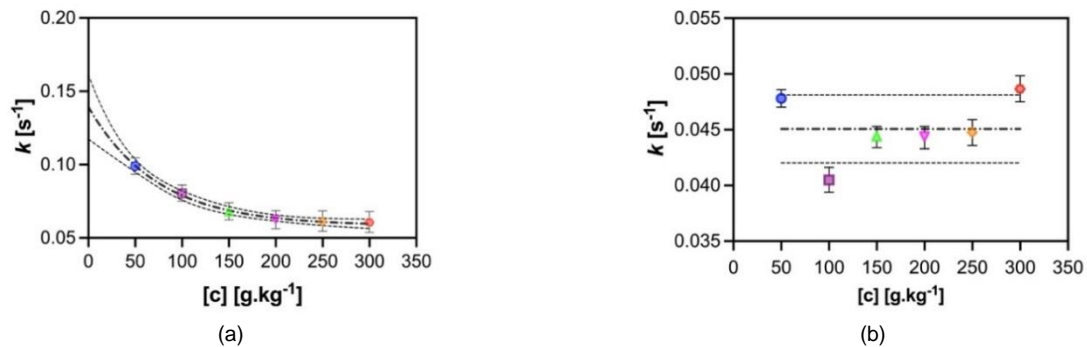

(a) (b)

Figure 6. The photochromic system's: a) Growth phase rate constant, b) Decay phase rate constant under continual irradiance mode.
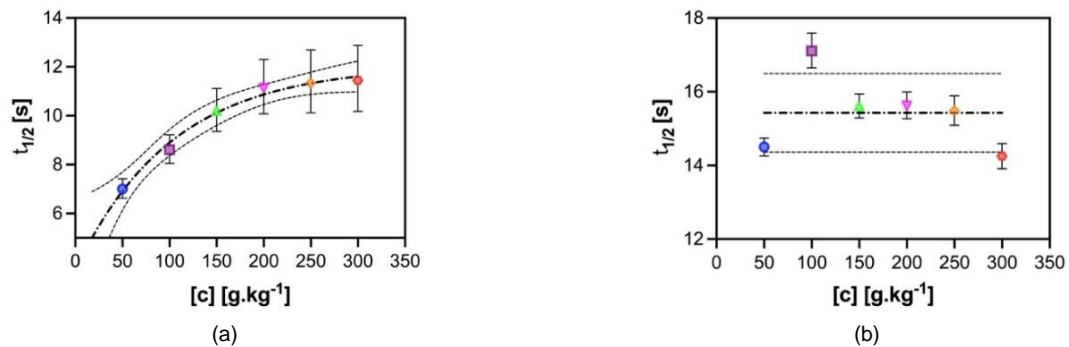

(a) (b)

Figure 7. The photochromic system's: a) Growth phase half-life (s), b) Decay phase half-life under continuous irradiance mode.
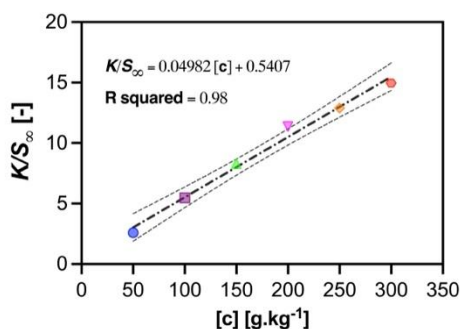
Figure 8. Dependency of photo colouration value vs. the concentration of photochromic dye under continuous UV irradiance.

CONCLUSION

The research study provided relevant information regarding photoreaction kinetics in a photochromic system. This reaction takes place under continuous irradiance mode and involves the process of photo colouration and decolouration. The reflectance vs. time curves produced during the photochromic cycle were used to analyse this process. The photochromic dye has a half-life of around six seconds when it is in a state of photo-excitation and a half-life of two seconds when the dye molecules are decolourising. The spiroxazine dye in textile print form was exposed to a continuous and uniform beam of monochromatic light. The light source used had a 360 nm wavelength and was stimulated by UV radiation. The measurements were taken at a temperature of 293.15 ± 2 K. Nevertheless, the transformation from a colourless state to a coloured one in the photoreaction is contingent upon the wavelength of light, namely within the visible spectrum, where the majority wavelength is found. Photodecolouration also occurs at the most prominent wavelength in the visible spectrum. The colour span values represent the highest colour intensity achieved during the phase of colour change caused by light exposure. These values are derived by analysing each photochromic system's reflectance versus time curves. The photodegradation during a single kinetic measurement is insignificant, as it only occurs and can be detected during a series of UV irradiation cycles during the growth phase of a photochromic cycle. The rate constants for photocolouration and decolouration adhere to the decay model, with the former increasing as the dye concentration within the photochromic system increases, while the latter remains relatively constant. The colour yield of the photochromic system is directly proportional to the dye concentration within the system, resulting in a linear relationship.

Credit authorship contribution statement: <u>Solanki U.B.</u>: *Conceptualization, Experimentation, Data curation,* *investigation, data analysis, writing – Original draft, review, editing, project administration.* <u>Viková M.:</u> *Review and editing.* <u>Vik M.:</u> *Review and editing.*

REFERENCES

1. Pimienta V., Frouté C., Deniel M.H., et al.: Kinetic modelling of the photochromism and photodegradation of a spiro [indoline-naphthoxazine]. Journal of Photochemistry and Photobiology A: Chemistry, 122(3), 1999, pp. 199-204. https://doi.org/10.1016/S1010-6030(99)00023-4

2. Biteau J., Chaput F., Boilot J.P.: Photochromism of spirooxazine-doped gels. The Journal of Physical Chemistry, 100(21), 1996, pp. 9024-9031. https://doi.org/10.1021/jp953607o

3. Vik M., Periyasamy A.P.: Chromic materials: fundamentals, measurements, and applications. CRC Press, 2018.

4. Little A.F., Christie R.M.: Textile applications of photochromic dyes. Part 2: factors affecting the photocoloration of textiles screen‐printed with commercial photochromic dyes. Coloration Technology, 126(3), 2010, pp. 164-170. https://doi.org/10.1111/j.1478-4408.2010.00242.x

5. Little A.F., Christie R.M.: Textile applications of photochromic dyes. Part 3: factors affecting the technical performance of textiles screen‐printed with commercial photochromic dyes. Coloration Technology, 127(5), 2011, pp. 275-281. https://doi.org/10.1111/j.1478-4408.2011.00307.x

6. Viková M.: Photochromic Textiles, Heriot-Watt University, Scottish Borders Campus, Edinburgh, UK, 2011, pp. 53–147. http://hdl.handle.net/10399/2439

7. Vikova M., Vik M.: Photochromic textiles and measurement of their temperature sensitivity. Research Journal of Textile and Apparel, 18(3), 2014, pp. 15-21. https://doi.org/10.1108/RJTA-18-03-2014-B002

8. Solanki U., Vikova M.: FATIGUE STUDY OF SPIRO [INDOLINE-NAPTHOOXAZINES] PIGMENT USING COLORIMETRIC DATA IN A CONTINUOUS MODE OF UV IRRADIANCE. Fibres and Textiles, 28(4), 2021, pp. 93-101. http://vat.ft.tul.cz/2021/4/VaT_2021_4_13.pdf

9. Solanki U., Viková M., Vik M.: New Method for Prediction of Photochromic Textiles Fatigue Behavior. In Materials Science Forum. Trans Tech Publications Ltd, 1063, 2022, pp. 163-172 https://doi.org/10.4028/p-ld65c6

10. Pimienta V., Lavabre D., Levy G., et al.: Kinetic analysis of photochromic systems under continuous irradiation. Application to spiropyrans. The Journal of Physical Chemistry, 100(11), 1996, pp. 4485-4490. https://doi.org/10.1021/jp9531117

11. Bouas-Laurent H., Dürr H.: Organic photochromism (IUPAC technical report). Pure and Applied Chemistry, 73(4), 2001, pp. 639-665. https://doi.org/10.1351/pac200173040639

12. Maafi M.: Useful spectrokinetic methods for the investigation of photochromic and thermo-photochromic spiropyrans. Molecules, 13(9), 2008, pp. 2260-2302. https://doi.org/10.3390/molecules13092260

13. Seipel S., Yu J., Periyasamy A. P., et al.: Inkjet printing and UV-LED curing of photochromic dyes for functional and smart textile applications. RSC advances, 8(50), 2018, pp. 28395-28404. https://doi.org/10.1039/C8RA05856C

14. Seipel S., Yu J., Viková M., et al.: Color performance, durability and handle of inkjet-printed and UV-cured photochromic textiles for multi-colored applications. Fibers and Polymers, 20, 2019, pp.1424-1435. https://link.springer.com/article/10.1007/s12221-019-1039-6

15. Kellmann A., Tfibel F., Dubest R., et al.: Photophysics and kinetics of two photochromic indolinospirooxazines and one indolinospironaphthopyran. Journal of Photochemistry and Photobiology A: Chemistry, 49(1-2), 1989, pp. 63-73. https://doi.org/10.1016/1010-6030(89)87106-0

16. Bär R., Gauglitz G.: Limitations to the kinetic analysis of thermoreversible photoreactions of photochromic systems.

Journal of Photochemistry and Photobiology A: Chemistry, 46(1), 1989, pp. 15-26.
https://doi.org/10.1016/1010-6030(89)87029-7

17. Pimienta V., Micheau J.C.: Kinetic analysis of photoreversible photochromic systems under continuous monochromatic irradiation from Abs. vs time curves. Molecular Crystals and Liquid Crystals Science and Technology. Section A. Molecular Crystals and Liquid Crystals, 344(1), 2000, pp. 157-162.
https://doi.org/10.1080/10587250008023830

18. Pimienta V., Lavabre D., Levy G., et al.: Kinetic analysis of photochromic systems under continuous irradiation. Application to spiropyrans. The Journal of Physical Chemistry, 100(11), 1996, pp. 4485-4490.
https://doi.org/10.1021/jp9531117

19. Chowdhury M.A., Joshi M., Butola B.S.: Photochromic and thermochromic colorants in textile applications. Journal of Engineered Fibers and Fabrics, 9(1), 2014, 155892501400900113.
https://doi.org/10.1177/155892501400900113

20. Luccioni-Houzé B., Campredon M., Guglielmetti R., et al.: Kinetic analysis of fluoro-[2H]-chromenes at the photostationary states. Molecular Crystals and Liquid Crystals Science and Technology. Section A. Molecular Crystals and Liquid Crystals, 297(1), 1997, pp. 161-165.
https://doi.org/10.1080/10587259708036117

21. Ottavi G., Favaro G., Malatesta V.: Spectrokinetic study of 2, 2-diphenyl-5, 6-benzo (2H) chromene: a thermoreversible and photoreversible photochromic system. Journal of Photochemistry and Photobiology A: Chemistry, 115(2), 1998, pp. 123-128.
https://doi.org/10.1016/S1010-6030(98)00254-8

22. Parhizkar M., Zhao Y., Wang X., et al.: Photostability and durability properties of photochromic organosilica coating on fabric. Journal of Engineered Fibers and Fabrics, 9(3), 2014, 155892501400900308.
https://doi.org/10.1177/155892501400900308

23. Gaeva E.B., Pimienta V., Delbaere S., et al.: Spectral and kinetic properties of a red–blue pH-sensitive photochromic spirooxazine. Journal of Photochemistry and Photobiology A: Chemistry, 191(2-3), 2007, pp. 114-121.
https://doi.org/10.1016/j.jphotochem.2007.04.011

24. Deniel M.H., Lavabre D., Micheau J.C.: Photokinetics under continuous irradiation. In Organic photochromic and thermochromic compounds: Volume 2: Physicochemical studies, biological applications, and thermochromism. Boston, MA: Springer US, 2002, pp. 167-209.
https://link.springer.com/chapter/10.1007/0-306-46912-X_4

GARMENT DURABILITY ANALYSIS – INFLUENCE OF TEXTILE MAINTENANCE

WIENER, JAKUB[*]; **ŠUBROVÁ, TEREZA AND COETZEE, DIVAN**

Technical University of Liberec, Faculty of Textile Engineering, Studentská 1402/2, 461 17 Liberec 1, Czech Republic

ABSTRACT

Textiles used in clothing pose a large environmental burden from their initial manufacturing, maintenance and end of life. Garment production is a major problem whose environmental impacts can be easily quantified since it is a defined production process. To implement sustainable processes, it is necessary to evaluate the entire life cycle of a garment, including its maintenance and end-of-life. In this study, the maintenance phase of the garment is investigated. The garment maintenance is divided into real applied steps, and these individual steps are analysed in terms of raw material especially regarding potential/real damage to the treated garment fabric. The different maintenance steps are contextualised by the survey and results of the questionnaire used for the study. This investigated which gentle maintenance practices the respondents use in practice. The source of the analysed data is a questionnaire survey made in the Czech Republic. The result is a thorough analysis of the maintenance practices associated with garments and an analysis of ways to extend the lifetime of garments and thus reduce their environmental burden caused by excessive waste generation.

KEYWORDS

Garment; Durability; Textile maintenance.

INTRODUCTION

The textile industry is one of the largest contributors to environmental pollution. The increase in textile waste is usually perceived as the result of an increase in cheap products in a saturated market. Archetypal practices used during consumer use further contribute to this problem [1]. Textile durability is a key tool for achieving sustainability in the apparel sector. The longevity of garments is not only a matter of the textile materials used but also of the appropriate maintenance chosen and carried out.

Textile maintenance consists of stain removal (detaching), removal of impurities (washing, dry cleaning), removal of used solvent (drying, evaporation of organic solvents), minor repairs, surface alignment (ironing, mangling) and storage.

Table 1 summarizes the operations involved in garment maintenance. It gives the operation's main objective, the principle of the methods used, and the risks to the garment that can significantly reduce its service life.

The individual operations of garment maintenance are detailed below. The procedures used are:

Stain removal – detaching

One of the most common reasons for discarding garments is due to damage caused by stains and spots or their improper removal. Depending on the nature of the stain, several methods may be required to remove it. Once the chemical nature of the stain and the textile material have been correctly identified, the appropriate stain remover is selected. Often, stains can be easily removed without much difficulty or cost [2], [3].

The agents contain various oxidizing and dispersing agents as well as solvents. These agents are applied in a highly concentrated and effective form that can remove the stain or facilitate its removal in a subsequent step targeted at removing common soils. The used agents may cause local discoloration or otherwise damage the garment's fibres when applied. This can be due to an inappropriate choice of detaching agent for a given garment containing sensitive fibres or dyes [3], [4], [5]. Organic solvents are a potential risk for chemical fibres, and aqueous solutions are riskier for natural fibres [2].

Only a limited number of low-efficiency detachers are available for domestic use. Commercially available stain removers have low risk of damaging the garment. However, it is also likely that some stains

---

cannot be removed with these products. Figures 1 and 2 show an example of an unremoved stain on a knitted fabric.

However, if it is not difficult to remove the stain, using normal laundry detergents and cleaning agents could ensure the removal of the stain without adding a detachment agent. Water molecules can diffuse well between the fibres and the stain using surfactants, thereby weakening the bonding forces between the stain and the fabric. Several factors influence the ability to remove stains, such as fabric characteristics, type of soiling, water quality, washing technique, detergent composition, etc. [3], [6].

Removal of impurities

Routine washing

The main purpose of the washing process is to remove dirt and microorganisms from soiled textiles to ensure hygienic safety and decontamination. The textiles undergo a washing process that includes removing dirt using special detergents, bleaching, disinfection, neutralization, and soaking [7].

The outcome of the wash depends on several factors, including the amount and type of water, temperature, length of wash cycles, chemicals used, such as detergents, and the mechanical spinner used. Dirt can be removed either by higher temperature, mechanical force, interfacial processes, or chemical degradation by enzymes or bleaching agents. Prewashing, which is a short wash before the main wash, is commonly used to effectively remove various stains and soils. Prewashing was more common in the past because laundry was dirtier, took longer to accumulate before washing, and detergents were less effective [8].

Washing is commonly practiced in households and industrial laundries and is based on the use of aqueous dispersing and bleaching systems. Commonly used detergents may contain percarbonates (bleaching agents, sources of hydrogen peroxide), peroxide activators to increase the bleaching ability of percarbonates at low temperatures, pH-adjusting agents (usually alkaline in origin), detergent and emulsifying detergents, and enzymes to break down difficult-to-remove starch and protein-based impurities [3], [8].

Natural fibres, such as cotton and wool, are hydrophilic, which means they have places on their surface where water molecules bind. As a result, water remains trapped in these fibres, causing them to have a poor ability to transport and release moisture [9]. Washing cellulose-based fibres is always risky, as the fibres swell intensely during washing. The swelling of cellulose fibres causes a temporary shortening of the yarns, which usually results in shrinkage of the garment [10]. This occurrence should be expected by the user of the garment but is not usually a risk to the longevity of the garment. The second aspect of fibre swelling is the release of dyes from the fibres, which is promoted by the swelling of the polymer by water and by the opening of nano-pores in the fibre [11]. If less stable dyes are chosen, the colour of the garment may be significantly lost during washing, and the product's life may be significantly reduced. The swelling of cellulose fibres is not significantly affected by the temperature of the washing bath.

Table 1. Clothing maintenance operations.

	1. Stain removal	2. Removal of impurities	3. Removal of used solvent	4. Minor repairs	5. Surface alignment	6. Storage
Objective:	Elimination of visually localised impurities	Elimination of surface-deposited impurities, including odour	Remove the solvent used in the previous operation	Ensure functionality and eliminate mechanical damage to the garment	Fracture elimination, mechanical alignment of the garment	Keep the garment in usable condition
Principle:	Topical use of detergents, bleaches, solvents	Use of solvent and dispersion systems	Solvent evaporation by heat and vapour recovery	Restoration of garment	Temporarily stent clothing by exposure to temperature and humidity	Elimination of chemical, biological and mechanical influences on clothing
Risks to clothing:	Insufficient stain removal, fibre damage, localised discolouration	Insufficient impurities removal, mechanical and chemical damage to the garment, colour changes	Contamination of clothing with dirt, colour changes	Visibility of adjustments	Colour changes, thermal damage to the garment	Fracture formation, pest infestation, colour changes

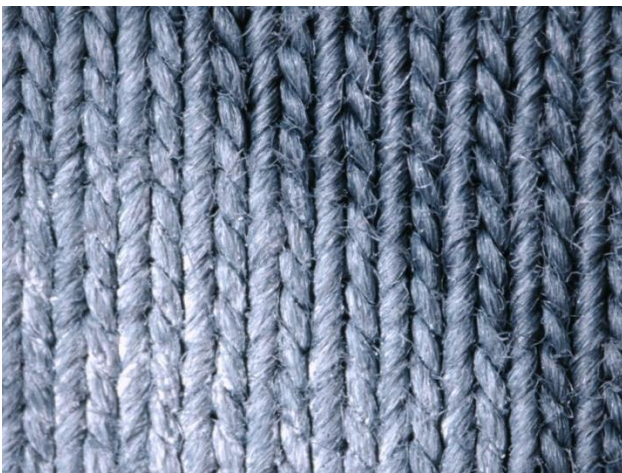**Figure 1.** Paint stain on cotton knitted fabric magnified 10x.

Figure 2. Paint stain on cotton knitted fabric, magnified 35x.

For wool and other protein fibres, the potential alkalinity of the washing solution is a risk, especially at higher temperatures. Under these conditions, there is a particular risk of felting of the wool, associated with a permanent change in the appearance and dimension of the garment [12]. Also, a problem for wool fibres is the presence of some enzymes used in detergents; these are various esterases and proteases that should break down the proteins contained in the dirt on the fibre [13]. Choosing gentle washing methods, minimizing mechanical action and controlling moisture during drying can help preserve the quality and appearance of wool garments.

Damage to synthetic polymer fibres is almost impossible at recommended washing temperatures. The recommended washing temperature is practically always below the fibre polymer's glass transition temperature, thus ensuring not only the fabric's mechanical stability but also the dye's stability during washing.

Wet cleaning

Wet cleaning is one of the methods of professional garment maintenance normally carried out by dry cleaners. This optimized washing procedure uses the basic principles and technologies of conventional washing. The risks to garments are comparable to conventional laundering [5].

Dry cleaning

It is one of the methods of professional garment maintenance and is typically carried out in dry cleaners. In contrast to washing and wet cleaning, non-aqueous solvents such as perchloroethylene and some liquid hydrocarbons are used [14]. Dry cleaning is gentler on the natural fibres and the dyes in them. The use of inappropriate solvents is a risk factor for synthetic materials. There is practically no risk when using standard textile fibres and standard dry-cleaning solvents [5]. The problem tends to be the design components of garments made of low-resistant polymers.

Removal of used solvent

Clothes are dried in different ways. They are usually dried using a combination of air or hot air, resulting in the evaporation of moisture and then removing it with a stream of air. Different forms of drying racks and lines are used, both indoors and outdoors. Drying chambers and separate drying rooms, such as drying cabins with or without heating, and, finally, tumble dryers, are also used. On average, about 32% of households in Europe use tumble dryers [8].

Air drying

Air drying is the most energy-efficient method, as it uses ambient air temperature as the energy source to evaporate water, which also removes evaporated moisture. Drying in direct sunlight is the fastest but also the most problematic regarding garment life. Direct sunlight generates active oxidising agents in wet textiles, which are particularly damaging to the fabric's colour. In addition, direct sunlight also damages the polymer, but this process is relatively slow [15], [16]. An example of the change in colour of the fabric is shown in Figure 3.

Drying in the tumble dryer

Drying in a tumble dryer is quick but less gentle on fabrics compared to air drying. The mechanical action in the dryer can cause slight abrasion between garments, gradually damaging them. Loose fibres tend to get caught in the tumble dryer filter. While this reduces the fabric's weight over time due to fibre loss, it also helps to remove microfiber deposits accumulated during washing. [17] Research shows that all fibre types release significant amounts of microfibres when washed, but cellulose-based fabrics release more microfibres than polyester with the same fabric structure. The physicochemical properties of fibres and yarns play an important role in forming microfibres. Fabrics with higher abrasion resistance, low pilling and higher yarn breaking strength have a lower tendency to form tufts and/or release microfibres when subjected to the mechanical

Figure 3. Colour change of cotton knitted fabric due to light and humidity (unexposed on top, exposed knitted fabric on bottom), magnified 12x.
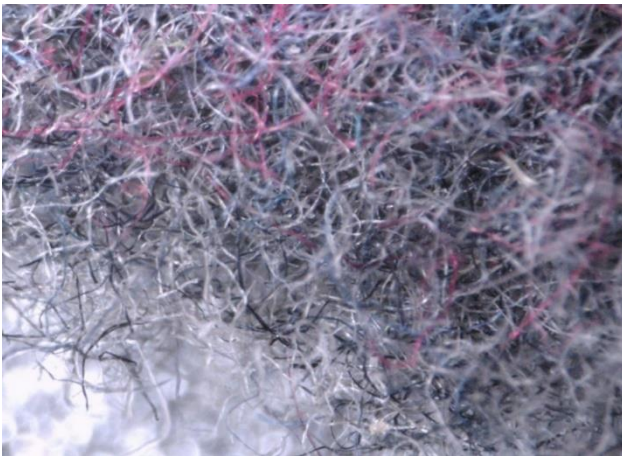

Figure 4. Fibrous microplastics caught on the tumble dryer filter magnified 100x.

action of washing [18]. A sample of the fibrous microplastics released during drying of the fabric is shown in Figure 4. The advantage of the tumble dryer is that there is no risk of photochemical decomposition of dyes, however, too high drying temperatures and mechanical movement can cause mechanical deformation of the fabric.

Minor repairs

Repair is essential as it can reduce garment consumption and textile waste, thereby improving the sustainability of garments throughout their life cycle and enhancing the circular economy [19]. Most of the time, clothes are mechanically damaged during use, and this damage is one of the main reasons why clothes are discarded from the wardrobe. However, some mechanical damage is repairable with relatively little effort. The most common is the reattachment of separated garment parts, the addition of lost buttons, etc. [20]. Examples of minor mechanical damages of garments are shown in Figures 5 and 6. Minor repairs indicate that the wearer values their garment; they generally do not require advanced skills, but

willingness is crucial. Each minor repair significantly contributes to prolonging the garment's life.

Various surveys indicate that while certain segments of society are starting to acknowledge the environmental and social advantages of garment repair, this perspective diverges from mainstream thinking. The prevailing attitude leans towards discarding damaged garments rather than repairing them [1].

There are many barriers that complicate garment repair. Among these are financial costs and lack of time and skills. The study also highlights that social and psychological reasons play a big role in repair. Traditionally, the imperfection of textile materials is strongly associated with a lack of finances, and wearing visibly worn or damaged clothing plays a significant role in characterising social conditions. However, the increasing visibility of repairs challenges traditional, outdated views of clothing repair. Designing visible repair patterns that are modern, stylish, accessible and can be deemed personalised offers the potential for a wider extension of repair techniques, making them personal, meaningful and socially acceptable to wear in the workplace [20].

Surface alignment

Ironing

Ironing is based on the application of high temperature, pressure and moisture to the garment material. The mechanism of action varies from fibre to fibre, but the result is similar for all garment fibres. Temperature has a significant effect on the ironing result for synthetic fibres, while moisture has a greater effect on natural fibres. Particularly for synthetic polymer fibres, a sufficiently high temperature is necessary but must not exceed a critical temperature close to the melting or decomposition temperature of the fibres. Significantly exceeding the ironing temperature leads to the destruction of the fibre structure in the case of fusible fibres and carbonisation or colour changes in the case of non-fusible fibres. If a synthetic fibre fabric (typically polyester) is dyed with a disperse dye for a non-standard short period of time, the dye is localised just below the surface of the fibres. The temperature effect of ironing causes a redistribution of the dye in proportion to the intensity of ironing, leading to irremovable and easily visible colour changes [21].

Mangling

The same principles used for mangling are also used for ironing. Due to the different geometry of the process, there is less risk of fibre damage and colour variations on the textile. Mangling is a process of smoothing clothing instead of ironing it after it has been dried. This is done by passing it between heavy rollers, which may be heated [22].
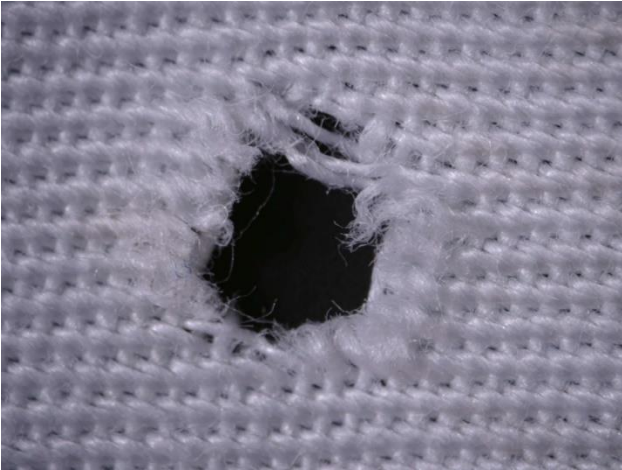
Figure 5. Mechanically damaged cotton fabric - perforations, suitable for repair, enlarged 25x.

Figure 6. Mechanically damaged cotton fabric - loose pocket, suitable for repair, enlarged 15x.

Storage

Textiles are not usually exposed to intensive processes from their surroundings during storage, but rather to low-intensity, long-term processes. However, the result can be the destruction of the garment. The problem in storage is usually moisture, which promotes hydrolysis reactions and thus damages the fibres, such as in the case of polyamide. Moisture also promotes the activity of insects, moulds and bacteria, which can degrade textiles, although it is more common for hard-to-remove odours or coloured stains to appear on textiles [23]. Another problem is direct sunlight, which, when exposed for long periods, can significantly damage the exposed areas both at the polymer level and at the level of the fabric's colour. Clothing should be stored in a dark area with low humidity and adequate temperature to avoid the aforementioned problems.

EXPERIMENT

A questionnaire-based method was chosen to collect data on reasons for which clothes were discarded from the wardrobe and, simultaneously, to collect data on the users' behaviour towards the clothes at the time of their discarding. The questionnaire was created using Google Forms and distributed to the public. Considering the topic of the questionnaire, an increased proportion of respondents from the circle of those interested in fashion and clothing can be expected. Given the creation of the questionnaire in a university setting, an increased proportion of student respondents can also be expected. The questionnaire presented here is in English; a questionnaire in the Czech language was used to collect data for this study. The respondents are, therefore, mainly from the Czech Republic. For this research, responses were collected from a total of 498 respondents.

The collection of responses using this questionnaire took place from 15.2 to 17.4 2024.

Asked questions:

1. <u>Which of these maintenance practices do you use to make your clothing last longer? (you can select more than one option).</u>

   · Proper storage (dry, dark, clean environment...)

   · Gentle washing (following care label instructions)

   · Removing stains with special agents

   · Minor textile repairs (preventing knitwear from pilling, patching holes...)

   · I don't dry textiles in direct sunlight

2. <u>How often do you repair or alter clothing instead of discarding it due to minor damage or wear and tear?</u>

   · Often (once a week)

   · Occasionally (once a month)

   · Rarely (once a year)

   · Never

RESUTLS AND DISCUSSION

Evaluation of questionnaire data:

Many respondents were women (81%), with the remainder (19%) being men (Figure 1). No other gender was indicated by the respondent. The higher percentage of women is related to the higher percentage of women in our university (Faculty of Textile Engineering TU Liberec) and the expected higher percentage of women interested in clothing and fashion.

The age distribution of respondents is relatively even, encompassing the entire range of adults (18+), though a few respondents under 18 also participated. The higher proportion of individuals in the 19 to 26-year-old category can be attributed to the significant number of respondents from our university. Refer to Figure 8.
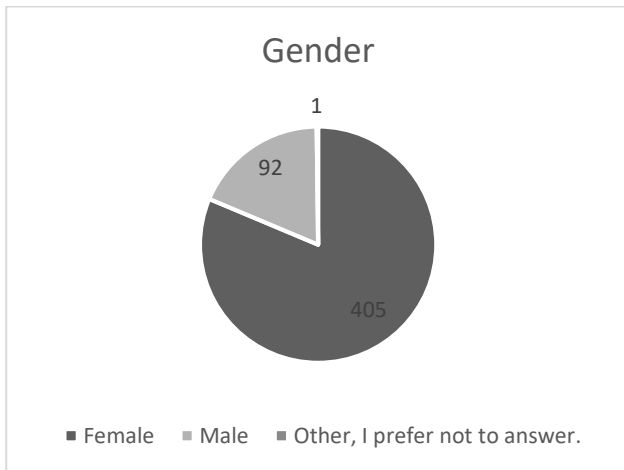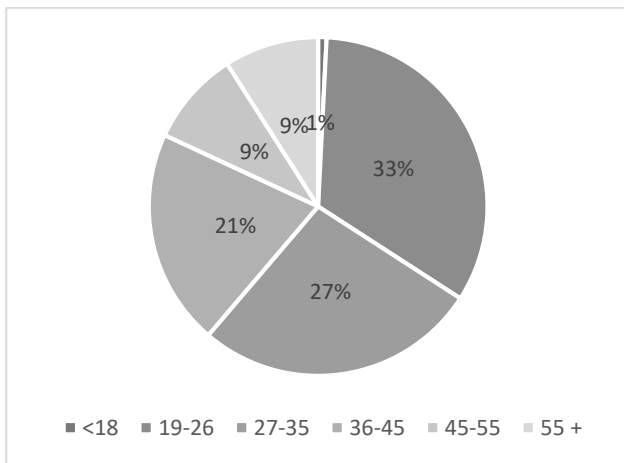
Figure 7. Gender of respondents.

Figure 8. Age distribution of respondents (only 1% of respondents below 18 years).

This question received 1328 responses. The following is a multiple-choice question. The least preferable method is drying in direct sunlight. Only 20.5% of respondents chose this option. The theory of drying textiles in direct sunlight should spread more widely among the public. It is scientifically proven that progressive tendering of fibres occurs on exposure to sunlight for long periods, and serious losses in strength can occur, particularly with lightweight fabrics. The different fibres lose strength at different rates and range from sensitive silk to resistant polyacrylonitrile fibres, which withstand sunlight for long periods.[24].

On the other hand, the procedure followed the most is proper washing and following the procedure on the label. A total of 73.1% of respondents followed this procedure.

A significant number of respondents (68.3%) reported that they store textiles correctly. Factors such as a dry, dark and clean environment ensure that textiles are protected and maintained in optimal conditions, contributing to their long-term durability and quality. Such a clean environment is crucial not only for private households but also for industrial storage facilities or museums.

Many respondents prolong the life of their garments with minor and relatively simple repairs (61.8%). 43% of respondents choose to remove stains using special detaching products. The percentage of responses is summarized in Figure 9.

These responses suggest that consumers very often take care of their garments, thus prolonging their life. A related question focuses on how often users repair or alter their clothes instead of discarding them due to minor damage or worn-out items. Only 8% of respondents answered that they do not tend to maintain their garments in this way.
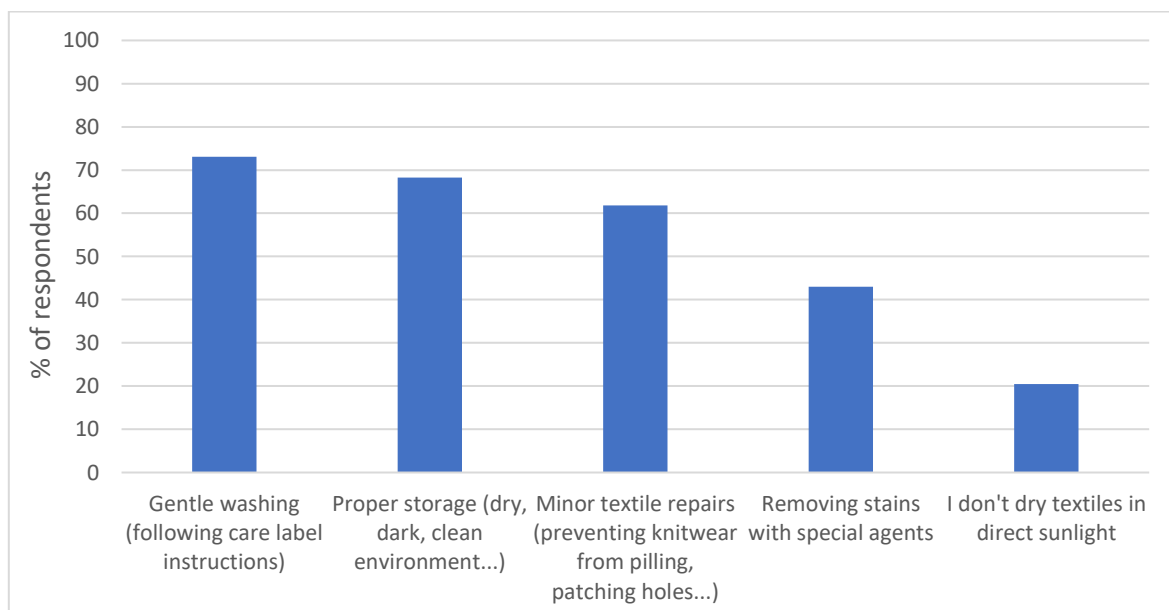

Figure 9. Percentage of respondents using this method of garment maintenance.
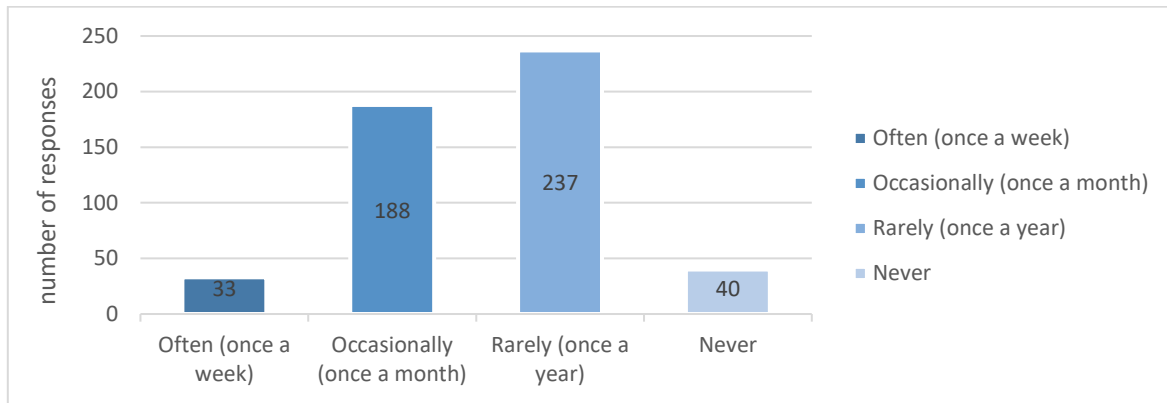
Figure 10. Frequency of small repairs and alterations to respondents' clothing.

When comparing clothing repairs by gender, it is found that 35% of men and 68% of women prefer to have their clothes repaired. 498 respondents answered the question on the frequency of minor clothing repairs. The questionnaire results show that 33 people in this group regularly repair their clothes once a week, indicating that they take considerable care of their clothes. 188 people choose to repair their clothes monthly, indicating a regular effort to maintain the quality of their wardrobe. A further 237 respondents choose to have their garments repaired once a year, which may indicate their intention to save the cost of new garments while maintaining their favourite items. Conversely, 40 people admitted that they never repaired their garments, which may reflect their preference for buying new pieces over repairing old ones. Frequency of small repairs is summarised in Figure 10.

CONCLUSION

In this study, the life cycle of garment maintenance was analysed to identify and quantify garment maintenance risks. The different stages of garment maintenance and the associated degradation of garments were discussed. Improperly selected maintenance or improperly performed garment maintenance mainly leads to changes in garment colour but can also lead to permanent damage to the fibre structure of the garment. Damage to the garment is a common reason for removing it from the wardrobe and thus ending its life. Damaged garments are usually not suitable for reuse, and it can, therefore, be said that any damage to a garment leads to a significant shortening of the garment's life. Much of the damage to garments is caused by incorrect maintenance, and therefore, garment maintenance needs to be popularised. At the same time, garments that require easy and risk-free maintenance need to be industrially produced. A questionnaire survey was conducted to verify consumer awareness of garment maintenance methods and risks. The questionnaire survey results are satisfactory; most respondents employ suitable methods for garment maintenance and understand the risks associated with improper care on garment durability.

REFERENCES

1. Gwilt A.: What prevents people repairing clothes?: an investigation into community-based approaches to sustainable product service systems for clothing repair. 2014, online: http://orcid.org/0000-0002-2557-7098
2. Roberson N., Hard G., Russel M.: Removing Stains from Clothing. Texas Agricultural Extension Service, 1958.
3. Saunders B.: Stain Removal Chart For Washable Clothing. Texas Agricultural Extension Service, 1984.
4. Whittelsey A.H., Lang H.A.: Removal of stains from clothing and other textiles. Washington, D.C.: U.S. Dept. of Agriculture, 1917.
5. Roberts J.C.: The chemistry of paper, Royal Society of Chemistry, 2007, 204 p.   Brant W. E. T.: Dry Cleaner, Scourer, and Garment Dryer, 2nd Edition. Philadelphia: Henry Carey Baird & CO., 1907, online: http://www.hathitrust.org/access_use#pd
6. Shi W., Pei L., Gu X., et al.: Stain removal performance of moisture-wicking fabric during home laundry. Tenside, Surfactants, Detergents, 60(3), 2023, pp. 203–213. https://doi.org/10.1515/tsd-2022-2436
7. Tufan H.A., Gocek I., Sahin U.K., et al.: A novel washing algorithm for underarm stain removal. In IOP Conference Series: Materials Science and Engineering, Institute of Physics Publishing, 2017. https://doi.org/10.1088/1757-899X/254/8/082001
8. Pouillard V., Dubé-Senécal V.: The Routledge History of Fashion and Dress, 1800 to the Present. Taylor and Francis, 2023. https://doi.org/10.4324/9780429295607
9. Su C.-I., Fang J.-X., Chen X.-H., et al.: Moisture Absorption and Release of Profiled Polyester and Cotton Composite Knitted Fabrics. Textile Research Journal, 77(10), pp. 764–769, 2007. https://doi.org/10.1177/0040517507080696
10. Budtova T., Navard P.: Cellulose in NaOH–water based solvents: a review. Cellulose, 23(1), Springer Netherlands, pp. 5–55, 2016. https://doi.org/10.1007/s10570-015-0779-8
11. Paul R., Teli M.D.: Effect of swelling and reactive dyeing on the accessibility of cotton to cellulase enzymes. J Appl Polym Sci, 121(4), pp. 1946–1950, 2011. https://doi.org/10.1002/app.33772
12. Feldtman H.D., Mcphee J.R.: The Effect of Temperature on the Felting of Shrink-Resistant Wool.
13. Silva C.J.S.M., Prabaharan M., Gübitz G., et al.: Treatment of wool fibres with subtilisin and subtilisin-PEG. Enzyme Microb Technol, 36(7), pp. 917–922, 2005. https://doi.org/10.1016/j.enzmictec.2005.01.017
14. McLendon V.I.: Removing stains from fabrics: home methods. Washington, D.C.: U.S. Department of Agriculture,

1964, online: https://hdl.handle.net/2027/ufl1.ark:/13960/t0ms4t08m

15. Groeneveld I., Kanelli M., Ariese F., et al.: Parameters that affect the photodegradation of dyes and pigments in solution and on substrate – An overview. Dyes and Pigments, vol. 210, Elsevier Ltd, 2023. https://doi.org/10.1016/j.dyepig.2022.110999

16. Gavor M.E.: The Photodegradation of Cotton Dyeings in the Presence of Binary Mixtures of Direct Dyes. University of Manitoba, Winnipeg, 1990.

17. Yousef S., Eimontas J., Zakarauskas K., et al.: A new strategy for using lint-microfibers generated from clothes dryer as a sustainable source of renewable energy. Science of the Total Environment, vol. 762, 2021. https://doi.org/10.1016/j.scitotenv.2020.143107

18. Zambrano M.C., Pawlak J.J., Daystar J., et al.: Microfibers generated from the laundering of cotton, rayon and polyester based fabrics and their aquatic biodegradation. Mar Pollut Bull, vol. 142, pp. 394–407, 2019. https://doi.org/10.1016/j.marpolbul.2019.02.062

19. McQueen R.H., Jain A., McNeill L.S., et al.: The role of resources in repair practice: Engagement with self, paid and unpaid clothing repair by young consumers. Textile Research Journal, 93(3-4), pp. 576–591, 2023. https://doi.org/10.1177/00405175221123067

20. McLaren A., McLauchlan S.:Crafting sustainable repairs: practice-based approaches to extending the life of clothes. Laitala & Boks, 2015.

21. Cheriaa R., Ben Marzoug I., Sakli F.: Effects of industrial ironing on mechanical and dimensional properties of cotton, wool and polyester fabrics. 2016.

22. Tudor J.: Sanitary laundering, or, The story of "Through the wash." 1916.

23. Dhiman G., Chakraborty J.N.: Antimicrobial performance of cotton finished with triclosan, silver and chitosan. Fashion and Textiles, 2(1), 2015. https://doi.org/10.1186/s40691-015-0040-y

24. Little A.H.: The Effect of Light on Textiles. 1963.

THE EFFECT OF COMPRESSION STOCKING ON LEGS' GEOMETRY CHANGES WITHIN DIFFERENT MOVEMENT

KYZYMCHUK, OLENA[1][*]; RIABCHYKOV, MYKOLA[2]; KYOSEV, YORDAN[1]; MELNYK, LIUDMYLA[3] AND BOLL, JESSIKA[1]

[1]   Technische Universität Dresden, Hohe Str. 6, 01069 Dresden, Germany
[2]   Lutsk National Technical University, Lvivska str. 75, Lutsk, 43018, Ukraine
[3]   Kyiv National University of Technologies and Design, Mala Shyianovska St., 2, Kyiv, 01011, Ukraine

ABSTRACT

In this study, the changes in leg size and shape as well as pressure at different sites of a lower leg were investigated using advanced tools such as the Move4D scan system and Texsens pressure measuring device. The effect of the class of compression stocking, wearing time, and movement type was analyzed for one volunteer. It is the basis for the high-accuracy ready-to-wear compression stocking development based on the concept of personalization.

INTRODUCTION

The demand for compression clothing and rehabilitation goods increases every year. Today's market for compression products is not limited to medical applications [1]. They are widely used in sports and everyday life. With the improvement of human needs and the development of technology, more and more attentions are paid to the comfort [2] and quality of the products used. Particular emphasis in this matter is on the items and products that can help maintain health levels [3]. It was stated [4] that satisfactory compression textiles should possess the following characteristics: compression comfort; biocompatibility; good dimensional stability; controlled elasticity, stiffness and hysteresis; dynamic and sustained pressure delivery; satisfied contractile perception in long-term use; moisture and thermo-physiological regulation.

The compression stockings are the most used compression garment because of spread such diseases as various types of chronic oedema, venous thromboembolism and venous ulcers, where compression therapy is widely used and had good results [5]. Many scientists and therapists paying a crucial attention to study stocking performance and pressure prediction. It was found that knitted structure [6] [7], as well as inlay yarn count [8] and amount [9] together with yarn nature [10] and treatment type affect the material properties and stocking performance [11] [12].

Simultaneously ensuring the necessary functional properties, namely the pressure level at different areas, and high levels of comfort of the compression clothing is problematic within the mass production of the products of standard sizes. Most of the research for compression stocking development was done for standard legs using in-vitro pressure measurements on extremities dummies [13] and/or virtual soft mannequins [14]. In-vivo measurement has been usually used in clinical research [15]. On the other side, the emerging technologies in the textile industry as 4D scanning [16], 3D design [17], and CAD systems enable manufacturers to produce bespoke textiles on demand [18]. Investigation of the geometry changes of body legs with compression stocking in the static position [19] showed that 3-4D scanning allows the quick estimation of the compression clothes functionality and it can be a promising means for assessing the dimensional changes of the body parts.

This research aims to study the changes in sizes and shapes of the lower legs within the wearing time of compression stockings and different activities as well as changes in pressure that occurred at the same time. The research results are the basis for the development of a tool for high-accuracy ready-to-wear compression garment design.

MATERIALS AND METHODS

Compression stockings

Conventional knee-high 40 den stockings and two classes of compression stockings (I CCl and II CCl) of the same manufacturer were used. 85 % nylon and 15 % spandex are the yarns composition provided by manufacture. One volunteer took the part in the study. He is using compression stockings of size 3 [20] according therapist prescription. He did their usual routine activity between scanning without any limitations.

Scanning procedure

The MOVE 4D system from Valencia Polytechnic University at ITM TU Dresden was used for the investigation of the changes in the size and shape of the lower legs. Five following movements were performed: walking, stepping, bending over, sitting down, and rising on tiptoes. The scanning time for each movement was 4 seconds with a frequency of 15 frames per sec (Fig. 1). Scans were made for the control leg (without stocking) and within stocking wearing: just after putting on stockings (0 hour) and after wearing time of 1 and 4 hours.

The 4D scanning data gives a possibility for a quick comparison of the legs. The evaluation can be done not only by leg circumference and cross-sectional area at certain sites but by the contours as well. The slicing of the legs scans and data transfer were done by ParaView 5.11.0, and MeshLab 2022.02 was used for the planar section (Fig. 2 b), area and circumference measurements. The left and right legs were studied separately.

Pressure measurement

The Texsens force and pressure measuring device [21] was used for pressure investigation. Measurement time was 60 sec (1 min) with 0.02 sec frequency. The measurements were done just after putting on stockings (0 hour) and after the first and fourth hours of wearing during all activities. The measurements were performed according RAL-GZ 387/1 [20] at three levels recommended by this standard: B (ankle), B1 (lower calf) and C (calf), They were fixed for the volunteer at 10, 23 and 30 cm from the floor (Figure 2.a). These levels were marked on the legs and on the stockings because within activity the distance between them is changed.

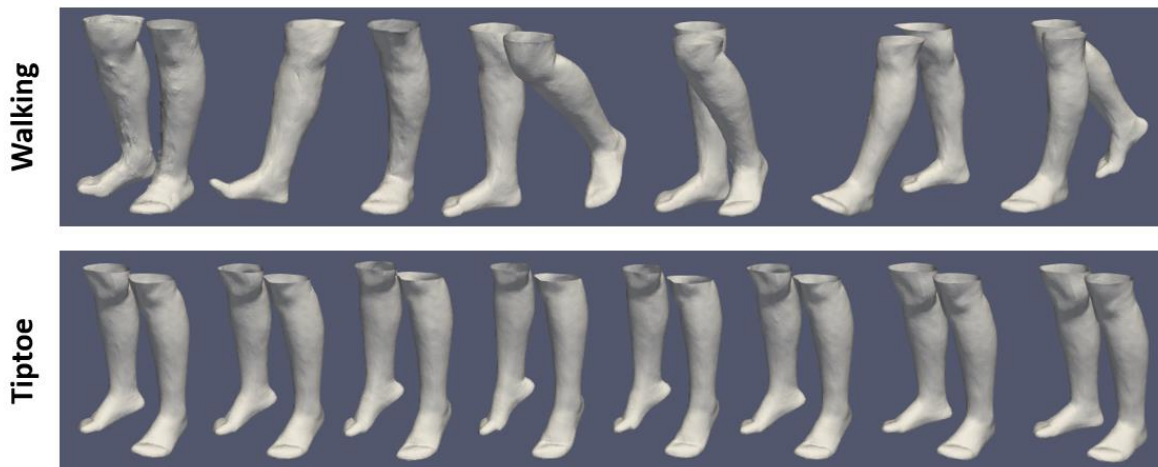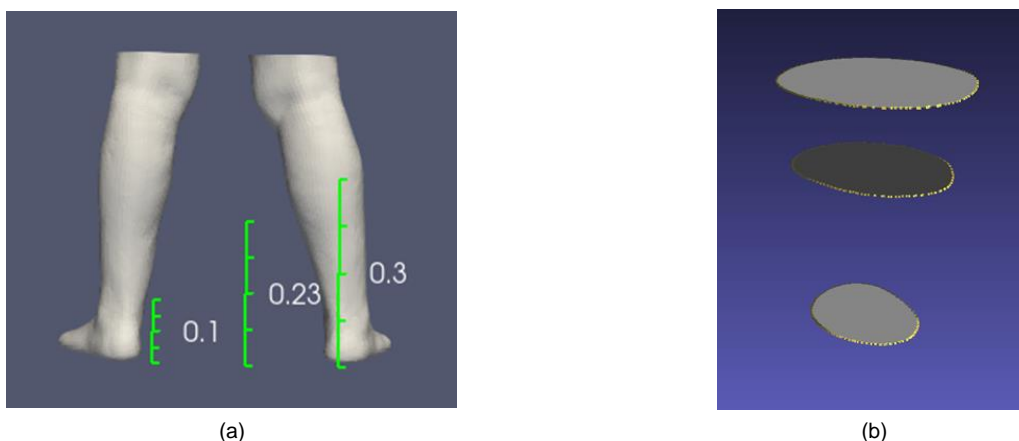**Figure 1.** Example of a scan captions during different movements.

(a)   (b)

Figure 2. Legs scan processing: (a) measurement levels; (b) the leg's slicing.

RESULTS AND DISCUSSION

The research was conducted in a few steps. Firstly, the leg shapes and sizes as well as their changes over time and used stocking's type were studied in static position. The values of existing changes at three levels were calculated and analyzed. Then, the effect of compression stocking and wearing time on the lower legs' sizes was studied during five different activities. After that the pressure level of stockings were analyzed as well.

Lower leg's size at static position

There is an increasing in leg's size within wearing time of conventional stocking due to legs swelling. In our previous study [19] was confirmed differences in left and right legs due to body's asymmetry. The example of cross-sectional contours at 30 cm level for both right (RL) and left (LL) legs are presented in Fig. 3. The cross-section area increases up to 11 % at the calf and up to 17 % at the ankle after 4 hours of conventional stockings wearing. The values for circumference increasing are smaller and are up to 5.3 % and 7.6 % respectively. It can affect the pressure delivered by compression stocking within wearing time. Using II CCl stockings are more effective for scanned person: the leg's circumference

and cross section area were kept at initials value at all studied levels for both legs.

Lower leg's size during movement (conventional stockings)

It is clear that leg shape and volume are changing during different movement due to muscles volume changes [22]. Thus, the greatest changes will be at level. An example of measurements of legs circumference at 30 cm level during bending over and rising on tiptoe are presented in Figure 4. The differences in the left and right legs are observed. The right leg is thicker by 10 mm in circumference. The changes in legs' size are within 10 mm for both movements. Both legs are swelling but the right leg swells more which is clear when comparing the control leg with the leg after 4 hours conventional stockings wearing during bending over (Fig. 4 a). The plots in Fig. 4 b give clear understanding how the legs circumference changes within one cycle of movement, namely rising on tip toe and back to initial position.

The research result for changes (Δ) in the leg cross section area (S) compared to control leg is presented in Table 1. The right leg and 30 cm level were chosen for presentation because of its higher swelling and data representativity. The presented data show that leg's size changes not only over time but during different activities as well. The highest changes of

(a)   RL Conventional   (b)   RL I CCl   (c)   RL II CCl

(d)   LL Conventional   (e)   LL I CCl   (f)   LL II CCl

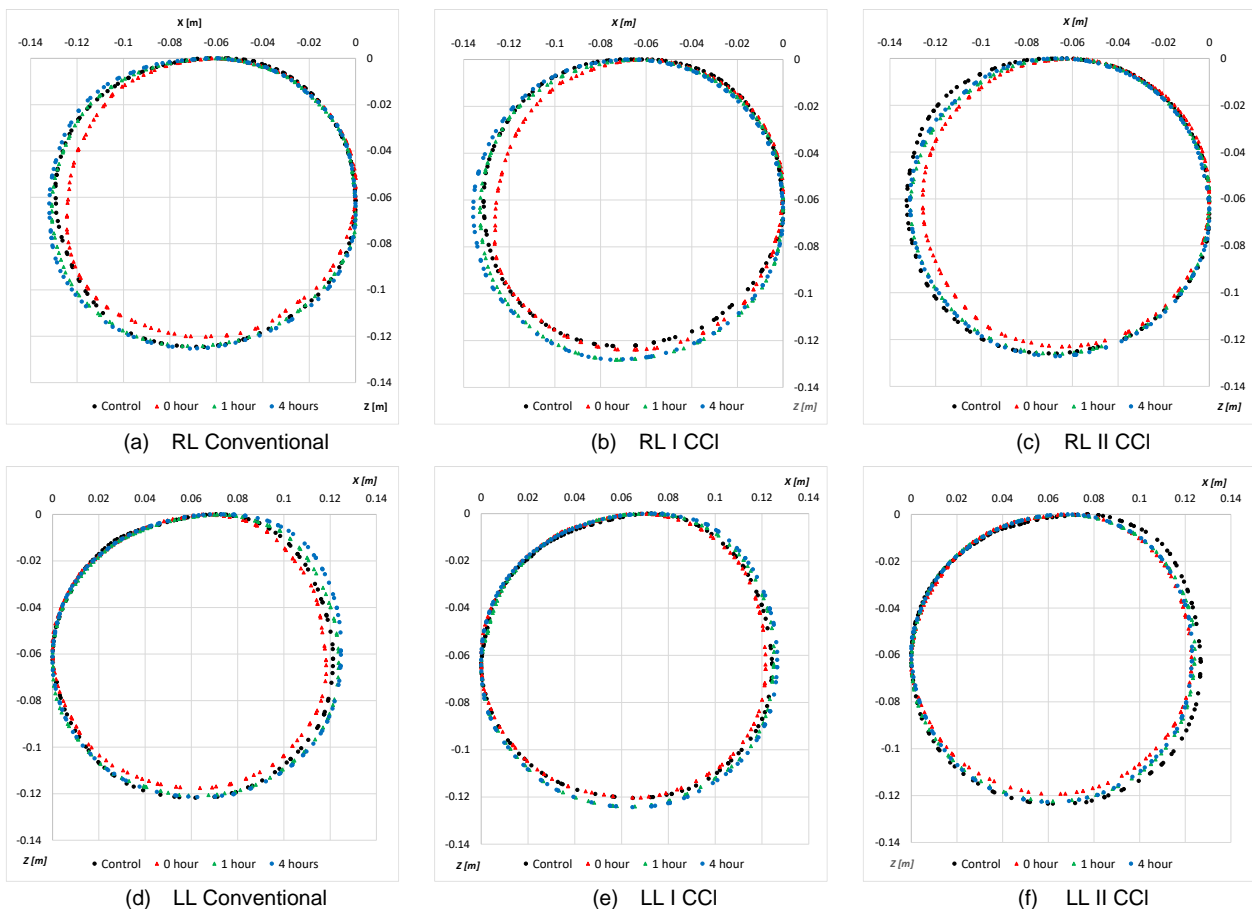**Figure 3.** Changes in the legs' shape at 30 cm level at the static position within wearing time for different stockings.

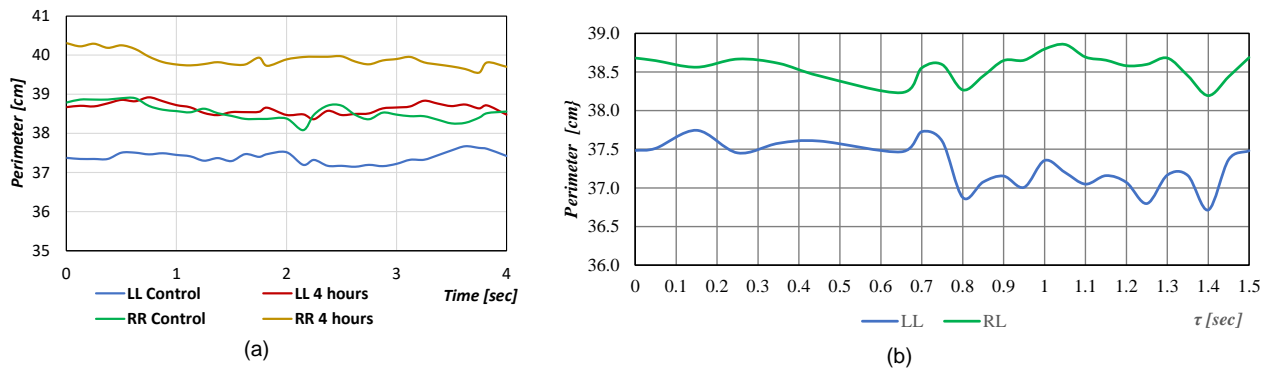(a)   (b)

Figure 4. Legs circumference changes at 30 cm level during bending over (a) and rising on tiptoe (b).

Table 1. Right leg cross section area (maximal value) at 30 cm level.

Conditions		Type of stocking					
Activity	*Wearing time*	Conventional		I CCL		II CCI	
		S [cm^2]	*Δ* [%]	*S* [cm^2]	*Δ* [%]	*S* [cm^2]	*Δ* [%]
Static	Control leg	119	-	128	-	134	-
	0 hour	119	0.0	126	- 1.9	124	- 7.9
	1 hour	130	9.1	136	6.3	131	- 2.1
	4 hours	133	11.1	138	7.5	131	- 2.4
Walking	Control leg	119	-	128	-	129	-
	0 hour	119	0	126	- 1.6	126	- 2.3
	1 hour	130	9.2	133	3.9	127	- 1.6
	4 hours	132	10.9	135	5.5	131	1.6
Rising on tiptoes	Control leg	118	-	122	-	128	-
	0 hour	118	0	121	- 0.8	123	- 3.9
	1 hour	127	7.6	130	6.6	127	- 0.8
	4 hours	128	8.5	131	7.4	127	- 0.8
Stepping	Control leg	118	-	124	-	126	-
	0 hour	118	0	120	- 3.2	122	- 3.2
	1 hour	124	5.1	130	4.8	128	1.6
	4 hours	127	7.6	133	7.2	127	0.8
Bending over	Control leg	116	-	124	-	125	-
	0 hour	116	0	122	- 1.6	121	- 3.2
	1 hour	123	6.0	129	4.0	125	0
	4 hours	125	7.8	131	5.6	125	0
Sitting down	Control leg	151	-	155	-	162	-
	0 hour	151	0	154	- 0.6	159	- 1.8
	1 hour	166	9.9	164	5.8	159	- 1.8
	4 hours	167	10.6	164	5.8	163	0.6

legs cross section areas after 4 hours of conventional stocking wearing were fixed during walking and sitting down with 10.9 % and 10.6 % correspondently. The I CCI stockings reduce values up to twice mostly. The I CCI stockings reduce swelling and values decrease, but the best results have been got with the usage of II CCL stockings. No swelling was fixed even after 4 hours of stockings wearing. Thus, obtained results give the clear opportunity for evaluation of compression stockings effectiveness.

Pressure value

The change in the leg's size leads to changes in stocking pressure on a lower limb. As we can see in Fig. 5 the pressure during bending over is changing within 3 kPa for I CCL and 5 kPa for II CCL stockings. The differences in pressure exerted to left and right legs are due to differences in their sizes. The pressure delivered by II CCI stocking is 2 times higher than those by I CCI stocking.

Thus, for left leg with 1 CCI stocking the pressure during bend over was from 3.2 to 4.5 kPa just after stocking wearing and in the 3.9-5.2 kPa range within 1 hour of wearing. The pressure rose to 5-6 kPa (over 50% increase) after 4 hours of wearing due to leg swelling. For the right leg there is different tendency: the delivered pressure is decreasing withing wearing time. This is probably because the stocking is not fitting well and slipping during wearing time.

The II CCI stocking with a higher level of delivered pressure keeps it more stable (Fig. 5 b). The changes in pressure during bend over just after stocking wearing was within 5 kPa, but after 1 hour of wearing it was only 2 kPa with similar mean values. After 4 hours of wearing the pressure goes up due to leg swelling and necessity to keep legs in initial state. The increase is within 20 %. The tendencies are similar for both legs. The differences in pressure value for left and right legs is due to their different size and swellings.
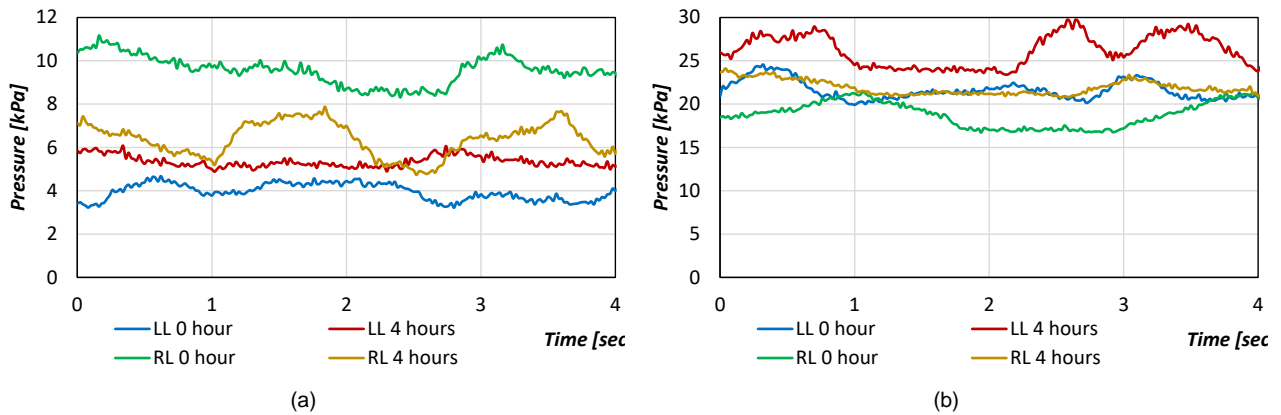
Figure 5. Pressure at 30 cm level within bending over for compression stockings: (a) I CCl; (b) II CCl.
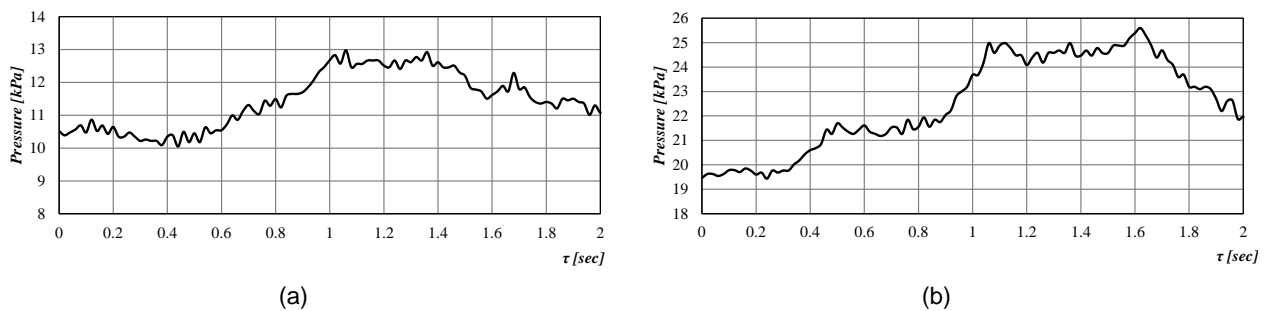

Figure 6. Pressure at 30 cm level within rising on tiptoe just after compression stockings wearing (0 hour): (a) I CCl; (b) II CCl.

The plots in Fig. 6 show how the pressure value on right leg changes within one cycle of movement, namely rising on tip toe and back to initial position. It is clear that highest value is at the top position and it correlates with circumference changes (Fig. 4 b). There is the similarity in plots for I CCl (Fig. 6 a) and II CCl (Fig. 6 b), the different is only in pressure values.

The plots for legs sizes changes and for delivered pressure for correspondent movements show similarity in tendencies thus 4D scan data can be used for the evaluation of compression stocking performance for certain persons and future development of high-quality personal products.

CONCLUSION

The investigation of the geometry changes of lower legs with compression stockings of two classes during wearing time and different activity confirmed that the shape and size of lower leg increased over time due to legs swelling and over different activity due to muscles volume changes. It was found that for studied volunteer the right leg is bigger and has higher swelling level. The highest changes in leg circumference at calf level was occurred during bending over and rising on tip toe (10-15 mm). The leg area increases up to 11 % at calf level, that were obtained after 4 hours at static position and during both walking and sitting down.

The conducted research has shown a correlation between the leg size (circumferences and areas) and the pressure level delivered by compression stockings. By processing data, it was clarified the compression stocking of which class more effective and more useful for scanned person. It could be concluded that the 4D scanning allows the quick estimation the compression stockings functionality.

The study results with stockings of two compression classes within wearing time and different activity are the basis for future development the algorithm for a customization of compression stocking to individual body geometry.

REFERENCES

1. Xiong Y., Tao X.: Compression Garments for Medical Therapy and Sports. Polymers (Basel), 10(6):663, 2018, pp. 1-19.
https://doi.org/10.3390/polym10060663
2. Zhang Q., et al.: Simple cellular automaton-based simulation of ink behaviour and its application to Suibokuga-like 3D rendering of trees, The Journal of Visualization and Computer Animation, 10(1), 1999, pp. 27-37. 2. Kyzymchuk O., Marmaralı A., Melnyk L., et al: The effect of weft yarn type and elastomer yarn threading on the properties of elastic warp knitted fabrics. Part II: Thermal comfort properties. Journal of Engineered Fibers and Fabrics, 18, 2023, pp.1-9.
https://doi.org/10.1177/15589250231171582
3. Brubacher K., Tyler D., Apeagyei P., et al.: Evaluation of the Accuracy and Practicability of Predicting Compression

Garment Pressure Using Virtual Fit Technology. Clothing and Textiles Research Journal, 41(2), 2023, pp.107-124. https://doi.org/10.1177/0887302X21999314

4. Liu R., Guo X., Lao T.T., et al.: A critical review on compression textiles for compression therapy: Textile-based compression interventions for chronic venous insufficiency. Textile Research Journal, 87(9), 2017, pp. 1121-1141. https://doi.org/10.1177/0040517516646041

5. Rabe E., Földi E., Gerlach H., et al.: Medical compression therapy of the extremities with medical compression stockings (MCS), phlebological compression bandages (PCB), and medical adaptive compression systems (MAC) : S2k guideline of the German Phlebology Society (DGP) in cooperation with the following professional associations: DDG, DGA, DGG, GDL, DGL, BVP. Hautarzt. 72(Suppl 2), 2021, pp. 37-50. https://doi.org/10.1007/s00105-020-04706-z

6. Kumar B., Das A., Alagirusamy R.: Effect of material and structure of compression bandage on interface pressure variation over time. Phlebology, 29(6), 2014, pp. 376-385. https://doi.org/10.1177/0268355513481772

7. Melnyk L., Kyzymchuk O.: Novel elastic knitted fabric with perforation. Fibres and Textiles, 30(1), 2023, pp. 120-125. https://doi.org/10.15240/tul/008/2023-1-021

8. Shi Y., Liu R., Lv J.: Effects of Knitting Variables for Pressure Controlling of Tubular Compression Fabrics. World Academy of Science, Engineering and Technology, Open Science Index 199, International Journal of Materials and Textile Engineering, 17(7), 2023, pp. 90 - 94.

9. Özbayrak N., Kavuşturan Y.: The effect of inlay yarn amount and yarn count on extensibility and bursting strength of compression stockings. Tekstil ve Konfeksiyon (Textile and Apparel), 2, 2009, pp. 102-107.

10. Kyzymchuk O., Melnyk L., Marmaralı A., et al. The effect of weft yarn type and elastomer yarn threading on the properties of elastic warp knitted fabrics. Part 1: Structure and elasticity. Journal of Engineered Fibers and Fabrics, 18, 2023, pp. 1-14. https://doi.org/10.1177/15589250231167405

11. Werner B., Lun B., Jean-François U., et al.: Determinants of pressure exerted by medical compression stockings. Nuklearmedizin, 36, 2007, pp. 237 - 244. https://doi.org/10.1055/s-0037-1622191

12. Van der Wegen-Franken C.P.M., Mulder P., Tank B., et al.: Variation in the dynamic stiffness index of different types of medical elastic compression stockings. Phlebology, 23(2), 2008, pp. 77-84. https://doi.org/10.1258/phleb.2007.006018

13. Kumar B., Das A., Alagirusamy R.: Study on interface pressure generated by a bandage using in vitro pressure measurement system. The Journal of The Textile Institute, 104(12), 2013, pp. 1374–1383. https://doi.org/10.1080/00405000.2013.807020

14. Ye C.Y., Liu R., Wu X.B., et al.: New analytical model and 3D finite element simulation for improved pressure prediction of elastic compression stockings, Materials & Design, 217, 2022, 110634 p. https://doi.org/10.1016/j.matdes.2022.110634

15. Mosti G.B, Mattaliano V.: Simultaneous Changes of Leg Circumference and Interface Pressure Under Different Compression Bandages, European Journal of Vascular and Endovascular Surgery, 33 (4), 2007, pp. 476-482. https://doi.org/10.1016/j.ejvs.2006.11.035

16. Kuehn T., Kyosev Y.: 4D Scanning of Clothed Humans - Preliminary Results, Proc. of 3DBODY.TECH 2021 - 12th Int. Conf. and Exh. on 3D Body Scanning and Processing Technologies, Lugano, Switzerland, 2021, #25. https://doi.org/10.15221/21.25

17. Ryabchykov M., Mytsa V., Bondarenko M., et al.: Formation of complex 3D surfaces scans for garment CAD. Vlakna a Textil, 30 (3), 2023, pp. 13-18. https://doi.org/10.1524_0/tul/008/2023-3-002

18. Shi Y., Liu R., Ye C.: Personalized compression therapeutic textiles: digital design, development, and biomechanical evaluation. Front Bioeng Biotechnol, 2024, 12:1405576. https://doi.org/10.3389/fbioe.2024.1405576

19. Kyzymchuk O., Kyosev Y., Melnyk L., et al.: The Investigation of the geometry changes of body legs with compression stocking in a static position. Communications in Development and Assembling of Textile Products, 4(2), 2023, pp. 213-221. https://doi.org/10.25367/cdatp.2023.4.p213-221

20. RAL GZ 387-1: Medical compression hosiery. Quality assurance. Deutsches Institut F. Guetesicherung und Kennzeichnung, 2008.

21. Texsens®: mobile load measurement in the textile and garment industry, online: https://novel.de/products/texsens/

22. Liu R., Kwok Y.L., Li Y., et al.: Skin pressure profiles and variations with body postural changes beneath medical elastic compression stockings. Int J Dermatol. 46(5), 2007, pp. 514-523. https://doi.org/10.1111/j.1365-4632.2007.03175.x

SYNCHROTRON BASED X-RAY ABSORPTION SPECTROS-COPY FOR STRUCTURAL ANALYSIS OF BASALT FIBERS

LICHTENBERG, HENNING[1*]; MAHLTIG, BORIS[1]; KLYSUBUN, WANTANA[2]; PRANGE, ALEXANDER[1,3] AND HORMES, JOSEF[3,4]

[1]   Hochschule Niederrhein University of Applied Sciences, Reinarzstr. 49, D-47805 Krefeld, Germany
[2]   Synchrotron Light Research Institute, 111 University Ave. Muang District, Nakhon Ratchasima 30000, Thailand
[3]   Center for Advanced Microstructures and Devices, Louisiana State University, 6980 Jefferson Hwy., Baton Rouge LA 70806, USA
[4]   Rheinische Friedrich-Wilhelm-University, Nussallee 12, D-53115 Bonn, Germany

ABSTRACT

X-ray Absorption Near Edge Structure (XANES) spectroscopy at the Synchrotron Light Research Institute (Thailand) was used to investigate temperature related structural changes in basalt fibers. As a first step, XANES spectra of fiber samples cut from a basalt roving heated for 1 hour at 800 °C were recorded at the K absorption edges of three chemical elements and compared with the spectra of the untreated fibers. Silicon and calcium K-edge XANES spectra of the fibers were not affected by heating, whereas iron K-edge XANES spectra were significantly influenced by heating at 800 °C. The high iron content in basalt fibers has been attributed to their higher thermal stability compared to common natural or synthetic fibers. As a next step, iron K-edge XANES spectra of two types of fibers (basalt roving and uncoated chopped fibers) were recorded after heating at temperatures between 600 °C and 900 °C. In both cases, with increasing temperature the absorption edge shifts to higher energies, indicating progressing oxidation of the iron atoms in the fibers. These experiments demonstrate the potential of X-ray absorption spectroscopy as a powerful analytical tool to investigate structural changes in basalt fibers upon heating and to correlate them with changes in their mechanical properties.

KEYWORDS

Basalt fibers; Thermal stability; Synchrotron; X-ray absorption spectroscopy.

INTRODUCTION

Inorganic fiber materials are known for their high thermal stability even in presence of oxygen from air [1] [2]. To inorganic fibers, different types of fiber materials are counted, e.g. carbon fibers, glass fibers or ceramic fibers from oxidic or non-oxidic composition [3-6]. Glass fibers are built up by mixtures of amorphous inorganic oxides as silica and alumina [3]. There are also glass fibers with special properties available, as e.g. a special resistance against alkaline liquids [3] [4]. Such extraordinary properties are often directly connected to the special composition of these fibers. The mentioned alkaline resistance, for example, is related to the presence of zirconia as glass fiber component [4] [7]. In a certain way similar to glass fibers are basalt fibers. Basalt fibers consist of different inorganic oxides and are also X-ray amorphous. However, basalt fibers are produced from natural volcanic rocks, which are molten for fiber production by spinning [8-10]. The composition of basalt fibers is determined by the composition of the rocks originally used. Compared to conventional glass fibers, basalt fibers contain a significant amount of iron oxide, giving them a typical brown coloration. Basalt fibers also contain titania in certain amounts [10-13]. Of course, there are also bulk-glass materials available which contain iron oxides or other iron compounds – with the aim to realize colored glass products, as e.g. used as bottles for beer or red wine [14-16]. However, for glass fibers such compositions containing iron oxides are quite unusual, especially for industrial products. Due to their origin, basalt fibers are sometimes offered as kind of a natural product from volcanic stones. Compared to common natural or synthetic fibers, they exhibit higher thermal and chemical stability and are also used in fiber composite reinforcements [10] [17] [18]. Their main component is silica, followed by titania, alumina, and iron oxide. A protective effect against heat radiation has been attributed to the iron oxide content [13] [19]. In general, the thermal stability of basalt fiber has been attributed to its high iron content [12] [20], and related to the iron redox state, specifically the iron oxides ratio, in the fiber [21] [22]. Changes in the structure and mechanical

---

properties of industrially used basalt fibers caused by heating and chemical treatment with acidic and alkaline solutions were investigated earlier [23]. It was reported that temperature had a significant influence on the fibers´ strength, which slightly decreased at ~300 °C, and rapidly at ~480 °C, finally resulting in complete disintegration. It should be noted that the maximum temperature of usage of basalt fibers is often given in the temperature range between 700 °C to 900 °C depending on the type of material and reference [10]. However, even treatments of these fibers at lower temperatures can decrease their strength. In earlier investigations [23], scanning electron microscopy before and after different thermal treatments did not indicate changes in fiber morphology, whereas energy-dispersive spectro-scopy (EDS) showed significant changes in surface composition (removal of carbon) even after moderate heating. These changes were related to the decrease in strength and partly attributed to decomposition of the sizing agents on the fiber surface, which were obviously burned away. These conclusions were in agreement with the results of thermogravimetric and calorimetric analyses, and similar effects leading to similar conclusions were observed after acidic and alkaline treatments. Besides these changes in surface properties at lower temperature it was expected that thermal treatment at higher temperature leads to a change in bulk structure by crystallization and further damage which could be controlled by doping with other elements (e.g. Zr) [19-21] [23-25]. X-ray absorption spectroscopy (XAS) is an element specific and nondestructive characterization method giving access to detailed information about the atomic environment of selected chemical elements in the sample [26] [27]. X-ray Absorption Near Edge Structure (XANES) spectra provide information about the oxidation state and coordination geometry of the absorber atoms, while from Extended X-ray Absorption Fine Structure (EXAFS) data structural parameters like interatomic distances, types of neighboring atoms and coordination numbers can be extracted [28]. Both EXAFS and XANES spectroscopy are well established and widely used analytical tools, covering a broad bandwidth of applications in diverse fields of research such as nanomaterials, biological, environmental and agricultural research, cultural heritage, mineralogy, geochemistry, biomedical applications, chemical engineering, catalysis, battery research and sensors [29-35]. In contrast to other characterization techniques, XAS is not limited to crystalline materials but also applicable to amorphous solids, liquids and gases without elaborate sample preparation. Due to the penetration strength of X-rays, XANES and EXAFS spectroscopy can be used for bulk analysis of solids and interfaces, and the measurements can be performed *in situ*, e.g. during heating or in reactive gas atmosphere. The objective of this study was to use XANES spectroscopy as

characterization method complementary to commonly used (mostly surface sensitive) laboratory techniques to analyze structural changes in basalt fibers upon thermal treatment in order to gain further insights into the mechanisms leading to the fibers´ decreasing mechanical stability. The results obtained can serve as a basis for future *in situ* XAS studies (e.g. using heatable sample cells), and ultimately contribute to the development of modified basalt fibers with enhanced temperature stability. Since the basalt fibers were expected to be mostly X-ray amorphous, XAS was considered as the ideal analytical tool for these investigations. This study covered absorption edges of different chemical elements and therefore included XAS measurements in a broad photon energy range. Accordingly, a tunable and highly intense X-ray source covering a wide range of energies was required, which is only accessible at a synchrotron light source.

EXPERIMENTAL SECTION

Samples and sample preparation

For a first series of XANES measurements, ca. 15 mm long pieces of a basalt fiber were cut from a basalt roving supplied by Incotechnology GmbH (Pulheim, Germany, type A) and heated for 1 hour in a muffle furnace at 800 °C. Infrared and EDS spectra of this type have been reported earlier [36] [37]. X-ray absorption spectra of these samples were measured at the absorption edges of three different chemical elements (silicon, calcium and iron). The silicon and calcium K-edge XANES spectra of these samples were identical to those of the untreated fiber, whereas the iron K-edge spectra of heated and untreated fibers showed significant differences. Consequently, the iron K- absorption edge was selected for a more systematic XANES investigation: First, the fiber sample from the roving was heated also at 480 °C (based on [23]) for 1 hour, and measured at the iron K-edge. The absorption spectrum of this sample was identical with the spectrum of the untreated fibers. Therefore, as a next step, fibers were subjected to the temperature treatment shown in Fig. 1 in the furnace: A heating rate of 5 °C/min was applied, and four target temperatures defined (600 °C, 700 °C, 800 °C and 900 °C). Each time a target temperature was reached the temperature was kept constant for 1 hour, and immediately afterwards a certain portion of the fibers (sample 1 – 4 in Fig. 1) was removed from the oven and prepared for iron K-edge XANES measurements. The remaining fibers in the furnace were heated to the next target temperature (plateau). This procedure was later also applied to prepare a different set of samples (type B) from uncoated chopped fibers (UCF) supplied by the company Deutsche Basalt Faser GmbH (Sangerhausen, Germany) for iron K-edge XANES spectroscopy. The use of these fibers as coating additives was reported
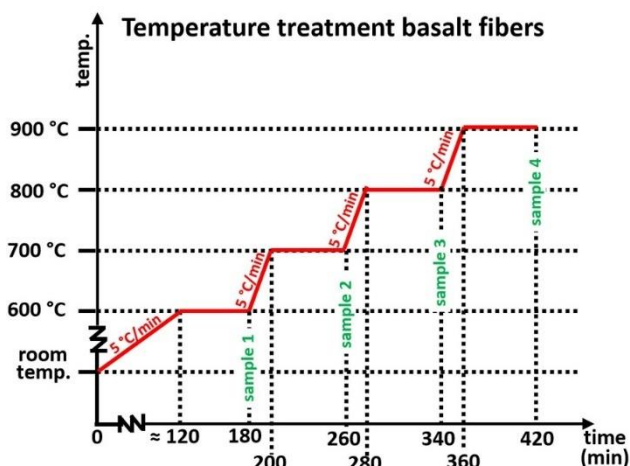
Figure 1. Temperature profile of temperature treatment applied to basalt fibers before iron K-edge XANES measurements.

earlier [38]. They were not cut, since they were already received chopped in ca. 0.5 cm long pieces. As expected, heating led to a clearly visible colour change in the fibers (from gold towards dark brown), which also became increasingly brittle.

For all XANES measurements, the fiber samples (either untreated or after heating) were on one side fixed with self-adhesive Kapton tape on a teflon sample holder, and on the opposite side (facing the beam) covered with polypropylene foil.

XANES measurements

XANES spectra of the basalt fibers were recorded at beamline BL8 [39-41] at the Synchrotron Light Research Institute (SLRI, Thailand, Siam Photon Source, 1.2 GeV electron storage ring) using bending magnet radiation. The chemical composition of basalt rock, glasses and fibers is well known from numerous publications [12] [17] [20] [42-46]: SiO_2 clearly dominates (in terms of mass fraction between ca. 40 and 60 wt.%), followed by Al_2O_3, iron oxides (FeO, Fe_2O_3), CaO, MgO, Na_2O, TiO_2 and K_2O. The values for the mass fraction for the individual components vary from publication to publication by a few percent, probably to a great extent due to the different origins of the basalt samples investigated. For this XANES study, the three chemical elements with the highest reported mass fraction (in wt.%) and K absorption edges in the X-ray energy range between 1.8 keV and 10 keV were chosen: Silicon, calcium and iron. XANES spectroscopy at energies below 1.8 keV is generally also possible at beamline BL8 (down to ca. 1 keV, i.e. covering the absorption edges of aluminum, magnesium and sodium), however, such experiments are quite challenging (require rather uncommon monochromator crystals and thin foils as window and sample support materials) and will therefore be part of future studies.

For this project, the double crystal monochromator at BL8 was equipped with either InSb(111) crystals (for spectroscopy at the silicon K-edge, 1839 eV) or Ge(220) crystals (calcium and iron K-edge at 4039 eV and 7112 eV, respectively). The scan parameters for the measurements at these absorption edges are shown in table 1. The beamsize at the sample position was 10 mm x 1 mm. During XANES measurements the incident and transmitted monochromatic X-ray intensities were measured with ionization chambers, and the intensities of the K_α X-ray fluorescence lines of silicon, calcium and iron (at 1.74 keV, 3.69 keV and 6.41 keV) were measured with a 13-element germanium detector (Canberra) or a 7-element silicon drift detector (SGX Sensortech) positioned perpendicular to the beam direction in the plane of the beam. Fiber samples were oriented at 45° to the incident beam. During the measurements at the Si and Ca K absorption edge, the sample chamber was flushed with helium to minimize the attenuation of the fluorescence radiation by ambient air. All fiber samples were measured in fluorescence mode. For energy calibration of the monochromator, absorption spectra of silicon powder, calcium carbonate powder ($CaCO_3$) and an iron foil were recorded in transmission mode. The first maximum of the first derivative of the Si powder spectrum was set to an energy of 1839 eV. For calibration at the calcium K-edge the first resonance (´white line´, absolute maximum) in the XANES spectrum of the $CaCO_3$ reference sample was set to an energy of 4049 eV.

To calibrate the set-up for iron K-edge spectroscopy the first maximum of the first derivative of the Fe foil spectrum was set to an energy of 7112 eV. XANES spectra (absorption coefficient as function of the photon energy E, in arbitrary units) were extracted from the raw data by background subtraction and normalization (and averaging over several spectra in cases where more than one XANES spectrum of the same sample was measured) using the Athena program [47].

RESULTS AND DISCUSSION

X-ray absorption near edge spectra at the K absorption edges of silicon, calcium and iron

Fig. 2 (a) shows silicon K-edge XANES spectra of untreated basalt fibers cut from the roving (type A) along with the spectra of the same fiber type heated for 1 hour at 800 °C. These spectra do not indicate any influence of this thermal treatment on the absorption behavior of silicon in these fibers. For comparison, a silicon K-edge XANES spectrum of quartz powder, measured on self-adhesive Kapton tape in transmission mode, is shown in Fig. 2 (b). The spectra of the basalt fibers and the quartz reference both show a pronounced absorption maximum („white line") at 1847 eV (1s → 3p transition [48-50]) and a broader „shape resonance" at ca. 1864 eV. Between these two spectral features, three additional absorption maxima appear in the quartz spectrum,

Table 1. Scan parameters for XANES measurements at different absorption edges.

Edge	Energy range (step size)			Integration time
	Pre-edge region	*Near edge region*	*Post-edge region*	
Si K	1789 - 1819 eV (3 eV)	1819 - 1909 eV (0.2 eV)	1909 - 1939 eV (3 eV)	1 s
Ca K	3950 - 4020 eV (2 eV)	4020 - 4120 eV (0.2 eV)	4120 - 4200 eV (1 eV)	3 s
Fe K	7000 - 7100 eV (2 eV)	7100 - 7160 eV (0.5 eV)	7160 - 7300 eV (1 eV)	3 s
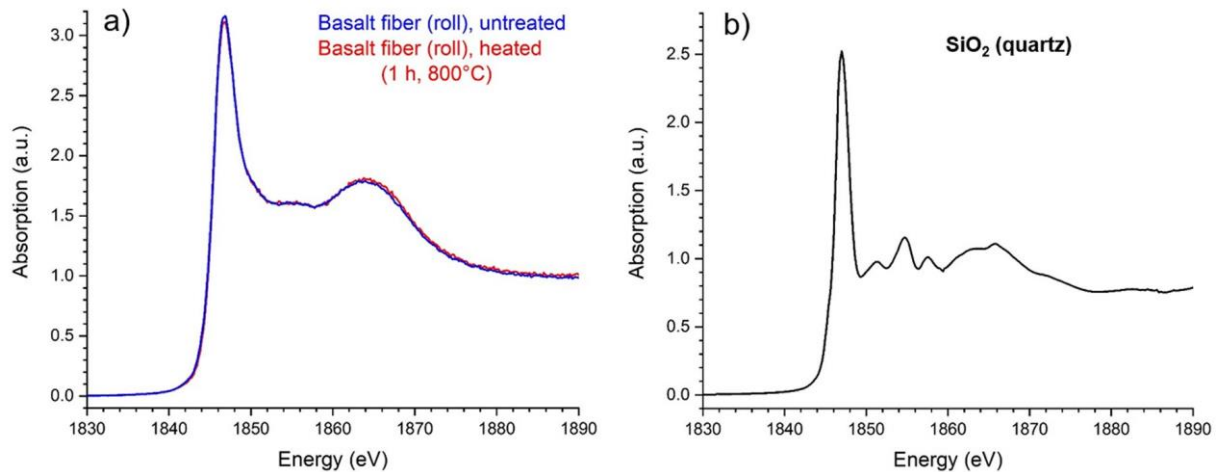
Figure 2. Silicon K-edge XANES spectra of: (a) basalt fibers cut from a roving (type A, ´roll´) and (b) CaO powder.
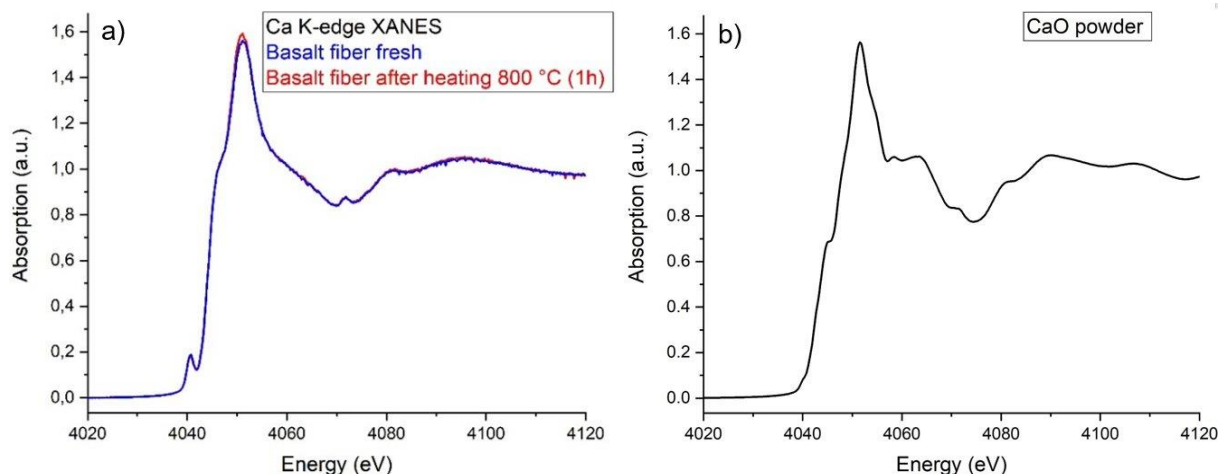
Figure 3. Calcium K-edge XANES spectra of: (a) basalt fibers cut from a roving (type A) and (b) quartz powder.

which are well known in the literature [48] and have been assigned by Li et al. [49] [50] to electronic transitions (1s → 3d/p) and multiple scattering processes. In the silicon K-edge absorption spectra of other stable crystalline modifications of SiO_2 like coesite and cristobalite, weak but clearly pronounced characteristic local absorption maxima above the white line are visible as well [48] [51-53].

In contrast, in the spectra of the basalt fibers (Fig. 2(a)) such features are not observed. In general, in amorphous SiO_2 they are suppressed in intensity and the absorption spectra are generally more diffuse due to the inherent disordered nature of such materials, featuring a broad range of Si-O-Si angles and Si-O and Si-Si distances compared to their crystalline counterparts [48] [54-57]. Accordingly, the spectra in

Fig. 2(a) indicate an atomic environment of silicon very similar to amorphous SiO_2, as expected: Such basalt fibers are produced by melting basalt rocks between ca. 1400 °C and 1700 °C [13] [58], followed by rapid cooling causing the basalt to solidify in a glass-like amorphous phase [59]. From Fig. 2(a) it is obvious that the thermal treatment does not cause any distinct spectral features to emerge in the energy range between 1847 eV and 1864 eV. Accordingly, these measurements do not indicate crystallization of SiO_2 upon heating at 800 °C for one hour.

Fig. 3(a) shows calcium K-edge XANES spectra of the same fiber type (roving, type A), untreated and after one hour of heating at 800 °C. In most publications providing tabulated values for the chemical composition of basalt, the calcium

containing component is listed as "CaO". A spectrum of CaO powder, measured on self-adhesive Kapton tape in transmission mode, is therefore shown in Fig. 3(b) for comparison. However, it clearly differs from the calcium K-edge spectra of the basalt fibers. Intensity, energy position and shape of the white line peak are roughly comparable (in both cases with a shoulder on the low energy side), but the basalt spectrum features a pronounced pre-edge resonance at ca. 4040 eV that does not appear in the CaO spectrum. On the other hand, above the white line two less intense peaks at 4059 eV and 4063 eV are observed in the CaO spectrum, but not in the absorption data of the fibers (assignment of absorption peaks in [48]). The spectra of the basalt fibers in Fig. 3(a) almost perfectly match several Ca k-edge XANES spectra of soda lime aluminosilicate glasses, which Cormier and Neuville compared with those of several Ca-bearing minerals [60]. The spectra of these crystalline references showed some additional features above the white line which were smoothed in the glass (except a weak local absorption maximum at ca. 4070 eV which occurs in most published Ca K-edge XANES spectra without physical interpretation). Occurrence and intensities of pre-edge features, which depend on the Ca site geometry (symmetry), varied from mineral to mineral. The comparatively high intensity of the pre-edge peak in the glasses was interpreted as an indication that the Ca environment is more distorted. The spectra of the basalt fibers in Fig. 3(a) also almost perfectly match the majority of XANES spectra of calcium aluminosilicate glasses [61], CO_2-bearing silicate glasses [62] and amorphous calcium silicate hydrates [63]. Moreover, the spectra of the basalt fibers in Fig. 3(a) resemble (although not as closely as the glasses mentioned above) the Ca K-edge XANES spectra of amorphous calcium carbonate which Brinza et al. [64] compared with spectra of the crystalline calcium carbonate phases calcite, aragonite and vaterite. In the post edge region (above the white line) these three crystalline references featured further absorption peaks and shoulders, whereas the amorphous calcium carbonate showed a smooth, relatively featureless decline from the white line to ca. 4068 eV. Qualitatively similar comparisons of amorphous and crystalline $CaCO_3$ polymorphs have been published by Kathyola et al. [65], Monico et al. [66] and Xto et al. [67], and also by Levi-Kalisman et al. [68] [69] and Lam et al. [70], who suggested an increase in structural disorder as a possible explanation for the observed decrease in the number of spectral features and their intensities in the post-edge regions of spectra when moving from the crystalline to the amorphous materials. Therefore, like the Si K-edge spectra in Fig. 2(a), the Ca K-edge spectra of the basalt fiber in Fig. 3(a) can be regarded as characteristic of a predominantly amorphous environment of the Ca or Si absorber atoms, which is

not measurably affected by heating for 1 hour at 800 °C.

Fig. 4(a) shows iron K-edge XANES spectra of the same fiber type (roving, type A), untreated and after heating for one hour at 480 °C and 800 °C. For comparison, transmission mode iron K-edge XANES spectra of reference compounds with iron in different oxidation states (powders spread on self-adhesive Kapton tape) are shown in Fig. 4(b). These reference spectra show that with increasing oxidation number of iron the rising edge of the white line in the absorption spectra is shifted to higher energies. The spectra in Fig. 4(a) indicate that moderate heating for one hour at 480 °C does not have a measurable impact on the iron speciation in the fibers, whereas heating at 800 °C leads to significant changes in the spectra: The intensity of the white line increases, and its rising edge is shifted to higher energies by ca. 2 eV, indicating oxidation of the iron atoms. Similar results are reported for iron K-edge XANES studies on bulk glass samples containing iron oxide and bulk basalt samples [71] [72]. Referring to an earlier investigation, changes in the bulk structure of basalt fibers upon heating at higher temperature are interpreted as result of crystallization processes [19-21] [23-25]. Based on the silicon and calcium absorption data shown in Fig. 2 and Fig. 3, there is no indication of crystallization of the fibers – at least not at the applied temperature (max. 800 °C) and the relatively short duration of heating. Earlier studies indicate that upon moderate heating predominantly the carbon containing sizing agent is pyrolyzed [23].

This effect on the sizing agent is probably not reflected in the spectra in Fig. 4(a), since XANES in the here applied fluorescence mode is not a surface sensitive technique, and the carbon absorption edge lies far below the operating range of the beamline. In the future such processes could be investigated using surface sensitive X-ray absorption spectroscopy, e.g. in electron yield mode, like in general the chemical bonds between the sizing and the basalt fiber.

Unfortunately, a quantitative analysis of the basalt fiber Fe-K-XANES spectra by fitting them to a linear combination of reference spectra was not possible with the reference compounds measured so far (iron foil and iron oxide powders), even when FeO reference spectra from a data base were included as representatives of divalent iron (not shown). This is obviously due to the complexity of the basalt fiber with its amorphous and multicomponent nature. In the future, further candidates for suitable reference compounds, including minerals and amorphous materials, will be tested in order to properly identify the chemical speciation of iron in the untreated and heated fibers. In any case, it can be assumed that the iron atoms in the basalt fibers are already in an "oxidized state" before the thermal treatment, and heating leads to further oxidation, probably through a change in the ratio of trivalent iron and the total iron content.
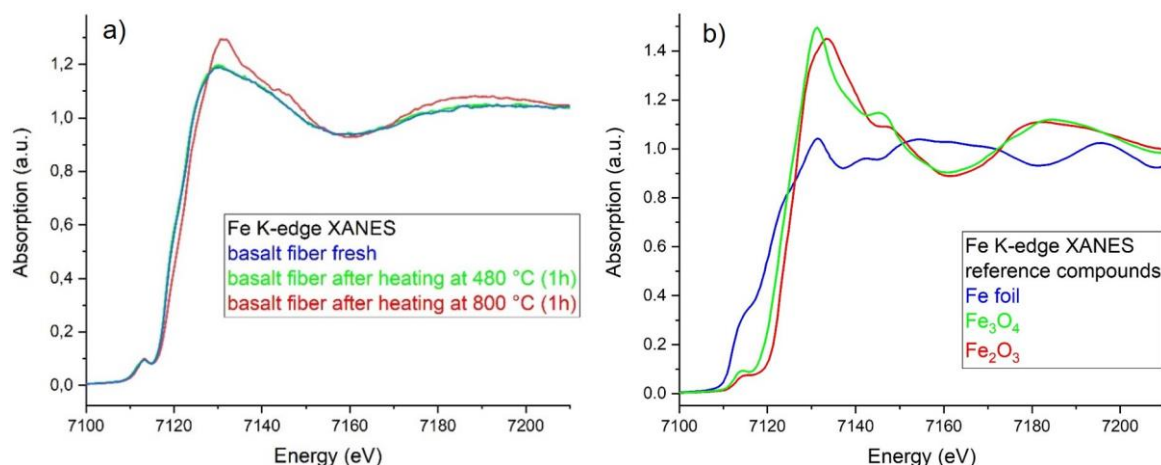
Figure 4. Iron K-edge XANES spectra of: (a) basalt fibers cut from a roving (type A) and (b) reference compounds.

Further investigation of temperature influence on iron atoms in the fibers

Since heating at 800 °C did not affect the silicon and calcium K-edge XANES spectra measured so far, and heating at 480 °C did not influence the X-ray absorption of iron atoms in the basalt fibers, focusing on the iron K- absorption edge and setting the first target temperature of the furnace to 600 °C seemed a reasonable starting point for further experiments. Of course, these first measurements cannot reveal to which extent, besides the applied temperature, the duration of heating affects structural changes measurable through XANES (i.e. whether longer heating can have the same effect as increasing the temperature).

Fig. 5 shows iron K-edge XANES spectra of the basalt fibers cut from the roving (type A) which were thermally treated according to the temperature profile in Fig. 1. Increasing temperature (and heating time in the furnace) causes an increase in white line intensity along with a shift of the rising edge of the white line towards higher energies in the spectra, indicating progressing (further) oxidation of the iron atoms. The most pronounced differences occur between the spectra of samples heated up to 600 °C and those heated up to 800 °C. It is not yet clear to which final state the fiber is oxidized at the end of the procedure and whether the oxidation is accompanied by crystallization (results shown in Fig. 2 and Fig. 3 suggest that this does not occur up to at least 800 °C). Given the penetration strength of X-rays, one can assume that this oxidation occurs in the bulk material and not predominantly at the surface of the fibers.

For comparison, a second type of basalt fiber (uncoated chopped fibers, type B) was subjected to the same thermal treatment (Fig. 1). The iron K-edge XANES spectra of these samples are shown in Fig. 6. The changes in the spectra as a result of heating to different temperatures are similar to the observed changes in absorption behavior of the fiber samples from the roving: With increasing maximum heating temperature the rising edge of the white line in the spectra is shifted to higher energies while the white line intensity increases. Interestingly, in contrast to the fiber from the roving, in the spectra of the uncoated chopped fiber (Fig. 6) also the weak pre-edge feature at 7114 eV seems to be affected by the thermal treatment (maximum of pre-edge peak shifted by ca. 0.7 eV when moving from maximum temperature 600 °C to maximum temperature 700 °C). Analysis of pre-edge peaks in iron K-edge XANES spectra, which are due to 1s→3d transitions, has been used to determine oxidation state (Fe^{2+} to Fe^{3+} ratio) and coordination of iron in different materials [48] [73-75]. Whether the pre-edge shift in Fig. 6 is really caused by structural changes or an artefact due to a shift in the monochromator´s energy calibration needs to be carefully investigated.

In Fig. 7 iron K-edge XANES spectra of both fiber types A and B (roving and uncoated chopped fibers), subjected to the thermal treatment shown in Fig. 1, are directly compared (same data as in Fig. 5/6). In the ´fresh´ state and after being heated at 600 °C both fibers show the same absorption behavior: The spectra in Fig. 7(a) and (b) are identical within the noise level of the measurements. These results indicate that the atomic environment of the iron atoms in both types of fibers is very similar in this temperature range. After heating at 700 °C and 800 °C (spectra after heating at 900 °C not shown) the absorption behavior of the two fibers is different (Fig. 7 (c-d)): In the spectra of the uncoated chopped fiber (type B) the white line is more intense and the rising edge of the white line at higher energies compared to type A. However, based on these first results one should not jump to the conclusion that in this temperature range the iron atoms in the uncoated chopped fibers are more susceptible to (further) oxidation compared to fiber samples cut from the roving. Such conclusions, especially when based on relatively small differences the spectra of both fiber types (Fig. 7(c) and (d)), would require that the

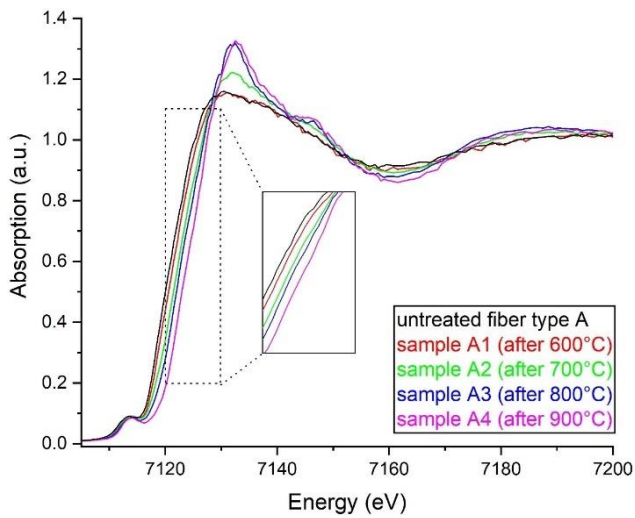thermal treatment for both fibers was exactly identical. This

Figure 5. Iron K-edge XANES spectra of basalt fibers from the roving (type A) heated at different temperatures according to the temperature profile in Fig. 1.
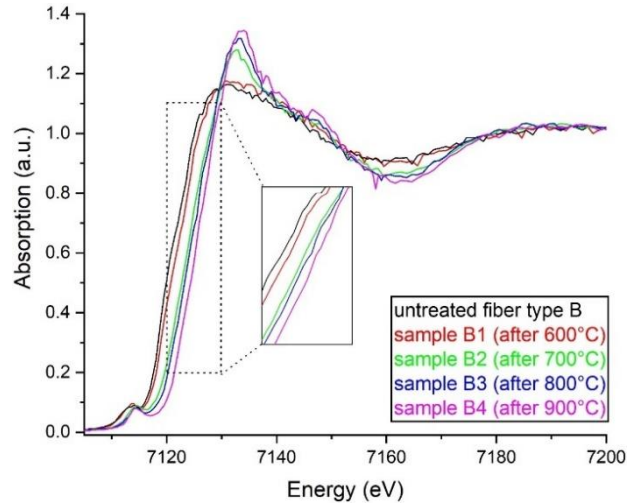

Figure 6. Iron K-edge XANES spectra of uncoated chopped basalt fibers (type B) heated at different temperatures according to the temperature profile in Fig. 1.
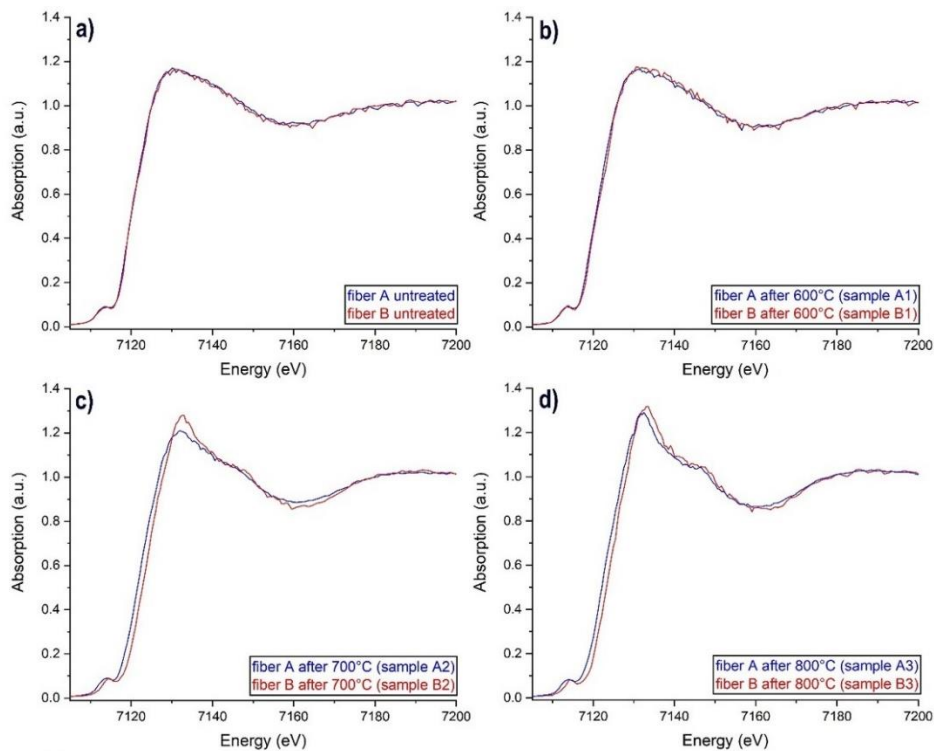

Figure 7. Iron K-edge XANES spectra: Comparison of two types of basalt fiber (type A: fiber samples cut from roving, type B: uncoated chopped fibers) heated to different maximum temperatures: (a) untreated, (b) 600 °C, (c) 700 °C, (d) 800 °C.

condition is not strictly fulfilled: The uncoated chopped fibers were heated after the XANES spectra of the thermally treated samples from the roving were recorded. Therefore, when preparing samples for future experiments the different types of fiber to be compared should be heated together in the furnace for better comparability. Further parameters to be taken into account for a comparison are potential differences in the physical properties of the fibers (e.g. diameter, density), and in the chemical composition.

SUMMARY AND OUTLOOK

These XANES measurements show how X-ray absorption spectroscopy can be used to investigate structural changes in basalt fibers resulting from heating. As a first step, the K- absorption edges of silicon, calcium and iron were selected for recording XANES spectra of basalt fiber samples, which were cut from a roving and then heated for one hour at either 480 °C or 800 °C. The silicon and calcium K-edge spectra indicate an amorphous structure in the

basalt fibers. Since these spectra were not influenced by heating, there is no sign of crystallization at temperatures up to 800 °C during this, relatively short, duration of the thermal treatment. In contrast, the iron K-edge spectra of heated fibers showed significant differences compared to the untreated fibers, indicating a progressing oxidation of the iron atoms somewhere above 480 °C. The results suggest that the atomic environment of at least one chemical element (iron) in the fibers changes upon heating above a specific temperature, while other chemical elements (here silicon and calcium) apparently remain unaffected by thermal treatment – at least when heated at 800 °C for one hour. As a next step, the furnace used for sample preparation was programmed to ramp up the temperature to four target values between 600 °C and 900 °C and keep it constant at these points for one hour before proceeding to the next target temperature. After each temperature plateau, portions of fiber samples were taken from the furnace for iron K-edge XANES measurements. This thermal treatment was also applied to uncoated chopped fibers. In general, iron K-edge XANES spectra of both types of fibers show an increase in white line intensity and a shift of the rising edge of the white line towards higher energies with increasing maximum temperature. This shift can be attributed to a progressing oxidation of the iron atoms, the majority of which was most likely already in an oxidized state before heating. The thermal treatment then obviously leads to an increase in the relative concentration of trivalent iron compared to iron species with lower oxidation numbers. Small differences between the iron K-edge XANES spectra of the two fiber types heated at a maximum temperature above 600 °C may potentially indicate a higher susceptibility of the uncoated chopped fibers to oxidation compared to the fiber samples cut from the roving. However, a verifiable statement in this direction requires further systematic investigations, making sure that the two types of fiber were exposed to an identical thermal treatment, and considering their physical properties and chemical composition.

The results of this study demonstrate the high potential of XANES spectroscopy for the characterization of basalt fibers and their structural changes during heating, opening new perspectives in this field of research, especially when more systematic XANES studies are performed and extended to include further chemical elements in the fibers, or when set-ups for *in situ* X-ray absorption spectroscopy (with heatable sample cells) are used in order to correlate the spectroscopic data with temperature related changes in the mechanical properties of the fibers for a knowledge based development of modified basalt fibers with enhanced temperature stability (e.g. by surface treatment or doping with other chemical elements). However, the results of this first series of experiments leave some questions open for future studies under improved

experimental conditions: The thermal treatment applied to the basalt fibers prior to the XANES measurements seemed to be the most practicable procedure for sample preparation at the beginning of the project. However, when following this protocol, a sample heated up to a specific maximum temperature was prior to reaching that specific target temperature already heated during ramping up from room temperature and in most cases (except the maximum 600 °C samples) also exposed to one hour heating at each lower temperature plateau. For future experiments one should invest more time in sample preparation, prepare separate batches of fibers to be heated at only one specific constant temperature for a specific time and wait each time until the furnace has reached this target temperature before placing the batch in it. On the other hand, different types of fibers to be compared later based on their XANES data should be placed in the furnace together to make sure that they were subjected to identical heating conditions for better comparability. The initial structure of the fibers before the thermal treatment could not be identified based on the data recorded so far, since this requires XANES spectra of special reference compounds beyond the ´standard´ oxide powders commonly used for quantitative analysis. Suitable reference compounds to be acquired for such studies should be as similar as possible to the basalt fibers´ (amorphous) structure and chemical/mineral composition. The data recorded so far do not provide information about processes on the fibers´ surface, since ´standard´ fluorescence mode XANES spectroscopy is not a surface sensitive technique. Moreover, it is not yet clear to which extent the observed oxidation of iron species is accompanied by crystallization. This could be investigated by powder X-ray diffraction or Extended X-ray Absorption Fine Structure (EXAFS) spectroscopy. Crystallization should result in more pronounced EXAFS oscillations with stronger contributions of higher coordination shells compared to the amorphous phase.

REFERENCES

1. Cooke T.F.: Inorganic fibers - a literature review, J. Am. Ceram. Soc. 74(12), 1991, pp. 2959-2978. https://doi.org/10.1111/j.1151-2916.1991.tb04289.x
2. Mahltig B.: Introduction to inorganic fibers. Book chapter in: Inorganic and composite fibers, Mahltig B., Kyosev Y. (Eds.) Woodhead Publishing – Elsevier, Duxford, UK, 2018, pp. 1-30.
3. Teschner R.: Glasfasern, Springer-Vieweg, Berlin, 2019, 2nd Edition.
4. Pico D., Wilms C., Seide G., et al.: Natural volcanic rock fibers, Chem. Fibers Int. 61(2), 2011, pp. 90-92.
5. Schawaller D., Clauß B., Buchmeiser M.R.: Ceramic filament fibers–a review, Macromol. Mater. Eng. 297(6), 2012, pp. 502-522.

https://doi.org/10.1002/mame.201100364

6. Mahltig B., Kyosev Y.: Inorganic and composite fibers, Woodhead Publishing – Elsevier, Duxford, UK, 2018

7. Ylmaz V.T., Lachowski E.E., Glasser F.P.: Chemical and microstructural changes at alkali‐resistant glass fiber‐cement interfaces, J. Am. Ceram. Soc. 74(12), 1991, pp. 3054-3060.
    https://doi.org/10.1111/j.1151-2916.1991.tb04301.x

8. Kumbhar V.P.: An overview: basalt rock fibers-new construction material, Acta Eng. Intl. 2(1), 2014, pp. 11-18.

9. Ivanitskii S.G., Gorbachev G.F.: Continuous basalt fibers: production aspects and simulation of forming processes I: State of the art in continuous basalt fiber technologies, Powder Metall. Met. C+ 50(3), 2011, pp. 125-129.
    https://doi.org/10.1007/s11106-011-9309-x

10. Mahltig B., Kyosev Y. (ed.): Basalt fibers, Book chapter in: Inorganic and composite fibers, Woodhead Publishing – Elsevier, Duxford, UK, 2018, pp. 195-218.

11. Ding L., Liu Y., Liu J., et al.: Correlation analysis of tensile strength and chemical composition of basalt fiber roving, Polym. Composite. 40(7), 2019, pp. 2959-2966.
    https://doi.org/10.1002/pc.25138

12. Deák T., Czigány T.: Chemical composition and mechanical properties of basalt and glass fibers: a comparison. Textile Res. J. 2009, 79(7), pp. 645-651.
    https://doi.org/10.1177/0040517508095597

13. Jamshaid H., Mishra R.: A green material from rock: basalt fiber – a review, J. Text. I. 107(7), 2016, pp. 923-937.
    https://doi.org/10.1080/00405000.2015.1071940

14. Donald S.B., Swink A.M., Schreiber H.D.: High-iron ferric glass, J. Non-Cryst. Solids 352(6-7), 2006, pp. 539-543.
    https://doi.org/10.1016/j.jnoncrysol.2005.11.042

15. Schreurs J.W., Brill R.H.: Iron and sulfur related colors in ancient glasses, Archaeometry 26(2), 1984, pp. 199-209.
    https://doi.org/10.1111/j.1475-4754.1984.tb00334.x

16. Bacon F.R., Billian C.J.: Color and spectral transmittance of amber bottle glass, J. Am. Ceram. Soc. 37(2), 1954, pp. 60-66.
    https://doi.org/10.1111/j.1151-2916.1954.tb14006.x

17. Dhand V., Mittal G., Rhee K.Y., et al.: A short review on basalt fiber reinforced polymer composites, Compos. Part B-Eng. 73, 2015, pp. 166-180.
    https://doi.org/10.1016/j.compositesb.2014.12.011

18. Khandelwal S., Rhee K.Y.: Recent advances in basalt-fiber-reinforced composites: Tailoring the fiber-matrix interface. Compos. Part B-Eng. 192, 2020, 108011 p.
    https://doi.org/10.1016/j.compositesb.2020.108011

19. Hao L., Yu W.: Evaluation of thermal protective performance of basalt fiber nonwoven fabrics, J. Thermal Anal. Calor. 100(2), 2010, pp. 551-555.
    https://doi.org/10.1007/s10973-009-0179-0

20. Moiseev E.A., Gutnikov S.I., Malakho A.P., et al.: Effect of iron oxides on the fabrication and properties of continuous glass fibers, Inorg. Mater. 44, 2008, pp. 1026–1030.
    https://doi.org/10.1134/S0020168508090215

21. Gutnikov S.I., Manylov M.S., Lipatov Ya.V., et al.: Effect of the reduction treatment on the basalt continuous fiber crystallization properties, J. Non-Cryst. Solids 368, 2013, pp. 45–50.
    https://doi.org/10.1016/j.jnoncrysol.2013.03.007

22. Gutnikov S.I., Manylov M.S., Lazoryak B.I.: Crystallization and thermal stability of the P-doped basaltic glass fibers. Minerals 9(10), 2019, pp. 615.
    https://doi.org/10.3390/min9100615

23. Overkamp T., Mahltig B., Kyosev Y.: Strength of basalt fibers influenced by thermal and chemical treatments. J. Ind. Text. 47(5), 2018, pp. 815-833.
    https://doi.org/10.1177/1528083716674905.x

24. Fiore V., Scalici T., Di Bella G., et al.: A review on basalt fibre and its composites, Compos. Part B-Eng. 74, 2015, pp. 74–94.
    https://doi.org/10.1016/j.compositesb.2014.12.034

25. Lipatov Y.V., Arkhangelsky I.V., Dunaev A.V., et al.: Crystallization of zirconia doped basalt fibers, Thermochim. Acta 575, 2014, pp. 238–243.

https://doi.org/10.1016/j.tca.2013.11.002

26. Bunker G.: Introduction to XAFS, Cambridge University Press, 2010.

27. Calvin S.: XAFS for Everyone, CRC Press, 2013.

28. Newville M.: Fundamentals of XAFS, Rev. Mineral. Geochem.78 (1), 2014, pp. 33–74.
    https://doi.org/10.2138/rmg.2014.78.2

29. Sharma S.K., Verma D.S. (ed.): Handbook of materials characterization, Cham: Springer, chapter 13, 2018.

30. D'Amico S., Venuti V. (ed.): Handbook of cultural heritage analysis, Cham: Springer (Springer nature reference), 2022.

31. Gates W.P., Bergaya F., Theng B.K.G., et al. (ed.): X-ray absorption spectroscopy, Handbook of Clay Science, Chapter 12.3, Developments in clay science 1, 2006, pp. 789 – 864.

32. Buzanich A.G.: Recent developments of X-ray absorption spectroscopy as analytical tool for biological and biomedical applications, X-Ray Spectrom. 51(3), 2022, pp. 294–303.
    https://doi.org/10.1002/xrs.3254

33. Iglesias-Juez A., Chiarello G.L., Patience G.S., et al.: Experimental methods in chemical engineering: X-ray absorption spectroscopy — XAS, XANES, EXAFS. Can. J. Chem. Eng. 100(1), 2022, pp. 3–22.
    https://doi.org/10.1002/cjce.24291

34. Iwasawa Y., Asakura K., Tada M. (ed.): XAFS techniques for catalysts, nanomaterials, and surfaces, Cham: Springer International Publishing, 2017, online:
    http://dx.doi.org/10.1007/978-3-319-43866-5

35. Prange A., Modrow H.: X-ray absorption spectroscopy and its application in biological, agricultural and environmental research., Rev. Environ. Sci. Bio. 1(4), 2002, pp. 259–276.
    https://doi.org/10.1023/A:1023281303220

36. Mahltig B.: High-performance fibres – A review of properties and IR-spectra, Tekstilec 64, 2021, pp. 96-118.
    https://doi.org/10.14502/Tekstilec2021.64.96-118

37. Mahltig B., Grethe T.: High-performance and functional fiber materials—A review of properties, scanning electron microscopy SEM and electron dispersive spectroscopy EDS, Textiles 2, 2022, pp. 209-252.
    https://doi.org/10.3390/textiles2020012

38. Ruffen C., Mahltig B.: Basalt fibers as functional additives in coating of textiles, J. Coat. Technol. Res. 18, 2021, pp. 271-281.
    https://doi.org/10.1007/s11998-020-00383-8

39. Klysubun W., Sombunchoo P., Wongprachanukul N., et al.: Commissioning and performance of X-ray absorption spectroscopy beamline at the Siam Photon Laboratory, Nucl. Instrum. Meth. A 582, 2007, pp. 87–89.
    https://doi.org/10.1016/j.nima.2007.08.067

40. Klysubun W., Tarawarakarn P., Thamsanong N., et al.: Upgrade of SLRI BL8 beamline for XAFS spectroscopy in a photon energy range of 1–13 keV, Radiat. Phys. Chem. 175, 2020, 108145 p.
    https://doi.org/10.1016/j.radphyschem.2019.02.004

41. Klysubun W., Sombunchoo P., Deenan W., et al.: Performance and status of beamline BL8 at SLRI for X-ray absorption spectroscopy, J. Synchrotron Radiat. 19, 2012, pp. 930–936.
    https://doi.org/10.1107/S0909049512040381

42. Cooper R.F., Fanselow J.B., Poker D.B.: The mechanism of oxidation of a basaltic glass: Chemical diffusion of network-modifying cations, Geochim. Cosmochim. Ac. 60(17), 1996, pp. 3253–3265.
    https://doi.org/10.1016/0016-7037(96)00160-3

43. Yilmaz S., Özkan O.T., Günay V.: Crystallization kinetics of basalt glass, Ceram. Int. 22(6), 1996, pp. 477–481.
    https://doi.org/10.1016/0272-8842(95)00118-2

44. Morozov N.N., Bakunov V.S., Morozov E.N., et al.: Materials based on basalts from the European north of Russia, Glass Ceram+ 58 (3/4), 2001, pp. 100–104.
    https://doi.org/10.1023/a:1010947415202

45. Burkhard D.J.M.: Crystallization and oxidation of Kilauea basalt glass: Processes during reheating experiments, J. Petrology 42(3), 2001, pp. 507–527.
    https://doi.org/10.1093/petrology/42.3.507

46. Chen X., Zhang Y., Hui D., et al.: Study of melting properties of basalt based on their mineral components, Compos. Part B-Eng. 116, 2017, pp. 53–60. https://doi.org/10.1016/j.compositesb.2017.02.014

47. Ravel B., Newville M.: ATHENA, ARTEMIS, HEPHAESTUS: data analysis for X-ray absorption spectroscopy using IFEFFIT, J. Synchrotron Radiat. 12, 2005, pp. 537–541. https://doi.org/10.1107/S0909049505012719

48. Henderson G.S., De Groot F.M.F., Moulton B.J.A.: X-ray absorption near-edge structure (XANES) spectroscopy. Henderson G.S., Neuville D.R., Downs R.T. (ed.): Spectroscopic methods in mineralogy and materials sciences, Boston, Chantilly, Virginia: DE GRUYTER; Mineralogical Society of America, Rev. Mineral. Geochem. 78, 2015, pp. 75–138.

49. Li D., Bancroft G.M., Kasrai M., et al.: X-ray absorption spectroscopy of silicon dioxide (SiO_2) polymorphs: The structural characterization of opal, Am. Mineral. 79, 1994, pp. 622–632.

50. Li D., Bancroft G.M., Fleet M.E., et al.: Silicon K-edge XANES spectra of silicate minerals, Phys. Chem. Miner. 22, 1995, pp. 115-122.

51. Gilbert B., Frazer B.H., Naab F., et al.: X-ray absorption spectroscopy of silicates for in situ, sub-micrometer mineral identification, Am. Mineral. 88, 2003, pp. 763–769. https://doi.org/10.2138/am-2003-5-605

52. De Ligny D., Neuville D.R., Cormier L., et al.: Silica polymorphs, glass and melt: An in situ high temperature XAS study at the Si K-edge, J. Non-Cryst. Solids 355, 2009, pp. 1099-1102.

53. Hormes J., Klysubun W., Göttert J., et al.: A new SOLARIS beamline optimized for X-ray spectroscopy in the tender energy range, Nucl. Instrum. Meth. B 489, 2021, pp. 76–81. https://doi.org/10.1016/j.nimb.2020.12.017

54. Davoli I., Paris E., Stizza S., et al.: Structure of densified vitreous silica – silicon and oxygen XANES spectra and multiple-scattering calculations, Phys. Chem. Miner. 19, 1992, pp. 171-175.

55. Henderson G.S., Fleet M.E.: The structure of titanium silicate glasses investigated by Si K-edge X-ray absorption spectroscopy, J. Non-Cryst. Solids 211, 1997, pp. 214-221.

56. De Wispelaere S., Cabaret D., Levelut C., et al.: Na-, Al- and Si K-edge XANES study of sodium silicate and sodium aluminosilicate glasses: influence of the glass surface, Chem. Geol. 213, 2004, pp. 63-70.

57. Cabaret D., Le Grand M., Ramos A., et al.: Medium range structure of borosilicate glasses from Si K-edge XANES: a combined approach based on multiple scattering and molecular dynamics calculations, J. Non-Cryst. Solids 289(1-3), 2001, pp. 1–8. https://doi.org/10.1016/S0022-3093(01)00733-5

58. Militký J., Kovačič V., Rubnerová J.: Influence of thermal treatment on tensile failure of basalt fibers, Eng. Fract. Mech. 69(9), 2002, pp. 1025–1033. https://doi.org/10.1016/S0013-7944(01)00119-9

59. Tamás-Bényei P., Sántha P.: Potential applications of basalt fibre composites in thermal shielding, J. Therm. Anal. Calorim. 148(2), 2023, pp. 271–279. https://doi.org/10.1007/s10973-022-11799-2

60. Cormier L., Neuville D.R.: Ca and Na environments in Na_2O–CaO–Al_2O_3–SiO_2 glasses: influence of cation mixing and cation-network interactions, Chem. Geol. 213(1-3), 2004, pp. 103–113. https://doi.org/10.1016/j.chemgeo.2004.08.049

61. Neuville D.R., Cormier L., Flank A.M., et al.: Al speciation and Ca environment in calcium aluminosilicate glasses and crystals by Al and Ca K-edge X-ray absorption spectroscopy, Chem. Geol. 213(1-3), 2004, pp. 153–163. https://doi.org/10.1016/j.chemgeo.2004.08.039

62. Morizet Y., Trcera N., Larre C., et al.: X-ray absorption spectroscopic investigation of the Ca and Mg environments in CO_2-bearing silicate glasses, Chem. Geol. 510, 2019, pp. 91–102. https://doi.org/10.1016/j.chemgeo.2019.02.014

63. Guo X., Wu J., Yiu Y.M., et al.: Drug-nanocarrier interaction–tracking the local structure of calcium silicate upon ibuprofen loading with X-ray absorption near edge structure (XANES), Phys. Chem. Chem. Phys. 15(36), 2013, pp. 15033–15040. https://doi.org/10.1039/c3cp50699a

64. Brinza L., Schofield P.F., Hodson M.E., et al.: Combining μXANES and μXRD mapping to analyse the heterogeneity in calcium carbonate granules excreted by the earthworm Lumbricus terrestris, J. Synchrotron Radiat. 21(Pt 1), 2014, pp. 235–241. https://doi.org/10.1107/S160057751303083X

65. Kathyola T.A., Chang S.Y., Willneff E.A., et al.: X-ray absorption spectroscopy as a process analytical technology: Reaction studies for the manufacture of sulfonate-stabilized calcium carbonate particles, Indu. Eng. Chem. Res. 62(40), 2023, pp. 16198–16206. https://doi.org/10.1021/acs.iecr.3c02540

66. Monico L., Cartechini L., Rosi F., et al.: Synchrotron radiation Ca K-edge 2D-XANES spectroscopy for studying the stratigraphic distribution of calcium-based consolidants applied in limestones, Scientific Reports 10(1), 2020, pp. 14337. https://doi.org/10.1038/s41598-020-71105-8

67. Xto J., Wetter R., Borca C.N., et al.: Droplet-based in situ X-ray absorption spectroscopy cell for studying crystallization processes at the tender X-ray energy range, RSC Adv. 9(58), 2019, pp. 34004–34010. https://doi.org/10.1039/c9ra06084g

68. Levi-Kalisman Y., Raz S., Weiner S., et al.: X-Ray absorption spectroscopy studies on the structure of a biogenic "amorphous" calcium carbonate phase, J. Chem. Soc. Dalton Trans. (21), 2000, pp. 3977–3982. https://doi.org/10.1039/B003242P

69. Levi-Kalisman Y., Raz S., Weiner S., et al.: Structural differences between biogenic amorphous calcium carbonate phases using X-ray absorption spectroscopy. Adv. Funct. Mater. 12(1), 2002, pp. 43. https://doi.org/10.1002/1616-3028(20020101)12:1%3C43::AID-ADFM43%3E3.0.CO;2-C

70. Lam R.S.K., Charnock J.M., Lennie A., et al.: Synthesis-dependant structural variations in amorphous calcium carbonate, CrystEngComm 9(12), 2007, 1226 p. https://doi.org/10.1039/b710895h

71. Fiege A., Ruprecht P., Simon A.C., et al.: Calibration of Fe XANES for high-precision determination of Fe oxidation state in glasses: Comparison of new and existing results obtained at different synchrotron radiation sources, Am. Mineral. 102(2), 2017, pp. 369-380. https://doi.org/10.2138/am-2017-5822

72. Cottrell E., Kelley K.A., Lanzirotti A., et al.: High-precision determination of iron oxidation state in silicate glasses using XANES, Chem. Geol. 268(3-4), 2009, pp. 167-179. https://doi.org/10.1016/j.chemgeo.2009.08.008

73. Wilke M., Farges F., Petit P.E., et al.: Oxidation state and coordination of Fe in minerals: An Fe K- XANES spectroscopic study, Am. Mineral. 86(5-6), 2001, pp. 714–730. https://doi.org/10.2138/am-2001-5-612

74. Westre T.E., Kennepohl P., DeWitt J.G., et al.: A multiplet analysis of Fe K-Edge 1s → 3d pre-edge features of iron complexes, J. Am. Chem. Soc. 119(27), 1997, pp. 6297–6314. https://doi.org/10.1021/ja964352a

75. Boubnov A., Lichtenberg H., Mangold S., et al.: Identification of the iron oxidation state and coordination geometry in iron oxide- and zeolite-based catalysts using pre-edge XAS analysis, J. Synchrotron Radiat. 22(2), 2015, pp. 410–426. https://doi.org/10.1107/S1600577514025880

DATA ANALYSIS FOR THE PREDICTION OF TEXTILE WASTE RECYCLING IN UKRAINE

BUKHANTSOVA, LIUDMYLA[*]; ZACHARKEVICH, OKSANA; LUSCHEVSKA, OLENA; KRASNIUK, LARYSA; KOSHEVKO, YULIA; DITKOVSKA, OLESYA AND SHVETS, GALINA

Khmelnytskyi National University, 11, Instytutska str., Khmelnytskyi, 29016, Ukraine

ABSTRACT

The textile and sewing industry is known to be the second most environmentally harmful industry for the environment. To maintain a circular economy, textile sources should be recycled, repaired, and used as much as possible while retaining their value. This research provides primary information about the database of post-production textile waste. The data suggests that 30 garment companies produce 778.11 tons of post-production textile waste per year, with cotton accounting for 42.14% and polyester for 32.45%. It is important to consider processing waste using different technologies according to the certification of textile waste to determine its raw material composition and purity. For an effective waste management policy, it is essential to implement it systematically, continually assess outcomes and challenges, and involve all stakeholders and activities that generate and manage waste. This is crucial in formulating an effective waste management policy.

KEYWORDS

Recycling; Textile waste; Cotton waste; Polyester waste; Pre-consumer waste; Post-production waste.

INTRODUCTION

The urgency of climate change, loss of nature, and pollution is worsened by unsustainable production and consumption. The textile industry, a significant contributor to these issues, must step up and implement sustainable practices. The industry's value chain significantly contributes to global greenhouse gas emissions. There is a growing need for the industry to recycle and use sustainable materials, reduce textile waste, and achieve net-zero emissions [1]. By 2030, the sector's CO_2 emissions are projected to increase to nearly 2.7 billion tons annually, equivalent to one year of emissions from almost 230 million average passenger vehicles [2]. Transforming the textile value chain towards sustainability and circularity is not just a necessity but a crucial step toward a circular economy, and the industry's contribution to this transformation is vital.

Zero-waste design is a powerful tool for implementing a circular economy. The Zero Waste International Alliance defines it as an ethical, economical, efficient, and visionary objective that guides people in transforming their lifestyles and practices to mimic sustainable natural cycles [3] [4]. Zero-waste design aims to effectively consume resources throughout the product lifecycle by optimizing material usage, promoting reuse, recycling, and recovery, and

designing products that can be easily modified or repurposed [5]. These actions minimize textile waste, which can be categorized as pre-consumer or post-consumer waste streams. Circular fashion approaches mainly concentrate on used garments or post-consumer waste [6-8]. Less attention is paid to textile waste and remnants from garment manufacturing, known as post-production or pre-consumer waste [9-10].

World sustainable trends are increasing the recycling and collection of textile waste, which could lead to an annual reduction of around 18 million tons of CO_2 emissions. This would involve reducing incineration and landfill use and moving the industry towards a closed-loop system [1].

Now, efforts are being made to address global trade dynamics and support countries that cannot process the waste they receive, helping them establish effective recycling and safe waste management solutions. Textile incineration or destruction is not recommended unless the textiles are highly contaminated. Instead, textiles should be reused, recycled, or repurposed [2]. The study results [11] show that reusing textiles has a more significant positive impact than recycling. Both strategies should be integrated, and proper management through separate collection for reuse and recycling can help

---

reduce environmental impacts. Recycled fibers generally have lower environmental impacts than virgin fibers, except for some cases like polyester or cotton recycling. At the same time, regenerated textiles can have better properties than primary ones [12].

By 2030, the aim is to source all priority materials that have a low climate impact and do not negatively affect other Sustainable Development Goals. This includes having 25% of key raw materials with lower climate impact by 2025 and having 45% recycled polyester to achieve a 90% recycled volume share by 2030 [13].

Four archetypes of textile recycling (mechanical, thermo-mechanical, chemical, and thermo-chemical) are well-known [14-15]. They are used according to textile waste content [14] and have different parameters, such as open- or closed-loop, energy efficiency, and restoring or maintaining the original quality fibers [16-18]. That's why knowing the raw material content of textile waste is essential in developing a sustainable action roadmap and selecting the most appropriate technology for textile recycling.

There are enough examples of creating sustainable action plans and designing sustainable and circular products. Textiles and clothing are strategic pillars of the European economy, accounting for around 140,000 companies and employing more than 1 million people across the region. As announced by the European Commission, new regulations will be introduced by 1 January 2025, including the obligation to separate textile waste collection [19]. ReHubs was created as a joint initiative by EURATEX to upcycle textile waste and circular materials all over Europe [20]. Its goal is to establish a collective effort based on European recycling hubs to upcycle textile waste and increase the scale of collecting, sorting, processing, and recycling pre-consumer and post-consumer materials. This initiative aims to achieve fiber-to-fiber recycling for 2.5 million tons of textile waste by 2030. Europe faces a textile waste problem of 7-7.5 million tons, of which only 30-35% is collected today. While some countries are designing schemes to address the waste collection challenge, there is currently no large-scale plan to process the waste. Looking ahead, the textile recycling industry in Europe could bring about economic, social, and environmental benefits. Once matured and scaled, it could become a profitable sector with a total market size of 6-8 billion € and around 15,000 direct new jobs by 2030 [20].

The United Kingdom's sustainable initiative plans to transform the textile industry and close the loop on materials by adopting chemical or mechanical recycling of materials back into textile fibers. The UK will reduce the greenhouse gas footprint of new products by 50% to limit global warming to 1.5 °C per the Paris Agreement and achieve Net Zero by 2050. Also, the water footprint of new products will be reduced by 30%, and the use of virgin textile materials will be decreased to meet consumer needs [21].

Waste collection and processing, of course, have a regional aspect. For example, a Canadian pilot research project described key data collection and analysis methods to gain insight into the potential for implementing circular practices to reduce waste for Montréal [22] effectively. The study compared the circular processes in three main good green innovation stages: primary sorting, secondary sorting, and landfill or energy recovery in the Architecture, Engineering, & Construction Industries. Quantitative data from reports was collected and compared, but missing or unclear information was identified. In cases where information was unavailable, estimates were made using direct proportions and simple projections, assuming that the missing information had the same characteristics as the current data. This helped create a schematic diagram of the general function of waste management in the Montréal metropolitan area. It's important to note that much of the available information was related to Quebec as a region, so the authors extrapolated numbers logically to a city [22]. Therefore, gathering sufficient analytical data and applying them to a specific area is crucial in cases without a database.

In the pre-consumption textile waste study was based on five years of comprehensive field research in four Bangladesh, India, and Estonia factories. Upcycling design approaches were developed, and an accompanying business model was developed to integrate and implement them [10]. Authors recommended optimizing textile waste by cutting leftovers and minimizing overconsumption [10]. Therefore, to achieve maximum circularity, it is recommended that cutting leftovers unsuitable for upcycling be sent to mechanical recycling with the rest of the textile waste and that a design be implemented that minimizes cutting leftovers and the production of excess garments.

Based on this research results [10], it can be said that depending on the factory size, the textile waste and fabric leftovers generated in the garment manufacturing process range from 25 to 40% of the total fabric used. Generally, there are three main reasons for fabric leftover generation and fabric loss in garment manufacturing. These are the leftovers due to the technical particularities of production processes, problems with the quality of the fabric, and issues related to manufacturing and resource planning (e.g. order faults or cancellations, overproduction). Testing different upcycling design methods and leftover types shows that 50% of pre-consumption textile waste can be upcycled into new garments [10], and some tannery waste is used effectively in construction [23]. Thus, the sewing industry can significantly improve its overall circularity by redirecting streams of pre-consumer textile waste

back into production and upcycling them in-house or recycling.

Under the European Green Deal, electronics, furniture, and textiles are now Ukraine's top priorities due to their significant environmental impact and potential for circular use [24].

The European Green Deal is crucial to the EU's goal of achieving net zero emissions in Europe by 2050. Ukraine is working to align its domestic policies with European standards and has formed an interdepartmental working group for the European Green Deal. The country has initiated a targeted dialogue with the EU through the EU-Ukraine Green Deal Task Force to collaborate on climate issues. According to this, Ukraine will introduce new textile legislation as part of the European Green Deal. These changes aim to shift from traditional resource depletion to a circular and Zero-waste approach [25]. However, there is a lack of official statistical data in Ukraine regarding the textile industry's impact on the environment.

Due to Ukraine's extensive territory and the ongoing war, solving this problem requires a regional approach. The Khmelnytskyi region is located in the West of Ukraine. It has a significant presence of clothing manufacturers, accounting for 6% of Ukraine's total before the war. Moreover, Kharkiv, Odesa, and Dnipro clothing manufacturers have relocated to the Khmelnytskyi region. Thus, the Khmelnytskyi region presents an opportunity for further growth and development in the clothing manufacturing sector. So, it is crucial to implement innovation and technology to drive competitiveness and sustainability. The Khmelnytskyi region's strategic location and emerging role as a hub for the industry make it an attractive for an excellent case of regional circular economic development.

According to the information [26], the total number of sewing enterprises in the Khmelnytskyi region is 1173. On the other hand, the number of officially registered sewing enterprises in Khmelnytskyi city is about 683 [26], more than half of regional SMEs. Most clothes manufacturers use imported fabrics and primary raw materials to produce goods [27]. Only 32% of needed textiles are made by Ukrainian producers. Garment production efficiency is only 60% of India, China, England, and China's total production capacity. The main reasons are the ineffective garment production organization and older manufacturing technology [28].

Ukraine's textile and apparel industry is dominated by small and medium-sized enterprises (SMEs), many of which are micro-enterprises. According to [28], more than 92% of companies in the industry have fewer than ten employees.

Developing a circular economy policy in Ukraine requires taking several steps. These include creating transparent and competitive markets for secondary raw materials, improving and harmonizing Ukrainian legislation with relevant international laws, and reducing waste. It is possible to integrate Ukrainian clothing manufacturers into global value chains by digitalizing production, adapting industrial clothing manufacturing to international environmental requirements, implementing resource-efficient technologies, and providing comprehensive support for environmentally efficient businesses by the state [25].

Auditing existing garment production is essential to understand the amount of textile waste created after manufacturing. Analyzing this data will help identify areas where innovative solutions can effectively address the current textile waste issue [29-30]. Implementing an effective waste recycling model in the garment industry, preventing textile waste through the sustainable design of textile products, implementing eco-design for products, and promoting their consumption based on the principles of a circular economy are all very relevant. Therefore, it's crucial to establish the necessary conditions for sewing enterprises to transition to zero-waste production.

The lack of up-to-date statistical information on the volume of clothing production and the size of test waste in the production process requires conducting such studies. In the future, the expansion and digitization of similar statistical datasets will need high quality for application in circular business models. This involves opening up the data for financial institutions, research centers, and universities and harmonizing the methodology and information standards with the relevant EC standards [25].

Thus, the main goals for establishing the implementation of sustainable clothing production are:

• Study of volumes of post-production textile waste in separated regions;

• Determination of stakeholders' characteristics producing post-production textile waste capacity and production volumes;

• Establishing the raw material composition characteristics of textile waste for the processing technology selection;

• Definition of the stakeholders' behavior in textile waste management to form a mutually beneficial action plan for the circular economy.

METHODOLOGY

Due to advancements in sorting and mechanical recycling of textile waste, a decrease in the costs of secondary raw materials for textiles will be expected. This achievement appears to be a realistic possibility due to the establishment of a comprehensive action plan for textile waste recycling. For this, we needed to collect data on textile waste generation in garment enterprises in Khmelnytskyi.

The first step to a sustainable growth strategy for Ukraine's sewing industry involved gathering and analyzing waste data from stakeholders. At the same

time, we have used scientific theoretical research methods, such as analysis, synthesis, comparison, generalization of data on the problem, explanation, classification, and a systematic approach, as well as empirical methods like experiments, observation, and description.

Initially, stakeholders were divided into eight main categories: (S1) clothing manufacturers; (S2) manufacturers of other textile goods; (S3) government representatives; (S4) public figures; (S5) mass media; (S6) activists; (S7) public and environmental organizations; and (S8) consumers of goods and services. Relevant categories for conducting interviews were identified through the stakeholder selection process. These categories were further grouped into direct and indirect stakeholders based on their impact on post-production textile waste and management. The relevance of direct stakeholders was determined by their involvement in waste generation or management - (S1) and (S2). This approach allowed the inclusion of key decision-makers such as company directors and the production department head. They have direct involvement in textile product manufacturing and managing textile waste.

Two stages involved collecting waste data from direct stakeholders based on activity garment manufacturing indicators. In the first stage, respondents prepared for the survey by looking at and analyzing the company's data on crucial factors in the generation of textile production waste (Fig. 1).

In our survey, the key factors contributing to post-production textile waste included:

• A one-year time frame with high textile procurement indicators (1);

• The annual volume of garment production and, consequently, the annual volume of textiles (2);

• The proportion of different raw materials concerning the total annual textile quantity (3);

• The percentage of each clothing category to the total garment quantity (4);

• And the city area where the company is located, which is convenient for waste disposal (5).

Following this preparation, the survey was conducted in the second stage. We used a 17-question questionnaire with three question blocks according to the research goals (Table 1).

Two survey questions, QN7 and QN8 in QB2, had a branched structure consisting of a Textile raw classification (Table 2) and a Garment classification. We classified two key factors (raw materials - QN7 and clothing category - QN8) according to the standard classification of raw materials, process categories, product categories, and product details [31].

This classification can help select suitable textiles for procurement, inventory management, and product research and development. It ensures that materials and processes meet specific quality assurance standards. The Textile raw classification (Table 2) consists of 13 options for Material composition, which sewing enterprises used over one year. The Garment classification was based on the assortment manufactured by company respondents and included 10 Product categories.

RESULTS AND DISCUSSION

General information about the company (QB1)

During data collection, we contacted 45 heads of sewing companies, but only 30 provided data. Therefore, over 60% of sewing companies support textile waste recycling cooperation. The survey results were analyzed using Microsoft Power BI.

A survey revealed that 51.85% of sewing companies have a small capacity, 37% have a large capacity, and 11.12% have a medium capacity [32]. Some of our information about the company's capacity, including the use of an automatic cutting system and the percentage of textile leftover, was described in [32].

Our research found that 4883 tons of textiles are used, and these thirty sewing companies produce 778.11 tons of textile waste annually (Fig. 2). The survey also found that 44.93% of the waste created is from fabrics, and 55.07% is from knitted materials.
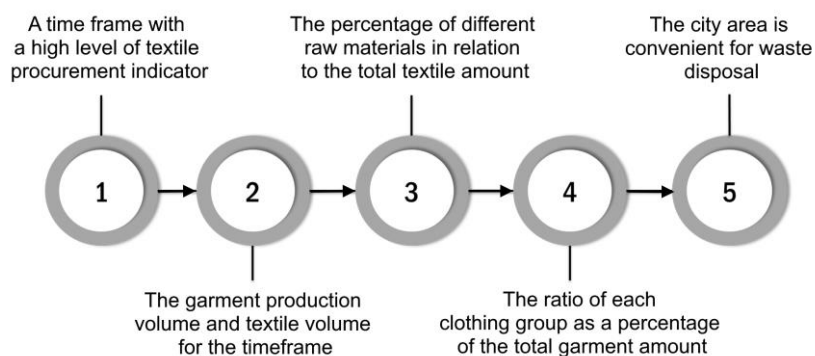

Figure 1. Procedure of data preparation about the generation of textile production waste.

Table 1. Sample interview questions for direct stakeholders (S1) and (S2).

Question block	Question Number (QN)	Sample Questions
General information about the company (QB1)	QN1	General information about a company
	QN2	Average production volume (units/year)
	QN3	How many seamstresses are there?
	QN4	The average volume of knitted materials (kg) used during the year
	QN5	The average volume of fabrics (per m) used during the year
	QN6	Is there software used to lay out the cut?
The characteristics of raw material composition textile waste and assortment (QB2)	QN7	How many materials of different raw materials do you have in manufacturing?
	QN8	How many types of products are there in your production?
	QN9	Is your clothing production seasonal?
	QN10	Is waste accounting kept?
	QN11	Average percentage of waste (approx. if no records are kept)
Stakeholder behaviour in textile waste management (QB3)	QN12	What does the company do with production waste?
	QN13	Are you ready to sell textile waste?
	QN14	Are you ready to sort textile waste by raw material?
	QN15	Are you ready to use containers for textile waste?
	QN16	Are you ready to pay for the service of collecting textile waste?
	QN17	Specify an area of the city convenient for unloading the company's waste

Table 2. Textile raw classification [31].

| Product category	Product detail	Material composition
Dyed fabrics (PC0025) Greige fabrics (PC0026) Undyed fabrics (PC0027)	Terry fabrics (PD0060) Denim fabrics (PD0061) Woven fabrics (PD0059) Knitted fabrics (PD0058)	Cotton 100% (RM0102 100%)
		Cotton 90%, other fibres (RM0102 90%, RM0262 10%)
		Cotton 75%, other fibres (RM0102 75%, RM0262 25%)
		Polyester 100% (RM0186 100%)
		Polyester 80%, other fibres (RM0186 80%, RM0262 20%)
		Polyester 30%, mixed fibers (RM0186 30%, RM0258 70%)
		Polyamide 100% (RM0182 100%)
		Polypropylene 90%, polyamide 10% (RM0202 90%, RM0182 10%)
		Linen up to 92%, other fibres (RM0108 92%, RM0262 8%)
		Linen 30%, viscose 70% (RM0108 30%, RM0238 70%)
		Linen up to 30%, mixed fibers (RM0108 30%, RM0285 70%)
		Wool 40%, acrilic 60% (RM0077 40%, RM0156 60%)
		Wool 30%, acrilic 70% (RM0077 30%, RM0156 70%)
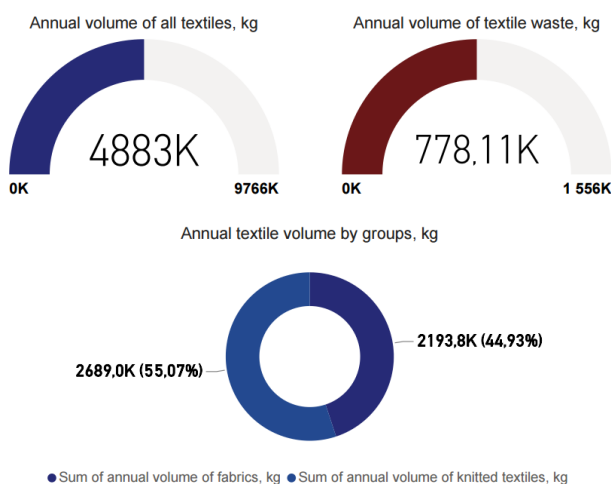
Figure 2. Annual textile volumes and waste by category.

Characteristics of raw textile waste (QB2)

The survey included a question about the types of products produced by sewing companies. The results showed that the most common types of products are knitted clothes (40.85%), sports clothes made of synthetic fabrics (15.21%), and clothes made of light woven fabrics (12.5%).

Annual textile waste volume by enterprise capacity and raw material composition is shown in Table 3.

Small sewing businesses accounted for the highest annual post-production textile waste, nearly 33.2%. Meanwhile, 23.9% of respondents did not disclose their enterprise capacity for various reasons.

The percentage of different raw materials in the total textile is shown in Fig. 3.

Material composition ratios in textile waste reveal that 42.14% of post-production textile waste contains more than 75% cotton, and 32.45% contains more than 80% polyester.

It has been determined that out of 327,888.94 kg of cotton textile waste, 56.92% (186,843.8 kg) is 75% cotton (RM0102 75%, RM0262 25%), and the lowest amount is 13.92% pure cotton (RM0102 100%) (Fig. 4).

Table 3. Annual textile waste volume by enterprise capacity.

Material composition (code)	Annual volume of textile waste by enterprise capacity [kg]				
	small	medium	large	not defined	total
Cotton 100% (RM0102 100%)	13 201.25	5 950.00	26 503.88	0	**45 655.13**
Cotton 90%, other fibres (RM0102 90%, RM0262 10%)	47 945.00	12 590.63	34 851.88	202.50	**95 590.01**
Cotton 75%, other fibres (RM0102 75%, RM0262 25%)	37 460.63	1 328.13	28 717.50	119 137.50	**186 643.80**
Polyester 100% (RM0186 100%)	34 366.88	6 693.75	27 366.75	1 260.00	**69 687.38**
Polyester 80%, other fibres (RM0186 80%, RM0262 20%)	63 393.75	4 743.75	53 473.13	61 200.00	**182 810.60**
Polyester 30%, mixed fibers (RM0186 30%, RM0258 70%)	19 202.50	0	11 350.00	0	**30 552.5**
Polyamide 100% (RM0182 100%)	14 589.38	0	5 407.50	4 050.00	**24 046.88**
Polypropylene 90%, polyamide 10% (RM0202 90%, RM0182 10%)	13 087.50	90 131.25	618.75	0	**103 837.50**
Linen up to 92%, other fibres (RM0108 92%, RM0262 8%)	6 264.38	0	6 481.25	0	**12 745.63**
Linen 30%, viscose 70% (RM0108 30%, RM0238 70%)	3 168.75	0	3 490.63	0	**6 659.38**
Linen up to 30%, mixed fibers (RM0108 30%, RM0285 70%)	2 681.25	0	6 391.25	0	**9 072.50**
Wool 40%, acrilic 60% (RM0077 40%, RM0156 60%)	1 657.50	0	4 760.00	0	**6 417.50**
Wool 30%, acrilic 70% (RM0077 30%, RM0156 70%)	1 318.75	0	3 075.00	0	**4 393.75**
Total	**258 337.52**	**121 437.51**	**212 487.52**	**185 850.00**	**778 112.55**

Figure 3. Material composition ratios in textile waste.
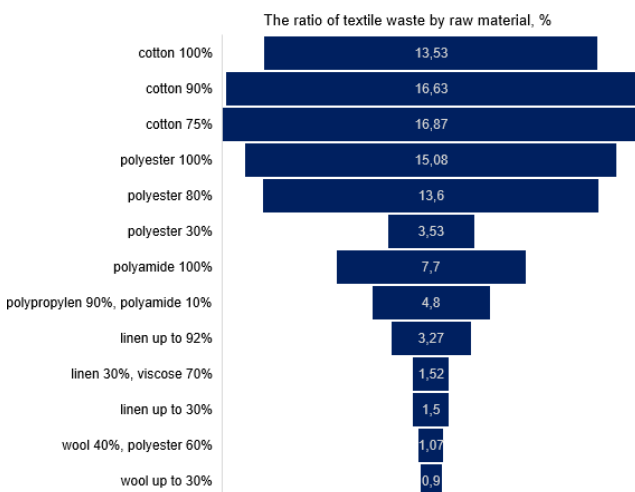
The results indicated that most textile waste (64.59%, equal to 182,810.6 kg) comprises 80% polyester waste (RM0186 80%, RM0262 20%). It was determined that 24.62% of the polyester waste, equivalent to 69,687.38 kg, comprises 100% polyester (RM0186 100%). Additionally, in our research, the textile waste of mixed raw materials (30% polyester and mixed fibers – RM0186 30%, RM0258 70%) is relatively tiny – 30,552.5 kg, 4% of the total amount (Fig. 5).

This information offers insights into the annual volumes of textile waste, enabling the development of practical technology and plans for processing the generated textile waste during production.
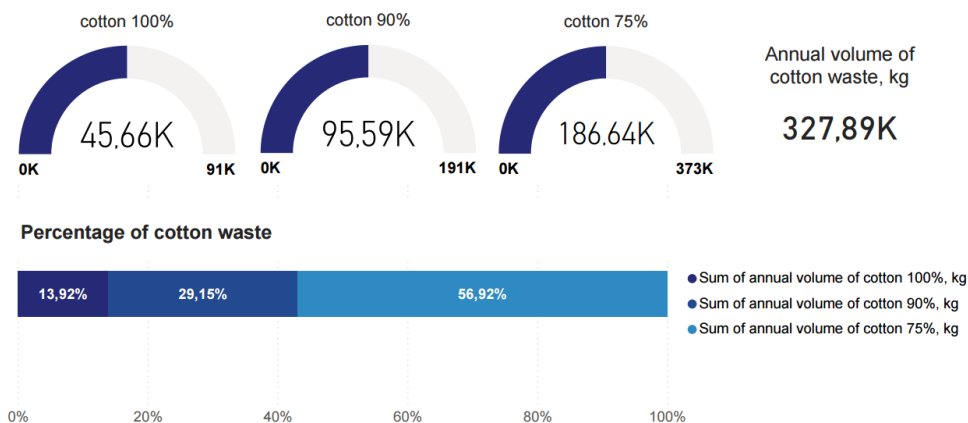

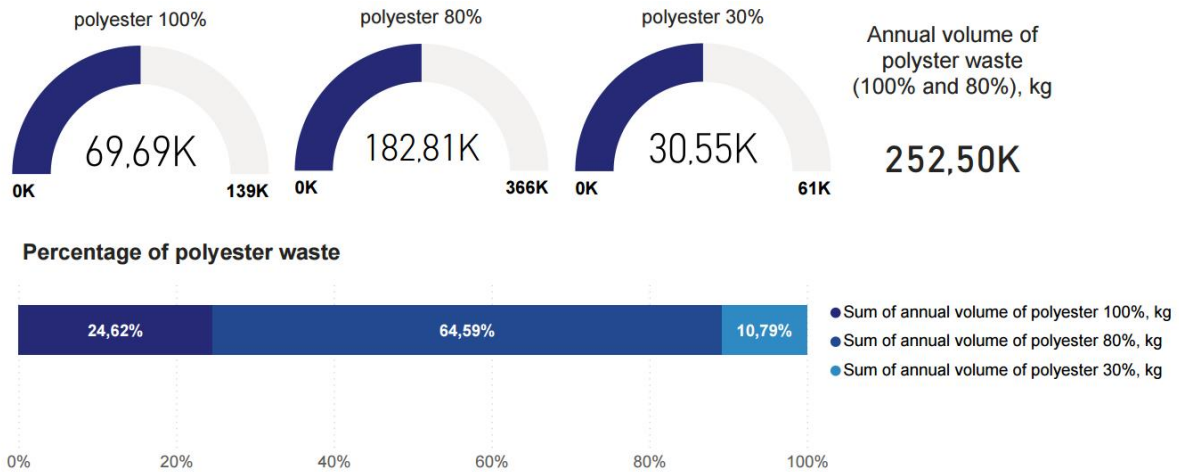**Figure 4.** Annual textile cotton waste volume.

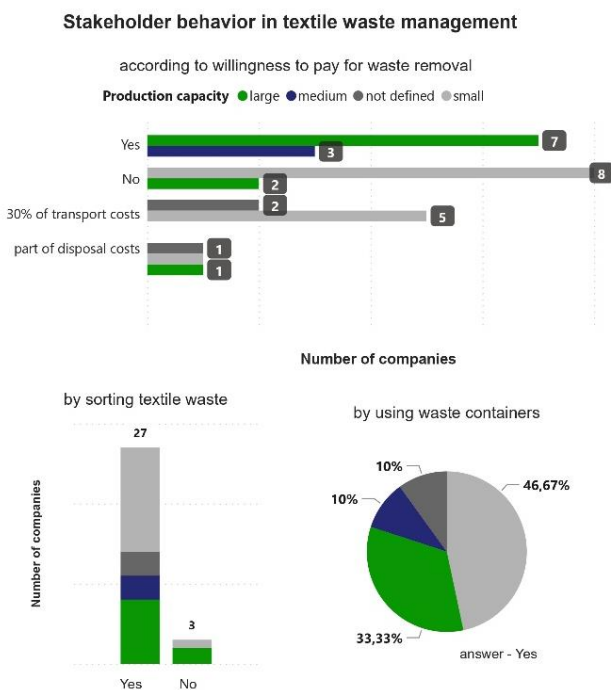**Figure 5.** Annual textile polyester waste volume.

Figure 6. Stakeholder behavior in textile waste management.

Stakeholder behavior in textile waste management (QB3)

It has been found that 90% of companies are prepared to sort the waste generated in the production process, and 50% of companies are willing to pay for waste collection services. Furthermore, all respondents have expressed their commitment to using containers for collecting and sorting waste (Fig. 6).

CONCLUSIONS

Waste management is crucial in achieving a sustainable environment and improving people's quality of life. The research shows that textile waste is a significant issue in Khmelnytskyi, which has over 600 sewing companies. It was determined that only 30 of them could regenerate almost 800 tons of post-production textile waste annually.

Introducing technologies for recycling textile waste as one of the Zero-waste design principles can substantially enhance the region's environmental situation and reduce the volume of waste in landfills. The volume of waste in 30 enterprises allowed for the extrapolation of data for further research and strategic planning. Based on these results, the Textile Waste Roadmap 2030 was created. Among its different actions to introduce sustainability principles into the Ukrainian sewing industry, it has provided gathering and certifying textile waste to determine the raw material and purity composition necessary for the precise selection of the recycling process. It is essential to implement Textile Waste Roadmap 2030 systemically and continually assess outcomes and challenges. That's why we plan to conduct more profound research on post-production textile waste regeneration in the Khmelnytskyi region to determine the most intensive locations for its accumulation and create the logistic collection and sorting system. The involvement of all stakeholders in this process will form an effective waste management policy. This collaborative effort will help establish a closed cycle of recycling textile waste from the garment industry, promote sustainable clothing and textile production in Ukraine, reduce greenhouse gases, and conserve primary planet resources.

REFERENCES

1. McKinsey's: Sustainable materials hub, online: https://www.mckinsey.com/capabilities/sustainability/how-we-help-clients/sustainable-materials-hub [cit. 11.7.2024]
2. Sustainability and circularity in the textile value chain, a global roadmap, online: https://circulareconomy.europa.eu/platform/sites/default/files/2023-12/Full%20Report%20-%20UNEP%20Sustainability%20and%20Circularity%20in%20the%20Textile%20Value%20Chain%20A%20Global%20Roadmap_0.pdf [cit. 11.7.2024]
3. Zero waste, Design guidelines, Design strategies and case studies for a zero waste city, online: https://www.zerowastedesign.org/wp-content/uploads/2017/10/ZeroWasteDesignGuidelines2017_Web.pdf [cit. 11.7.2024]
4. Gupta R., Kushwaha A., Dave D., et al.: Waste management in fashion and textile industry: recent advances and trends, Life-Cycle Assessment, and circular economy, 2022, 418 p. https://doi.org/10.1016/B978-0-323-85403-0.00004-9
5. Understanding zero waste design: a guide for building professionals, online: https://ugreen.io/understanding-zero-waste-design-a-guide-for-building-professionals/ [cit. 11.7.2024]
6. Wiedemann S.G., Biggs L., Clarke S.J., et al.: Reducing the environmental impacts of garments through industrially scalable closed-loop recycling: Life Cycle Assessment of a recycled wool blend sweater, Sustainability 2022, 14, pp. 1-13. https://doi.org/10.3390/su14031081
7. Ribeiro P.R., Batista P., Mendes-Palma F., et al.: Consumers' engagement and perspectives on sustainable textile consumption, Sustainability 2023, 15, pp.1-23. https://doi.org/10.3390/su152215812
8. DeVoy J.E., Congiusta E., Lundberg D.J., et al.: Post-Consumer textile waste and disposal: differences by socioeconomic, demographic, and retail factors, Waste Management, Volume 136, 2021, pp. 303-309. https://doi.org/10.1016/j.wasman.2021.10.009
9. Akter M.Md.Kh., Haq U.N., Islam Md.M., et al.: Textile-apparel manufacturing and material waste management in the circular economy: a conceptual model to achieve sustainable development goal (SDG) 12 for Bangladesh, Cleaner environmental systems, Volume 4, 2022, pp. 1-12. https://doi.org/10.1016/j.cesys.2022.100070
10. Aus R., Moora H., Vihma M., et al.: Designing for circular fashion: integrating upcycling into conventional garment manufacturing processes, Fash Text, 2021, 8(34), pp. 1-18. https://doi:10.1186/s40691-021-00262-9
11. Abagnato S., Rigamonti L., Grosso M.: Life cycle assessment applications to reuse, recycling and circular practices for textiles: a review, Waste Management, Volume 182, 2024, pp. 74-90. https://doi.org/10.1016/j.wasman.2024.04.016
12. Basit A., Latif W., Baig S.A., et al.: The mechanical and comfort properties of sustainable blended fabrics of bamboo with cotton and regenerated fibers, Clothing and textiles research journal, 2018, 36(4), pp. 267-280. https://doi:10.1177/0887302X18782778
13. Our work on the sustainable development goals in Ukraine, online: https://ukraine.un.org/en/sdgs [cit. 11.7.2024]
14. Scaling textile recycling in Europe-turning waste into value, 2022, online: https://www.mckinsey.com/~/media/mckinsey/industries/retail/our%20insights/scaling%20textile%20recycling%20in%20europe%20turning%20waste%20into%20value/scaling%20textile%20recycling%20in%20europe%20turning%20waste%20into%20value.pdf?shouldIndex=false [cit. 11.7.2024]
15. Tang K.H.D.: State of the art in textile waste management: a review, Textiles, 2023, 3, pp. 454-467. https://doi.org/10.3390/textiles3040027
16. Ralph Lauren unveils first-to-market product innovation with the RLX Clarus® Polo, exclusively at the Australian Open 2022, online: https://corporate.ralphlauren.com/pr_220112_Clarus.html [cit. 11.7.2024]
17. Sanchis-Sebastiá M., Ruuth E., Stigsson L., et al.: Novel sustainable alternatives for the fashion industry: a method of chemically recycling waste textiles via acid hydrolysis, Waste Management, Volume 121, 2021, pp. 248–254. https://doi.org/10.1016/j.wasman.2020.12.024
18. Liu W., Liu Sh., Liu T., et al.: Eco-friendly post-consumer cotton waste recycling for regenerated cellulose fibers, Carbohydrate Polymers, Volume 206, 2019. https://doi.org/10.1016/j.carbpol.2018.10.046
19. Directive (EU) 2018/851 of the European Parliament and of the Council, online: https://www.legislation.gov.uk/cy/eudr/2018/851/body [cit. 18.8.2024]
20. ReHubs 2022: Circulating textile waste into value, online: https://euratex.eu/139/rehubs-2022-circulating-textile-waste-into-value/ [cit. 11.7.2024]
21. Sustainable textiles action plan, Textiles 2030, Re-use and recycling, Signatory pack, online: https://www.wrap.ngo/sites/default/files/2021-11/Textiles2030-Re-use-and-Recycling-Signatory-Pack%2018%2011.pdf [cit. 11.7.2024]
22. Keena N., Rondinel-Oviedo D.R., Demaël H.: Circular economy design towards zero waste: laying the foundation for constructive stakeholder engagement on improving construction, renovation, and demolition (CRD) waste management, IOP Conf. Series: Earth and environmental science, 2022, pp. 1-10. https://doi.org/10.1088/1755-1315/1122/1/012059
23. Mushahary J., Mirunalini V.: Waste management in leather industry - Environmental and health effects and suggestions to use in construction purposes, International Journal of Civil Engineering and Technology, 8(4), 2017, pp. 1394-1401, online: https://iaeme.com/MasterAdmin/Journal_uploads/IJCIET/VOLUME_8_ISSUE_4/IJCIET_08_04_157.pdf
24. Review of current EU policy in the field of low-carbon and circular economy, Огляд сучасної політики ЄС у сфері низьковуглецевої та циркулярної економіки, online: https://tapas.org.ua/wp-content/uploads/2024/02/Iurydychnyj-zvit.pdf (in Ukrainian) [cit. 11.7.2024]
25. Recommendations on the implementation of international standards and open data to support Ukraine's transition to a low-carbon and circular economy, online: https://tapas.org.ua/wp-content/uploads/2024/02/Rekomendatsii_shchodo_vprovadzhennia.pdf (in Ukrainian) [cit. 11.7.2024]
26. Business Guide, Enterprises, Industry, Processing industry, Light industry, online: https://business-guide.com.ua/enterprises?q=&v=186&o=1 (in Ukrainian) [cit. 11.7.2024]
27. Ishchuk S., Sozanskyy L.: Peculiarities of functioning and diagnostics of cross-sectoral economic links of the textile industry of Ukraine, Fibres and Textiles, 29(1), 2022, pp.17-27. https://doi.org/10.15240/tul/008/2022-1-003
28. National economic strategy 2030, Vectors of economic development, online: https://nes2030.org.ua/docs/doc-vector.pdf [cit. 11.7.2024]
29. Tat-Dat B., Thi T.V.N., et al.: Green manufacturing performance improvement under uncertainties: an interrelationship hierarchical model, International Journal of Production Economics, Volume 268, 2024. https://doi.org/10.1016/j.ijpe.2023.109117
30. Ellen MacArthur Foundation. Adaptive strategy for circular design, online: https://www.ellenmacarthurfoundation.org/adaptive-strategy-for-circular-design/rules [cit. 11.7.2024]
31. ASR-213-V1.3-2024.06.01/. The Materials, Processes, & Products Classification V1.3
32. Bukhantsova L., Zakharkevych O., Krasniuk L., et al.: Preconditions of the strategy of sustainable apparel production in Ukraine, Herald of Khmelnytskyi National University, Issue 1, 2024 (331), pp. 57-60. https://doi.org/10.31891/2307-5732-2024-331-8

IMAGE-BASED CROSS-SECTIONAL ANALYSIS AND MICROMECHANICAL MODELING OF YARN AND COMPOSITE MATERIALS

OVERBERG, MATTHIAS[*]; ZALEWSKA, EMILIA; ABDKADER, ANWAR AND CHERIF, CHOKRI

Faculty of Mechanical Science and Engineering, Institute of Textile Machinery and High Performance Material Technology (ITM), Technical University Dresden, Germany

ABSTRACT

This study aims to establish a comprehensive methodology for determining the microstructural properties of hybrid yarns used in composite materials. By developing accurate models of hybrid yarns and composites based on detailed microstructural information such as fibre orientation, fibre diameter and distribution, this approach lays the foundation for future advances. These models, enriched with accurate microstructural data, will facilitate the creation of new modelling techniques that can be used in future research to explore the correlation between microstructural properties and mechanical performance of composite materials.

KEYWORDS

Hybrid composite; Microstructural properties; Intermixing; Fiber distribution.

INTRODUCTION

Composite materials are particularly valued for their rigidity, strength relative to weight, and other tailored properties which make them indispensable across various applications in Aerospace, Automotive Industry, Biomedical Applications, Sports Equipment, Construction and Civil Engineering [1-3]. The correlation between microstructural properties and mechanical behavior is fundamental for the advancement of material science, leading to better predictive capabilities, enhanced material performance, and innovative processing techniques. Understanding this relationship allows for the strategic design and application of materials across various industries [4] [5]. Recent studies have explored various aspects to enhance performance and understand the mechanisms affecting their behavior. Hoang et al. [6] investigated postprocessing techniques' impact on carbon reinforced thermoplastic composites, focusing on materials like PPS, PEEK, and PEKK. They found that consolidation techniques significantly affect the final quality, including void content and crystallinity. Oztan et al. [7] examined the microstructure of 3D-printed continuous fiber composites, revealing that defects significantly impact stiffness and strength, necessitating further investigation to enhance performance. Ramaswamy et al. [8] studied the mechanical performance of CF/PEEK and CF/PEKK composites, highlighting the tunable nature of their semi-crystalline matrices. They found CF/PEKK to be durable and damage-tolerant but noted the need for more research on matrix properties and fiber-matrix interface behavior. Mehdikhani et al. [9] reviewed the effects of voids in fiber-reinforced polymers, showing that voids predominantly affect matrix-dominated properties. Tunak et. al investigated the blending quality of fibre components in hybrid yarns containing conductive stainless steel fibres [10]. The quality of these datasets depends on the data that are accurate measurement and understanding of microstructural properties remain challenging, requiring precise methodologies. Recent advances in machine learning, as demonstrated by Li et al. [11] and Shah et al. [12], have shown promise in predicting the mechanical properties of composites. While these models are effective, they highlight the need for further research on establishing methodologies to determine microstructural properties of composites to and making valuable datasets from these relyable informations. These advanced Datasets can be used in the future to fill gaps that remain in fully linking microstructural properties to mechanical performance. This study aims to bridge these gaps by providing methodology to find microstructural properties based on digital image correlation methods and preparation to find the correlations between mechanical properties of composites and their microstructural properties.

MATERIALS

Hybrid yarns, composed of stainless steel (StS), glass fibers (GF), and polypropylene (PP), were utilized in the fabrication of fiber-reinforced composites (FRP) for this study. These hybrid yarns combine the complementary properties of their constituents, optimizing the mechanical performance of the FRP. Stainless steel was incorporated due to its ductility, which enhances the toughness and impact resistance of the composites, while glass fibers were selected for their high tensile strength and cost-effectiveness. Polypropylene, serving as the matrix material, contributes chemical resistance, recyclability, and low density, making it ideal for lightweight applications. Table 1 outlines the key properties of the filament yarns used in this study.

METHODS

Fabrication of hybrid yarns

For the manufacturing of multi-material composites, hybrid yarns were produced using a newly developed multi-level-intermixing process. This process is designed to achieve efficient intermixing of components while maintaining low-damage processing. During the process, mechanical separating elements divide the filament yarns into smaller fiber bundles. These separated bundles are then recombined into a single coherent fiber bundle using a subsequent merging element. This method minimizes damage to the individual filaments, preserving their mechanical properties in the final hybrid yarn. The structure of the machines and detailed descriptions of their components are provided in [13]. In the next step, the hybrid yarns were wound into unidirectional (UD) fabrics using the winding technique on an FW122 winding machine (IWT, Germany). This winding method ensures precise alignment of the yarns to form the composite samples for further testing.

Fabrication of Composite Samples

The unidirectional (UD) fabric samples were consolidated by compression moulding using a P300 PV thermal laboratory press (COLLIN Lab & Pilot Solutions GmbH, Germany). The theoretical volume fractions of the components in the composite were 18.2% stainless steel (StS), 34.5% glass fibers (GF), and 47.3% polypropylene (PP). The consolidation process was performed at 220°C under a pressure of 188 MPa to ensure proper bonding between the fibers and matrix. Following consolidation, test specimens were cut from the composite plates in the 0° direction (parallel to the fiber axis) using a WOCO 50 precision table saw (Uniprec Maschinenbau GmbH, Germany) equipped with a TS322 galvanic-coated blade (TSP Hildebrand, Germany), specifically designed for fiber-reinforced composites. The dimensions of the specimens for microscopic imaging were 20 ± 1 mm in length, 10 ± 0.2 mm in width, and 2 ± 0.2 mm in thickness.

Methodology for determination of microstructural properties of hybrid yarns and FRP

The primary objective of this study is to develop a methodology for modeling hybrid yarns and fiber-reinforced composites (FRCs) by incorporating detailed information about their microstructural properties. This methodology focuses on the segmentation and classification of hybrid yarn and composite regions based on microscopic cross-sections. Key features analyzed include the location and type of fibers, as well as the presence of voids, which significantly influence the mechanical properties of the composites. The information gathered from this analysis is used to create accurate models that capture local variations in fiber distribution and void content, both of which are critical to understanding the mechanical behavior of fiber-reinforced composites.

The methodology is divided into the following key steps (see Fig. 1):

1. Image Acquisition – Microscopic images of hybrid yarns and composite cross-sections are captured to provide detailed visual data on the fiber and void distribution.

2. Image Analysis and Segmentation – Using specialized image analysis software, the images are processed to segment and classify different components such as fibers and voids.

Table 1. Specifications of filament yarns used to manufacture composites.

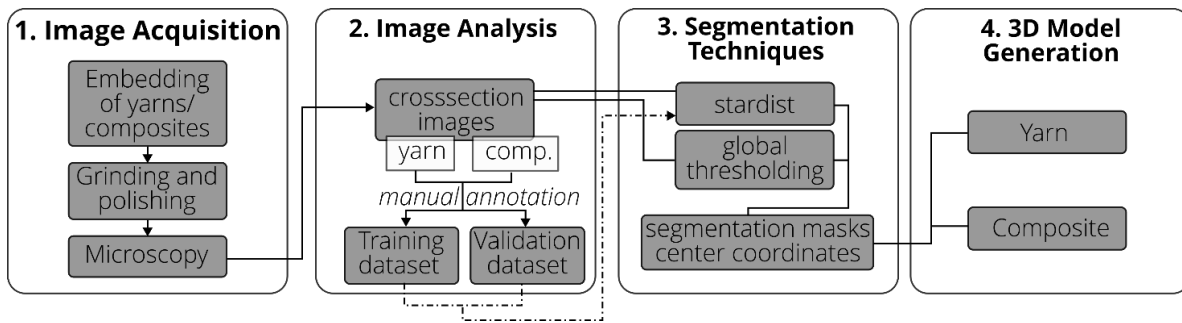|	Yarn properties			
	Notation	**Manufacturer**	**Diameter of single filament**	**Fineness filament yarn [tex]**
Stainless steel (StS)	chrome nickel steel wire 1.4301	Heinrich stamm GmbH	60±0.2	225
Glassfibre (GF)	EC9- 68tex- Z28 302P	P-D glasseiden GmbH oschatz	7.2±0.9	68
Polypropylene (PP)	Prolen HP 330/66, white, untwisted	Chemosvit fibrochem, s.r.o	15±1.5	2x33

Figure 1. Schematic representation of the methodology for image acquisition, analysis, segmentation, and 3D model generation.
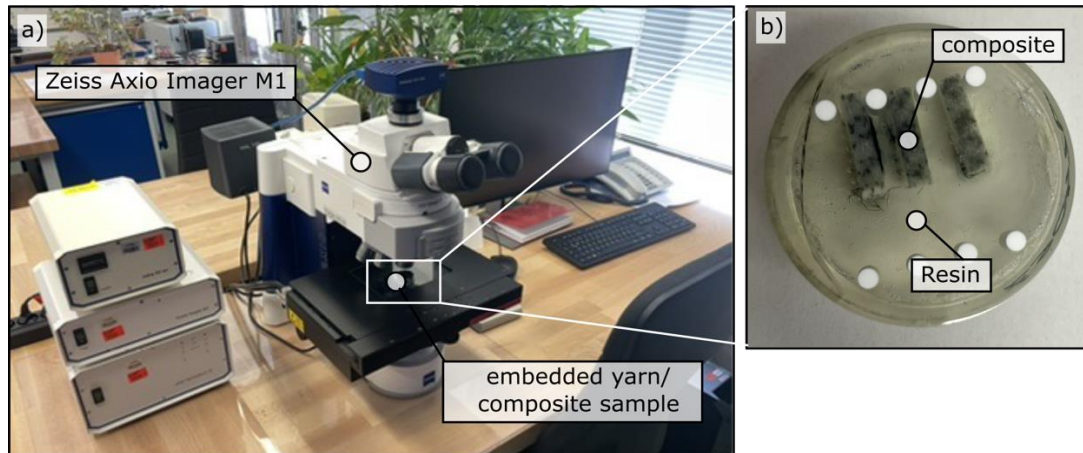

Figure 2. Experimental setup showing a) Zeiss Axio Imager M1 used for imaging composite and yarn cross-sections, and b) resin-embedded samples.

3. Segmentation Techniques – Advanced segmentation techniques are applied to accurately distinguish between fiber types and to identify voids within the composite structure.

4. 3D Model Generation – Based on the segmented data, 3D models are generated to simulate the internal structure of the hybrid yarns and composites, allowing for analysis of local variations in fiber and void content.

To capture detailed images of the yarn and composite cross-sections, both flatbed scanners and microscopy techniques were employed. The samples were first embedded in an epoxy resin matrix and cured at room temperature to preserve their structure during imaging. After curing, the samples were polished and cleaned to obtain smooth surfaces for analysis. High-resolution images of the cross-sections were captured using an Axio Imager M1m optical microscope (Carl Zeiss, Germany) at a magnification of 200x, with the magnification calibrated using Zeiss Zen software. The optical microscope enabled detailed visualization of the fiber and matrix interfaces, which is essential for analyzing the microstructural properties of the composite materials. Additionally, high-resolution images of the yarns' longitudinal sections were obtained using a Perfection V550 flatbed scanner (Epson, Japan). The flatbed scanner provided large-scale images that were particularly useful for observing the alignment of fibers within the yarn. These high-resolution images were critical for identifying and analyzing key microstructural features, such as fiber distribution, voids and fiber angle, which influence the mechanical performance of the composites. Fig. 2(a) shows the imaging technique used to obtain cross-sectional micrographs by microscopy, while Fig. 2(b) shows the composite sample prepared for analysis, with the composites embedded in an epoxy resin matrix.

RESULTS

Image acquisition

Microscopic analysis of the longitudinal sections of the hybrid yarns showed minimal fibre degradation, as indicated by the limited number of fibres protruding from the yarn core (Fig. 3(b)). Slight aggregations of glass and thermoplastic fibres were observed within the hybrid yarns (Fig. 3(a)). Composite cross section images (Fig. 3(c)) showed a uniform distribution of steel fibres. These findings were confirmed by subsequent image analysis and segmentation as discussed in Image analysis and segmentation section.
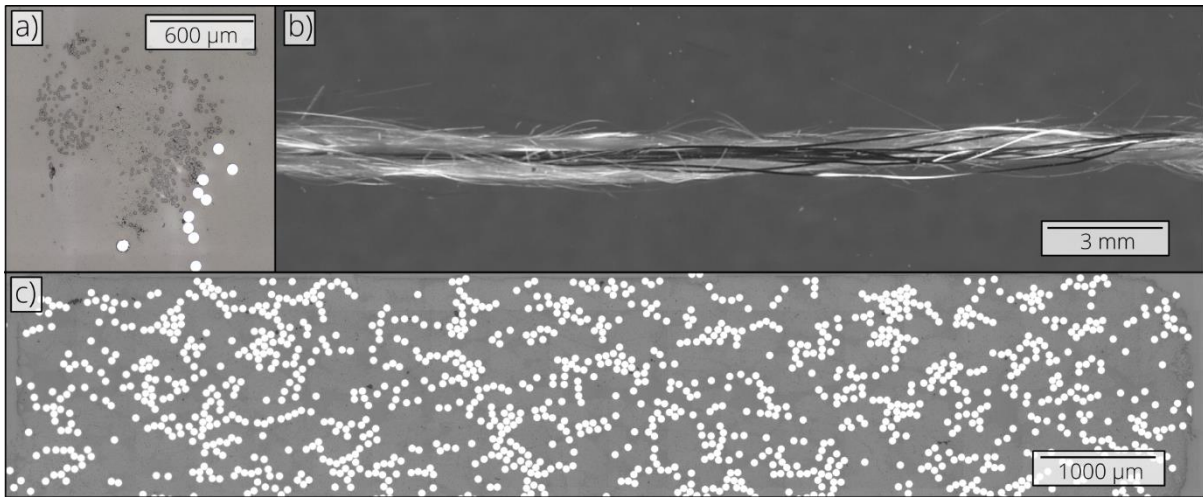
Figure 3. Microscopic images of: (a) hybrid yarn cross-section, (b) composite cross-section, and (c) yarn longitudinal view obtained by flatbed scanning.
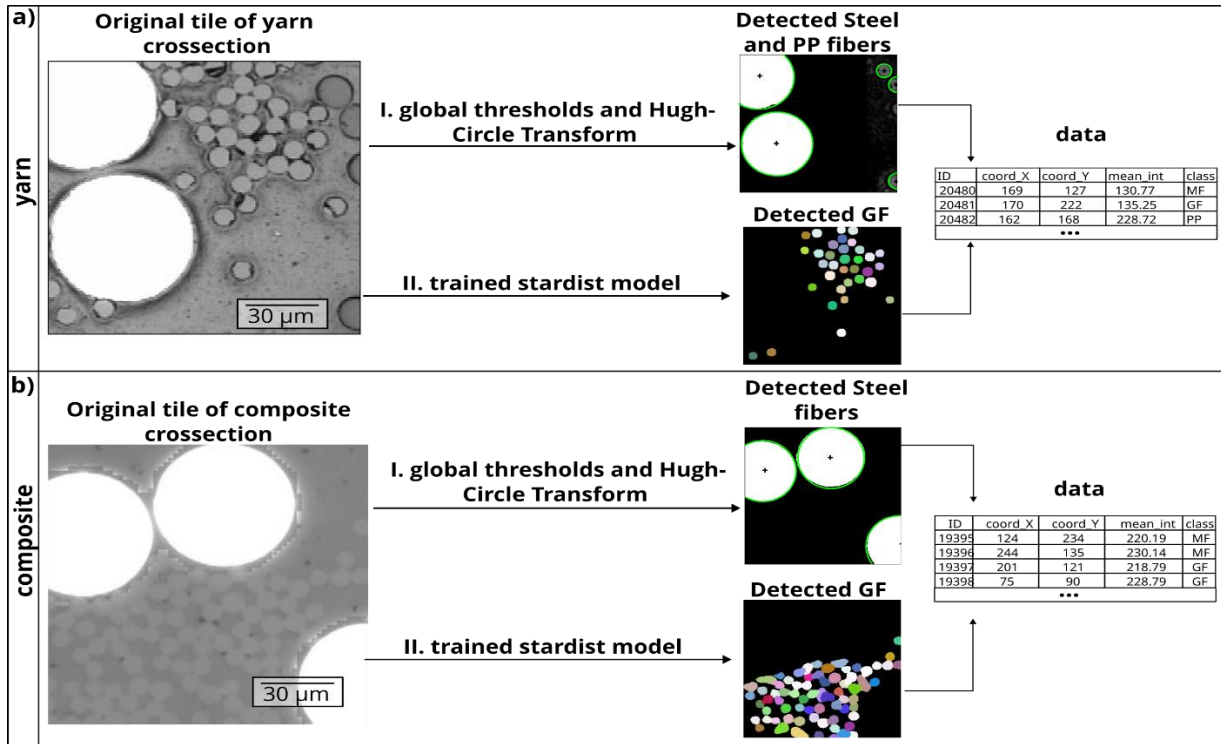

Figure 4. Methodology for determining microstructural properties of: (a) yarn and (b) composite.

Image analysis and segmentation

Digital image analysis was conducted using a combination of conventional and advanced segmentation techniques (Fig. 4). Initial segmentation was performed using global thresholding due to its computational efficiency, with manually set grayscale thresholds for steel, polypropylene (PP) fibers, and voids, which generated binary images. However, global thresholding was insufficient for accurately segmenting glass fibers (GF) due to the low contrast between fibers and the matrix. To improve segmentation accuracy, a machine learning-based approach was employed using the Stardist library [14], which relies on star-convex shapes for segmentation. The model training involved multiple steps: image preparation, manual annotation, data augmentation, and dataset division. Initially, 25 cross-sectional images of hybrid yarns were manually annotated using QuPath software [15], with each image divided into tiles of 256x256 pixels. These images were split into a training dataset (80%) and a validation dataset (20%). Data augmentation included variations in intensity and image flipping to improve model generalization. The model was trained using a convolutional neural network with a U-Net architecture as the backbone. The training process

used 30 epochs and a batch size of 4. For the Stardist model, 32 rays were set to describe the star-convex shapes. This method allowed for precise fiber boundary delineation, even in low-contrast images.

Additionally, the Hough-Circle Transform method was applied to identify fibers in the images, although it proved less effective for glass fibers. The Stardist model, however, achieved an Intersection over Union (IoU) accuracy of 93% for yarn cross-sections and 81% for composite cross-sections, demonstrating its suitability for fiber segmentation. Key local descriptors, including fiber center coordinates, void areas, mean image intensity, and fiber classification, were calculated and stored for further analysis.

In the composite analysis, the approach was modified to account for the consolidation of polypropylene (PP) fibers during the thermo-pressing process, which resulted in their absence from the composite cross-sections. Consequently, the focus shifted to identifying voids, which are known to significantly impact the mechanical properties of fiber-reinforced composites. Due to the high contrast between the voids and the surrounding matrix material, global thresholding was sufficient for detecting voids. This method efficiently identified voids, making it unnecessary to apply more advanced segmentation techniques in this case. The determined void content in composites is 2.8 ±0.5%.

Exploratory spatial analysis of fibers

Before initiating the modeling process, an exploratory spatial point pattern analysis of the yarn's cross-sections was performed to gain initial insights into the spatial distribution of fibers. This analysis helps in understanding fiber distribution, interactions, and potential clustering within the yarn, providing valuable information for optimizing textile performance, ensuring uniformity, and predicting mechanical properties. A representative example of this analysis is shown in Fig. 5.

In Fig. 5(a), the distribution of glass fibers (GF), stainless steel fibers (StS), and polypropylene fibers (PP) in a cross-section is displayed. To further investigate the spatial patterns of each fiber type, the fibers were plotted separately (Fig. 5(d)), providing a qualitative overview of their locations within the yarn. In addition, the spatial probability of occurrence for each fiber type was calculated and is displayed in Fig. 5(b), highlighting areas where specific fiber types are most likely to occur. For a more quantitative assessment, spatial distribution functions such as the K, J, F, and G functions were calculated. These functions are commonly used in spatial point pattern analysis to detect clustering or dispersion within a dataset. In this case, the analysis revealed a slight clustering of fibers in the hybrid yarn, as indicated by deviations in the calculated distribution functions compared to a Poisson distribution with complete spatial randomness (CSR). This clustering may be due to the manufacturing process and could influence the mechanical performance of the yarn by creating localized regions of higher or lower fiber density.

3D modeling based on microstructure

The microstructural information obtained from the segmentation process was used to generate 3D models of the yarn and composite structures (Fig. 6). The local descriptors, including the center coordinates of the fibers and their respective types, were used to set the starting points of the fibers in the model. Scans of longitudinal sections were analyzed to calculate the average fiber angle deviation from the yarn's longitudinal axis, an important factor due to the slight twist introduced during processing. These data were combined to create a realistic 3D representation of the yarn, which can be used to correlate microstructural features with mechanical properties.
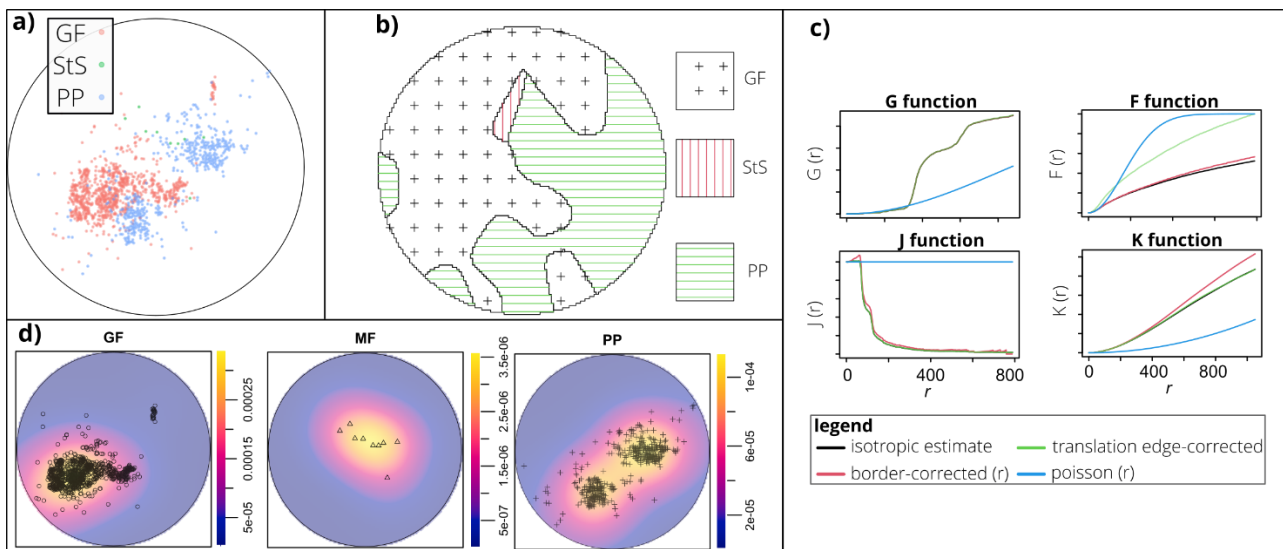

Figure 5. Example results of exploratory spatial analysis of yarn: (a) determined local positions of GF, StS, and PP in the yarn, (b) probability map of different fiber types, (c) resulting spatial summary functions, and (d) specific locations of different fibers.
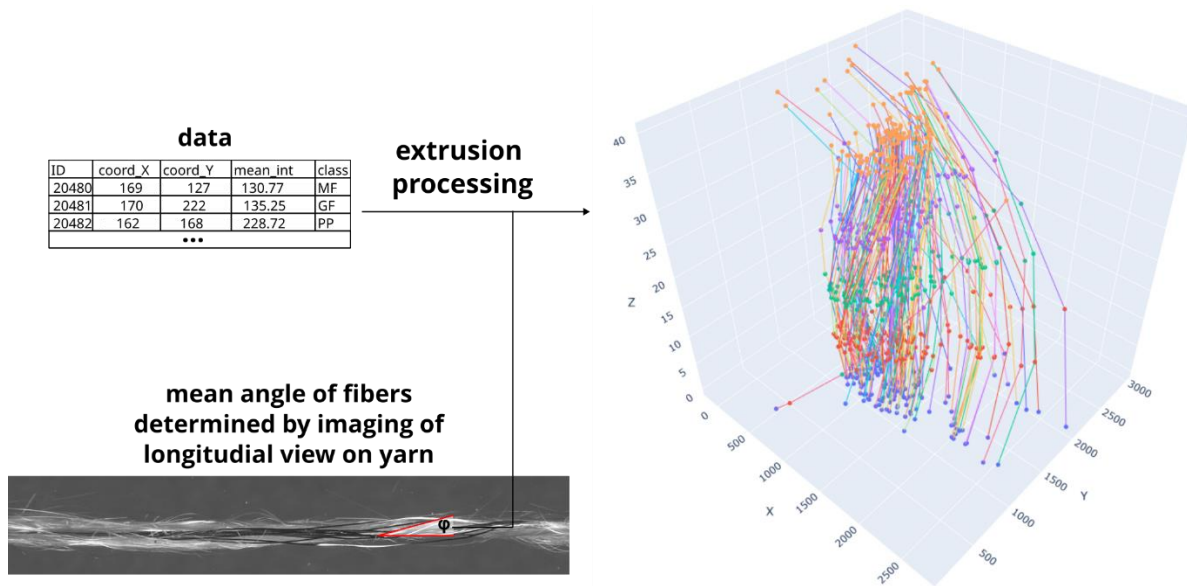
Figure 6. Example of the 3D model determined using the DIC-based method.

An algorithm was developed for this process, which takes the initial coordinates and corresponding fiber types as input. Then to represent the rotation of the yarn, the center of gravity was first determined by calculating the overall centroid of the x and y coordinate using the NumPy library. Subsequently, new planes were generated at equal intervals parallel to the initial plane. The coordinates, rotated relative to the initial points of the first plane, were positioned around the calculated centroid. These rotated points were then connected to their corresponding points on the adjacent planes, forming the desired representation.

The developed DIC-based process enables future work to include voids and fiber distribution in composite models, allowing for more accurate representations of the material's behavior under mechanical stress. By incorporating these features, particularly voids—known to significantly impact mechanical performance by serving as points of weakness—future research can leverage these enhanced 3D models to better predict and optimize the mechanical behavior of composites based on their internal microstructure.

CONCLUSION

In this study, a comprehensive methodology for the analysis and modeling of hybrid yarns and fiber-reinforced composites (FRCs) was developed. The combination of advanced image acquisition techniques, segmentation processes, and 3D modeling allowed for a detailed understanding of the microstructural features critical to the mechanical behavior of these materials. By utilizing optical microscopy and flatbed scanning, high-resolution images of both yarn cross-sections and longitudinal views were captured, enabling the precise identification and classification of fiber types and voids. The image analysis process was enhanced through the use of machine learning-based segmentation, particularly the Stardist algorithm, which significantly improved the accuracy of fiber and void identification. The resulting segmented data allowed for the construction of 3D models of the yarn and composite structures, incorporating key microstructural elements such as fiber orientation, distribution, and void content. These models provide valuable insights into how these features influence the overall mechanical properties of the materials.

The exploratory spatial analysis of the fiber distribution further revealed slight clustering, which could have implications for the material's uniformity and performance. The spatial distribution functions and probabilistic models enabled a deeper investigation into fiber interactions and clustering tendencies, shedding light on potential improvements for yarn manufacturing processes. Looking ahead, the developed DIC-based process opens new avenues for future research. The ability to incorporate detailed microstructural data, such as fiber distribution and void content, into composite models will enable more accurate predictions of material behavior under various mechanical stresses. This will not only enhance the understanding of how microstructural features affect performance but also facilitate the optimization of hybrid yarns and composites for a wide range of engineering applications.

In conclusion, the methodologies and models developed in this study offer a powerful framework for investigating and optimizing the microstructure and mechanical performance of hybrid yarns and fiber-reinforced composites, opening the way for improved material design and industrial applications.

REFERENCES

1. Curtis C.J., et al.: Computer-generated watercolor. In: Proceedings of the 24th annual conference on Computer graphics and interactive techniques, 1997, pp. 421-430. https://doi.org/10.1145/258734.25889
2. Rajak D.K., Pagar D.D., Kumar R., et al.: Recent progress of reinforcement materials: a comprehensive overview of composite materials, Journal of Materials Research and Technology, 8(6), 2019. https://doi.org/10.1016/j.jmrt.2019.09.068
3. Advanced Mechanics of Composite Materials: Elsevier, 2007.
4. Anisimov E., Manak J., Puchnin M., et al.: The Effect of Microstructural Features on Mechanical Properties, Key Engineering Materials, 606, 2014. http://dx.doi.org/10.4028/www.scientific.net/KEM.606.47
5. Plaza G.R., Pérez-Rigueiro J., Riekel C., et al.: Relationship between microstructure and mechanical properties in spider silk fibers: identification of two regimes in the microstructural changes, Soft Matter, 22, 2012. http://dx.doi.org/10.1039/C2SM25446H
6. Hoang V.T., Kwon B.S., Sung J.W., et al.: Postprocessing method-induced mechanical properties of carbon fiber-reinforced thermoplastic composites, Journal of Thermoplastic Composite Materials, 36(1), 2023. https://doi.org/10.1177/08927057209453
7. Oztan C., Karkkainen R., Fittipaldi M., et al.: Microstructure and mechanical properties of three dimensional-printed continuous fiber composites, Journal of Composite Materials, 53(2), 2019. https://doi.org/10.1177/0021998318781938
8. Ramaswamy K., Modi V., Rao P.S., et al.: An investigation of the influence of matrix properties and fibre–matrix interface behaviour on the mechanical performance of carbon fibre-reinforced PEKK and PEEK composites, Composites Part A: Applied Science and Manufacturing, 165, 2023. https://doi.org/10.1016/j.compositesa.2022.107359
9. Mehdikhani M., Gorbatikh L., Verpoest I., et al.: Voids in fiber-reinforced polymer composites: A review on their formation, characteristics, and effects on mechanical performance, Journal of Composite Materials, 53(12), 2019. https://doi.org/10.1177/0021998318772152
10. Tunak M.., Tunakova V., Schindler M., et al.: Spatial arrangement of stainless steel fibers within hybrid yarns designed for electromagnetic shielding. Textile Research Journal, 89(10), 2018. https://doi.org/10.1177/0040517518783354
11. Li M., Li S., Tian Y., et al.: A deep learning convolutional neural network and multi-layer perceptron hybrid fusion model for predicting the mechanical properties of carbon fiber, Materials & Design, 227, 2023. http://doi.org/10.1016/j.matdes.2023.111760
12. Shah V., Zadourian S., Yang C., et al.: Data-driven approach for the prediction of mechanical properties of carbon fiber reinforced composites, Materials Advances, 19, 2022. https://doi.org/10.1039/D2MA00698G
13. Overberg M., Badrul Hasan M.M., Abdkader A., et al.: Investigations on the development of impact-resistant thermoplastic fibre hybrid composites from glass and steel fibre, Journal of Composite Materials, 58(14), 2024. https://doi.org/10.1177/00219983241246128
14. Weigert M., Schmidt U.: Nuclei Instance Segmentation and Classification in Histopathology Images with Stardist, in 2022 IEEE International Symposium on Biomedical Imaging Challenges (ISBIC), Kolkata, India: IEEE, 2022, S. 1–4. https://doi.org/10.1109/ISBIC56247.2022.9854534
15. Bankhead P.: QuPath: Open source software for digital pathology image analysis, Sci Rep, Bd. 7, Nr. 1, S. 16878, 2017. https://doi.org/10.1038/s41598-017-17204-5

AIMS AND SCOPES

"Vlakna a Textil" is a peer-reviewed scientific journal serving the fields of fibers, textile structures and fiber-based products including research, production, processing, and applications.

The birth of this journal is connected with three institutions, Research Institute for Man-Made Fibers, Svit (VÚCHV), Research Institute of Chemistry of Textiles (VÚTCH) in Žilina and Department of Fibers and Textiles at the Faculty of Chemical Technology, Slovak Technical University in Bratislava, having a joint intention to provide, utilize and deposit results obtained through the research, development and production activities dealing with the aforementioned scopes. „Vlákna a Textil" journal has been launched as a consequence of a joing of existing magazines „Chemické vládkna" (VÚCHV) and „Textil a chémia" (VÚTCH). Their tradition should provide a good framework for the new journal with the main aim to create a closer link between the basic element of the product - fibre and its fabric - textile.

Since its founding in 1994, the journal introduces new concepts, innovative technologies and better understanding of textile materials (physics and chemistry of fiber forming polymers), processes (technological, chemical and finishing), garment technology and its evaluation (analysis, testing and quality control) including non-traditional applications, such as technical textiles, composites, smart textiles or garment, and nano applications among others. The journal publishes original research papers and reviews. Original papers should present a significant advance in the understanding or application of materials and/or textile structures made of them.

VLÁKNA A TEXTIL
Volume 31, Issue 2, Septemberh 2024

CONTENT